



THE HONG KONG
POLYTECHNIC UNIVERSITY

香港理工大學

Pao Yue-kong Library

包玉剛圖書館

Copyright Undertaking

This thesis is protected by copyright, with all rights reserved.

By reading and using the thesis, the reader understands and agrees to the following terms:

1. The reader will abide by the rules and legal ordinances governing copyright regarding the use of the thesis.
2. The reader will use the thesis for the purpose of research or private study only and not for distribution or further reproduction or any other purpose.
3. The reader agrees to indemnify and hold the University harmless from and against any loss, damage, cost, liability or expenses arising from copyright infringement or unauthorized usage.

IMPORTANT

If you have reasons to believe that any materials in this thesis are deemed not suitable to be distributed in this form, or a copyright owner having difficulty with the material being included in our database, please contact lbsys@polyu.edu.hk providing details. The Library will look into your claim and consider taking remedial action upon receipt of the written requests.

**STUDY OF THREE-DIMENSIONAL WOVEN
FABRICS WITH IN-PLANE NEGATIVE POISSON'S
RATIO**

MUHAMMAD ZEESHAN

PhD

The Hong Kong Polytechnic University

2024

The Hong Kong Polytechnic University

School of Fashion and Textiles

**Study of Three-Dimensional Woven Fabrics With
In-Plane Negative Poisson's Ratio**

Muhammad Zeeshan

A thesis submitted in partial fulfillment of the requirements for the
degree of Doctor of Philosophy

August 2023

CERTIFICATE OF ORIGINALITY

I hereby declare that this thesis is my own work and that, to the best of my knowledge and belief, it reproduces no material previously published or written, nor material that has been accepted for the award of any other degree or diploma, except where due acknowledgement has been made in the text.

_____ (Signed)

 Muhammad Zeeshan (Name of student)

*To my father (late) and mother
for their prayers, love, and support*

ABSTRACT

Different from conventional fabrics, auxetic fabrics possess negative Poisson's ratio (NPR), which means that they show an unusual lateral expansion when stretched longitudinally. Auxetic textile fabrics have received significant attention due to their extraordinary behavior and improved characteristics because of the NPR. Until now, several two-dimensional (2-D) and three-dimensional (3-D) woven and knitted auxetic fabrics have been developed by researchers using different approaches. Auxetic behavior in woven fabrics can be induced by two methods. The first and simple method is to use a special auxetic yarn in the warp, weft, or in both directions to achieve NPR. Although this is the simplest approach to produce auxetic effect, however, there are some drawbacks linked with auxetic fabrics made using this method. Those drawbacks include, unstable auxetic behavior, incomplete transfer of auxetic property from yarn to fabric due to structural limitations, and auxetic yarns need a special arrangement for auxetic effect which makes the weaving process more complicated. The second method to produce auxetic woven fabrics is to realize auxetic geometry by using conventional elastic and non-elastic yarns in the warp and weft directions. After many potential developments in knitted auxetic fabrics, this method has now gained extraordinary interest of researchers to develop woven auxetic fabrics. So far, 2-D uni-stretch and bi-stretch woven fabrics have been developed based on this method. However, there are some limitations associated with these fabrics that include, low NPR, higher longitudinal deformation under tension, and a decrease in auxetic effect at high deformation. In addition, the development of 3-D woven fabric having in-plane auxetic behavior is still unaddressed.

This study aims to design and develop a novel 3-D narrow woven fabric that will exhibit in-plane auxetic behavior. A 3-D multilayer orthogonal through thickness structure was specially

designed with three different yarn components to incorporate auxetic geometry. One type of yarn was used in warp direction, while the two weft yarn systems, comprised of elastic yarn and coarse binding yarn, were used. The auxetic geometry resembles the re-entrant hexagon that was achieved by the unusual arrangement of warp yarns. The fabric samples were fabricated using a conventional semi-automatic weaving machine with four different influencing parameters for in-depth study. All the developed samples were tested on a tensile testing machine (Instron 5982) to evaluate the mechanical and auxetic behavior. The 3-D fabrics showed auxetic effect even at higher tensile strain. The results show that the appropriate binding to warp yarn diameter can produce a higher NPR of the fabric. While the repeat size of elastic weft yarn can highly affect the NPR of the fabric. The low bending stiffness of coarse binding yarn and low to moderate stretch percentage of elastic weft yarn are favorable for generating higher auxetic behavior. Furthermore, among all the 3-D woven fabrics developed with different structural parameters, the maximum Poisson's ratio achieved was -1.61.

After the experimental study, a geometrical model is proposed for the 3-D auxetic woven structure based on the geometrical arrangement of yarns that causes the NPR effect. A unit cell of a structure is first identified and then a relationship between longitudinal and lateral deformations of the structure is established in the form of semi-empirical equations. For validation of the model, the experimental results of the developed woven fabrics were correlated with the calculated results from the geometrical model. It was found that the calculated results were in good agreement with the experimental results. After experimental validation, the model was used to calculate and discuss critical parameters that affect the auxetic behavior of the structure. Thus, the geometrical analysis is believed to help predict the auxetic behavior of 3-D woven fabrics with different structural parameters.

While experimental and geometrical studies of the 3-D auxetic woven structure provide primary information, these studies have limitations in explaining the auxetic behavior of the 3-D woven structure at the yarn level. In addition, predicting the auxetic behavior of the 3-D woven structure by varying material properties is only possible through finite element (FE) analysis. Therefore, a 3-D FE model of the structure was developed to simulate the auxetic behavior of the structure. The structure was studied with different binding yarn properties once a good agreement was found between simulated and experimental results. The FE analysis provides new insights and uncovers fresh discussions regarding the auxetic behavior of the 3-D woven structure. With all the scientific discussions in light of the developed FE model, this study is expected to provide a better foundation for the future development of 3-D auxetic woven structures.

LIST OF PUBLICATIONS

Refereed journal papers

1. **Zeeshan M**, Hu H, Zulifqar A. Three-dimensional narrow woven fabric with in-plane auxetic behavior. *Text Res J* 2022; 92: 4695–4708.
2. **Zeeshan M**, Hu H, Etemadi E. Geometric Analysis of Three-Dimensional Woven Fabric with in-Plane Auxetic Behavior. *Polymers (Basel)* 2023; 15: 1326.
3. **Zeeshan M**, Hu H. Three-Dimensional Auxetic Woven Fabric Structure with In-plane Negative Poisson's Ratio for Composite Reinforcement: A Finite Element Analysis, submitted to journal (under review).

Book Chapters

- 1) Zulifqar A, **Zeeshan M**. Stretchable or elastomeric textiles as wearables, smart and functional textiles. In: Handbook of Stretchable and Elastomeric Textiles. Accepted in Elsevier.

Refereed conference papers

1. **Zeeshan M**, Hu H. Development of three-dimensional auxetic woven fabric for advanced engineering applications. In: *International Conference On Recent Advance In Engineering And Technology*. Toronto, 2023, pp. 1–3.

ACKNOWLEDGEMENTS

I would like to express my heartfelt gratitude to my chief supervisor, Prof. Hong Hu, for his unwavering support, invaluable guidance, and intellectual insights throughout the journey of my PhD study. His mentorship and encouragement have been instrumental in the successful completion of this thesis. My sincere appreciation goes to the dedicated staff of the School of Fashion and Textiles, especially Mr. Ng Shui-wing, for his constant assistance, technical support, and helpful attitude during my extensive work in the laboratories. I would also like to extend my profound gratitude to my esteemed colleagues, Dr. Adeel Zulifqar, Dr. Amir Shehzad, Mr. Umer Mansoor, Mr. Husnain Tansar, Mr. Zahid Javid, Mr. Aamir Mehmood, Mr. Abasal Husain, Mr. Ayaz Akber, Mr. Rehan Cheema, and Mr. Imran Mehmood, for their valuable cooperation, fruitful discussions, and support throughout my research journey. I am deeply indebted to my beloved soulmate, my wife Malaika Mushtaq, and my dear daughter Izzah Zeeshan and son Zayan Zeeshan, for their unwavering love, understanding, and constant support during the challenging times of my PhD study. Their sacrifices and encouragement have been a source of strength for me. I would like to express my heartfelt appreciation to my parents and parents-in-law for their unconditional love, prayers, and unwavering support throughout my academic journey. Special thanks go to my elder brothers, and sisters for their continuous motivation, guidance, and belief in my abilities. I would like to express my sincere gratitude to my teacher and mentor, Prof. Yasir Nawab, for his valuable guidance, inspiration, and continuous support throughout my academic journey. I am also thankful to my former colleagues, Dr. Mumtaz Ali, Dr. Aima Anjum, Dr. Muslim Rehman, Dr. Muhammad Umair, Dr. Khubeb Shaker, for their professional assistance, collaboration, and support.

TABLE OF CONTENTS

ABSTRACT.....	I
LIST OF PUBLICATIONS	IV
ACKNOWLEDGEMENTS	V
TABLE OF CONTENTS	VI
LIST OF FIGURES	XI
LIST OF TABLES	XIX
CHAPTER 1 INTRODUCTION	1
1.1 Background and motivation of the study	1
1.2 Aims and objectives.....	5
1.3 Research Methodology.....	6
1.3.1 Designing a three-dimensional auxetic woven structure	6
1.3.2 Development of three-dimensional auxetic woven fabrics	7
1.3.3 Characterization and analysis of the auxetic effect	7
1.3.4 Geometrical analysis of the yarns forming the three-dimensional architecture ..	7
1.3.5 Finite element analysis of the three-dimensional auxetic woven structure.....	8
1.4 Significance and values.....	8
1.5 Thesis outline.....	9
CHAPTER 2 LITERATURE REVIEW	12
2.1 Introduction	12
2.2 Auxetic fibers and polymers.....	12

2.3	Auxetic yarns	16
2.4	Auxetic knitted fabrics	20
2.5	Auxetic woven fabrics.....	30
2.5.1	Auxetic woven fabrics developed with auxetic yarns.....	31
2.5.2	Auxetic woven fabrics developed with non-auxetic yarns.....	35
2.6	Auxetic non-woven fabrics.....	39
2.7	Three-dimensional auxetic fabrics.....	44
2.7.1	Three-dimensional auxetic knitted fabrics	44
2.7.2	Three-dimensional auxetic fabrics made by using non-weaving and knitting technology.....	46
2.7.3	Three-dimensional auxetic fabrics made by using weaving technology	48
2.8	Auxetic composites	50
2.9	Potential applications of auxetic textiles.....	55
2.10	Conclusions	57
CHAPTER 3 MATERIALS AND METHODS.....		59
3.1	Introduction	59
3.2	Development of three-dimensional auxetic woven fabrics	59
3.2.1	Structure design	59
3.2.2	Fabric manufacturing.....	62
3.3	Experimental testing for auxetic effect	69
3.4	Geometrical analysis	72

3.5	Finite element analysis	73
3.6	Conclusions	74
CHAPTER 4 DEFORMATION BEHAVIOR OF THREE-DIMENSIONAL AUXETIC WOVEN FABRICS..... 75		
4.1	Introduction	75
4.2	Typical deformation behavior	76
4.2.1	Effect of binding yarn diameter on negative Poisson's ratio	80
4.2.2	Effect of repeat size of elastic yarn on negative Poisson's ratio	81
4.2.3	Effect of bending stiffness of coarse binding yarn on negative Poisson's ratio	83
4.2.4	Effect of weft stretch (elastic yarn) during insertion	84
4.3	Conclusions	86
CHAPTER 5 GEOMETRICAL ANALYSIS OF THREE-DIMENSIONAL AUXETIC WOVEN FABRICS..... 89		
5.1	Introduction	89
5.2	Geometrical analysis	89
5.2.1	The architecture of a three-dimensional auxetic woven structure	90
5.2.2	Yarn analysis	92
5.2.3	Geometric model.....	93
5.2.4	Experimental observations of geometric parameters and model validation ...	101
5.2.4.1	<i>Determining the Poisson's ratio during the first stage of deformation ...</i>	<i>101</i>
5.2.4.2	<i>Determining the Poisson's ratio during the second stage of deformation</i>	<i>103</i>

5.2.5	Prediction of auxetic behavior	107
5.2.5.1	<i>Effect of binding yarn compression</i>	107
5.2.5.2	<i>Effect of binding yarn diameter</i>	108
5.2.5.3	<i>Effect of binding yarn spacing</i>	110
5.3	Conclusions	111
CHAPTER 6 FINITE ELEMENT SIMULATION OF THREE-DIMENSIONAL AUXETIC WOVEN FABRICS		113
6.1	Introduction	113
6.2	Simulation of three-dimensional auxetic woven structure	114
6.2.1	Background of three-dimensional auxetic woven structure	114
6.2.2	Numerical modeling.....	115
6.2.2.1	<i>Establishing a model of the fabric structure</i>	116
6.2.2.2	<i>Determining material properties for the model</i>	118
6.2.2.3	<i>Setting up the testing environment and executing the model</i>	121
6.2.3	Simulation results	123
6.2.3.1	<i>Model validation</i>	123
6.2.3.2	<i>Deformation of structure and stress distribution analysis</i>	125
6.2.3.3	<i>Insights into the deformation behavior of the 3-D auxetic structure</i>	126
6.2.3.4	<i>Prediction of auxetic behavior with FE model</i>	129
6.3	Conclusions	132
CHAPTER 7 CONCLUSIONS AND SUGGESTIONS FOR FUTURE RESEARCH. 134		

7.1	Conclusions	134
7.1.1	Design concept and development	134
7.1.2	Auxetic behavior and factors affecting Poisson's ratio	135
7.1.3	Geometrical analysis	136
7.1.4	Finite element analysis	137
7.2	Contributions	138
7.3	Limitations	139
7.4	Suggestions for future research	140
	REFERENCES.....	141

LIST OF FIGURES

FIGURE 1.1 DEFORMATION BEHAVIOR OF CONVENTIONAL AND AUXETIC MATERIALS: (A) AT FREE STATE, (B) UNDER TENSILE DEFORMATION, (C) UNDER COMPRESSIVE DEFORMATION.	2
FIGURE 2.1 SCHEMATIC REPRESENTATION OF MICROPOROUS PTFE STRUCTURE OBSERVER UNDER TENSILE LOADING IN THE X-DIRECTION, (A) INITIAL STATE BEFORE DEFORMATION, (B) TENSION IN A LONGITUDINAL DIRECTION CAUSING NODES DISPLACEMENT, (C) ROTATION OF NODES INCREASING THE WIDTH, (D) FULLY EXPANDED STATE OF THE NODES ⁸	13
FIGURE 2.2 SEM IMAGE OF AUXETIC HMPE FIBER ⁷	14
FIGURE 2.3 LENGTH-WIDTH AGAINST THE TIME OF, (A) CONVENTIONAL POLYPROPYLENE FIBERS, (B) AUXETIC POLYPROPYLENE FIBERS ¹⁷	15
FIGURE 2.4 THE LENGTH-WIDTH DATA AGAINST THE TIME OF POLYESTER FIBERS ¹⁶	16
FIGURE 2.5 SCHEMATIC OF DOUBLE HELIX YARN, (A) RELAXED FORM, (B) UNDER TENSION ¹⁸ . ..	17
FIGURE 2.6 AUXETIC PLIED YARN, (A) RELAX STATE, (B) STRETCH STATE ⁶³	18
FIGURE 2.7 BRAIDED AUXETIC YARN AT (A) FREE STATE AND (B) UNDER TENSILE DEFORMATION ⁶⁴	19
FIGURE 2.8 THE DEVELOPED BRAIDED AUXETIC YARNS AND HELICAL AUXETIC YARN ⁶⁴	19
FIGURE 2.9 POISSON'S RATIO VERSUS TENSILE STRAIN CURVES OF BRAIDED AUXETIC YARN AND HELICAL AUXETIC YARN AT THE FIRST AND FIFTH CYCLE ⁶⁴	20
FIGURE 2.10 IMAGES OF DEVELOPED KNITTED FABRICS IN A NORMAL STATE, (A) MICROSCOPIC IMAGE, (B) MORE MAGNIFIED IMAGE SHOWING THE SINGLE REPEAT UNIT OF TRIANGULAR LATTICE GEOMETRY ⁷¹	21
FIGURE 2.11 (A) LENGTH-WIDTH DATA VERSUS TIME, (B) TRANSVERSE STRAIN VERSUS TENSILE STRAIN ⁷¹	21

FIGURE 2.12 AUXETIC KNITTED STRUCTURE WITH ELASTIC INLAY YARN ⁷²	22
FIGURE 2.13 AUXETIC WEFT-KNITTED FABRICS: (A) FOLDABLE GEOMETRY WITH A RECTANGULAR FORM OF THE FACE AND REVERSE LOOPS, (B) FOLDABLE GEOMETRY WITH HORIZONTAL AND VERTICAL STRIPES FORM OF THE FACE AND REVERSE LOOPS FORM, (C) ROTATING RECTANGLES STRUCTURE, (D) REAL-RE-ENTRANT HEXAGONAL STRUCTURE, (E) PSEUDO-RE-ENTRANT HEXAGONAL STRUCTURE ⁴²	24
FIGURE 2.14 SCHEMATIC OF GEOMETRIC DESIGN OF WARP-KNITTED AUXETIC FABRICS: (A) NON- AUXETIC RECTANGULAR NETS, (B) ADDITION OF EXTRA HORIZONTAL RIBS USING ELASTOMERIC YARN, (C) FORMATION OF RE-ENTRANT HEXAGONAL GEOMETRY AFTER SHRINKAGE ³⁹	25
FIGURE 2.15 SCHEMATIC PRESENTATION OF THREE FABRICS FORMED WITH DIFFERENT RIB SIZES: (A) FABRIC 1, (B) FABRIC 2, (C) FABRIC 3 ³⁹	26
FIGURE 2.16 IMAGES OF THE PRODUCED KNITTED AUXETIC SAMPLES: (A) FABRIC 1, (B) FABRIC 2, (C) FABRIC 3 ³⁹	27
FIGURE 2.17 FABRIC SAMPLE MOUNTED ON TENSILE TESTING MACHINE ³⁹	28
FIGURE 2.18 POISSON'S RATIO VERSUS TENSILE STRAIN CURVE OF FABRIC 3 ³⁹	28
FIGURE 2.19 LAMINATION PROCESS OF FRAME AND BASE FABRICS ⁷⁷	29
FIGURE 2.20 POISSON'S RATIO BEHAVIOR OF LAMINATED FABRIC UNDER WARP AND WEFT TENSILE STRAIN ⁷⁷	30
FIGURE 2.21 AUXETIC WOVEN FABRIC MADE OF DOUBLE HELIX YARN (UNDER TENSION) ¹⁸	31
FIGURE 2.22 AUXETIC FABRIC DEVELOPED WITH HELICAL AUXETIC YARN: (A) FABRIC B, (B) FABRIC C ⁵⁴	33
FIGURE 2.23 AUXETIC WOVEN FABRIC DEVELOPED WITH 4-PLY AUXETIC YARN ⁵⁵	34

FIGURE 2.24 PR-LONGITUDINAL STRAIN CURVES OF THE DIFFERENT AUXETIC GEOMETRIES VISUALIZED IN UNI-STRETCH WOVEN AUXETIC FABRICS ³⁰	37
FIGURE 2.25 THE AUXETIC BEHAVIOR IN THE ZIG-ZAG GEOMETRY-BASED BI-STRETCH WOVEN FABRICS TESTED: (A) ALONG THE WARP, (B) ALONG THE WEFT, (C) THE BI-STRETCH AUXETIC FABRIC, (D) UNIT CELL OF RE-ENTRANT HEXAGONAL GEOMETRY ^{26,56}	39
FIGURE 2.26 SEM MICROGRAPHS THE CELLULOSE FIBER NETWORK STRUCTURE OF PAPER AT TWO GIVEN MAGNIFICATIONS FOR EACH SAMPLE: (A) COPY PAPER, (B) FILTER PAPER ⁸²	40
FIGURE 2.27 SCHEMATIC REPRESENTATION OF HEAT-COMPRESSSION PROCESSING TREATMENT OF NON-WOVEN FABRIC SAMPLES ⁴⁶	41
FIGURE 2.28 THE POISSON'S RATIO AGAINST THE AXIAL STRAIN OF THE SAMPLE AS-RECEIVED, COMPRESSION, AND HEAT-COMPRESSED: (A) FABRIC TYPE NW1 AND, (B) FABRIC TYPE NW2 ⁴⁶	42
FIGURE 2.29 MICRO-CT IMAGES OF AS-RECEIVED SAMPLE: (A) TOP-VIEW AND (B) SECTION VIEW, AND HEAT-COMPRESSED SAMPLE: (C) TOP VIEW, AND (D) SECTION VIEW ⁴⁶	43
FIGURE 2.30 THREE-DIMENSIONAL KNITTED FABRIC: (A) FABRIC KNIT PATTERN, (B) SCHEMATIC OF PARALLELOGRAM PLANES OF ZIGZAG PATTERN, (C) KNITTED FABRIC IN RELAXED FORM, (D) KNITTED FABRIC IN STRETCH FORM ⁸³	44
FIGURE 2.31 THREE-DIMENSIONAL AUXETIC KNITTED SPACER FABRIC: (A) SCHEMATIC REPRESENTATION, (B) PRODUCED FABRIC ⁸⁴	45
FIGURE 2.32 THREE-DIMENSIONAL AUXETIC WARP-KNITTED SPACER FABRIC DESIGN: (A) LOOP DIAGRAM OF RE-ENTRANT HEXAGON, (B) JACQUARD PATTERN OF ROTATING SQUARE ⁴⁰	46
FIGURE 2.33 STRUCTURE OF INNOVATIVE 3-D NON-WEAVING AND KNITTED AUXETIC STRUCTURE, (A), RELAX STATE, (B) UNDER COMPRESSION ⁵⁷	47
FIGURE 2.34 MECHANISM OF AUXETIC BEHAVIOR IN THE 3-D WOVEN FABRICS ⁵⁸	49

FIGURE 2.35 (A) 3-D AUXETIC PRE-FORM DEVELOPED WITH PARA-ARAMID YARN (YELLOW) AND UHMWPE YARN (WHITE), (B) POISSON’S RATIO VALUES OF DEVELOPED SAMPELS ³³	50
FIGURE 2.36 COMPOSITE SAMPLES: (A) AUXETIC FABRIC REINFORCED COMPOSITE, (B) 100% PURE MATRIX, AND (C) NON-AUXETIC FABRIC REINFORCED COMPOSITE ⁹⁵	51
FIGURE 2.37 (A) AUXETIC AND (B) NON-AUXETIC FABRIC REINFORCED COMPOSITES UNDER COMPRESSIVE LOAD ⁹⁵	53
FIGURE 2.38 COMPARISON OF COMPRESSION CURVES OF THE THREE SAMPLES: (A) COMPRESSIVE STRESS-STRAIN, (B) COMPRESSIVE SPECIFIC STRESS-STRAIN ⁹⁵	53
FIGURE 2.39 ENERGY-TIME CURVES OF AUXETIC COMPOSITE, NON-AUXETIC COMPOSITE, AND PU FORM ⁸⁵	54
FIGURE 3.1 CONVENTIONAL THREE-DIMENSIONAL ORTHOGONAL THROUGH THICKNESS STRUCTURE.....	60
FIGURE 3.2 SCHEMATIC REPRESENTATION OF SIDE VIEW AND TOP VIEW: (A) CONVENTIONAL 3-D ORTHOGONAL STRUCTURE WITH 1/1 PLAIN PATTERN OF BINDING YARN, (B) CHANGING WEAVE PATTERN OF BINDING YARN BY 2/2 TWILL PATTERN IN WEFT INTERLOCK MANNER, (C) INTRODUCTION OF FINE ELASTIC YARN IN THE WEFT DIRECTION, (D) MODIFIED 3-D ORTHOGONAL STRUCTURE WITH AUXETIC GEOMETRY IN A RELAXED STATE.	61
FIGURE 3.3 SCHEMATIC OF 3-D AUXETIC WOVEN STRUCTURE (A) INITIAL STATE, (B) UNDER TENSILE TENSION IN THE WARP DIRECTION.....	62
FIGURE 3.4 IMAGES OF WARP YARN, ELASTIC WEFT YARN, AND BINDING YARNS USED FOR PRODUCING THREE-DIMENSIONAL (3-D) AUXETIC WOVEN STRUCTURE.....	64
FIGURE 3.5 TENSILE LOAD VERSUS STRAIN CURVES OF THE WARP, ELASTIC WEFT, AND BINDING YARNS.....	65

FIGURE 3.6 (A) SCHEMATIC ILLUSTRATION OF WARP AND WEFT YARNS OF THE TWO LAYERS OF 3-D WOVEN FABRIC, (B) THE INTERLACING PATTERN OF 3-D AUXETIC WOVEN FABRIC, (C) TOP LAYER OF THE ORTHOGONAL THROUGH-THE-THICKNESS AUXETIC WOVEN STRUCTURE.	66
FIGURE 3.7 SEMI-AUTOMATIC WEAVING MACHINE USED FOR FABRICATION.....	67
FIGURE 3.8 PROCESS OF PREPARING SAMPLES FOR TENSILE TEST; (A) 3-D WOVEN SAMPLE, (B) APPLICATION OF EPOXY TO THE CLAMPING AREA, (C) APPLICATION OF TABS UNDER NEGATIVE PRESSURE, (D) SAMPLES WITH ALUMINUM TABS.....	71
FIGURE 3.9 POISSON'S RATIO EVALUATION OF THREE-DIMENSIONAL AUXETIC WOVEN FABRIC: (A) TENSILE TESTING SETUP ON UTM MACHINE, (B) SCHEMATIC REPRESENTATION TESTING PROCESS.	72
FIGURE 4.1 THE DEFORMATION BEHAVIOR OF FABRIC F2-S2: (A) TENSILE STRESS-STRAIN CURVE, (B) LATERAL-TENSILE STRAIN CURVE, (C) POISSON'S RATIO-TENSILE STRAIN CURVE.....	76
FIGURE 4.2 DECRIMPING OF WARP YARNS UNDER TENSILE TENSION AT, (A) 0%, (B) 2%, (C) 4%, (D) 6%, (E) 8%, (F) 10%.....	79
FIGURE 4.3 TENSILE LOAD-STRAIN CURVE OF SINGLE WARP YARN.	79
FIGURE 4.4 POISSON'S RATIO VERSUS TENSILE STRAIN CURVES BY VARYING THE DIAMETER OF THE BINDING YARN.....	81
FIGURE 4.5 TENSILE BEHAVIOR OF THREE-DIMENSIONAL AUXETIC WOVEN FABRIC: (A) STRESS-STRAIN CURVES OF WOVEN FABRIC, (B) POISSON'S RATIO-TENSILE STAIN CURVES OF WOVEN FABRIC.	82
FIGURE 4.6 COMPARISON OF POISSON'S RATIO-TENSILE STAIN CURVES OF FABRIC WITH HIGH-STIFF AND LOW-STIFF BINDING YARN.	83

FIGURE 4.7 (A) COMPARISON OF POISSON'S RATIO-TENSILE STRAIN CURVES OF FABRIC WITH HIGH-STRETCH AND LOW-STRETCH ELASTIC WEFT INSERTION, (B) TENSILE LOAD-STRAIN CURVE OF ELASTIC WEFT YARN, (C) MECHANISM OF TENSILE FORCE AND RESTORING FORCE DURING DEFORMATION.....	85
FIGURE 5.1 THREE-DIMENSIONAL AUXETIC WOVEN STRUCTURE: (A) SCHEMATIC REPRESENTATION, (B) REAL FABRIC	90
FIGURE 5.2 BINDING YARN COMPRESSION TEST ASSEMBLY.....	93
FIGURE 5.3 SCHEMATIC DIAGRAM OF 3-D AUXETIC WOVEN STRUCTURE: (A) TOP VIEW, (B) TOP CROSS-SECTIONAL VIEW.....	93
FIGURE 5.4 GEOMETRICAL MODEL OF 3-D AUXETIC STRUCTURE: (A) DECRIMPING OF WARP YARNS UNDER TENSILE DEFORMATION, (B) ELONGATION OF WARP YARNS UNDER TENSILE DEFORMATION.	94
FIGURE 5.5 FIRST STAGE OF DEFORMATION OF A UNIT-CELL: (A) INITIAL STATE, (B) DEFORMED STATE.....	97
FIGURE 5.6 SECOND STAGE OF DEFORMATION OF A UNIT-CELL: (A) DECRIMPED, (B) ELONGATION OF WARP YARN.....	100
FIGURE 5.7 TENSILE FORCE-STRAIN CURVE OF ELASTIC WEFT YARN.....	102
FIGURE 5.8 COMPRESSIVE FORCE-EXTENSION CURVE OF COARSE BINDING YARN.....	102
FIGURE 5.9 TREND OF THE DIAMETER OF WARP YARN AGAINST THE TENSILE STRAIN.....	104
FIGURE 5.10 COMPARISON OF CALCULATED AND EXPERIMENTAL RESULTS OF POISSON'S RATIO AGAINST THE TENSILE STRAIN.....	106
FIGURE 5.11 EFFECT OF BINDING YARN'S COMPRESSION ON AUXETIC BEHAVIOR OF 3-D WOVEN STRUCTURE.....	108

FIGURE 5.12 EFFECT OF BINDING YARN DIAMETER ON AUXETIC BEHAVIOR OF 3-D WOVEN STRUCTURE.....	109
FIGURE 5.13 EFFECT OF BINDING YARN SPACING ON AUXETIC BEHAVIOR OF 3-D WOVEN STRUCTURE.....	110
FIGURE 6.1 SCHEMATIC ILLUSTRATION OF (A) CONVENTIONAL THREE-DIMENSIONAL ORTHOGONAL THROUGH-THE-THICKNESS STRUCTURE, (B) MODIFICATION OF BINDING YARN, (C) MODIFICATION OF WEFT YARN, AND (D) MODIFIED THREE-DIMENSIONAL AUXETIC STRUCTURE.....	115
FIGURE 6.2 ESTABLISHMENT OF FABRIC STRUCTURE MODEL FOR FINITE ELEMENT ANALYSIS; (A) REAL FABRIC STRUCTURE, (B) MODELED FABRIC STRUCTURE.....	118
FIGURE 6.3 TENSILE STRESS-STRAIN CURVE OF WARP YARN.	120
FIGURE 6.4 BOUNDARY CONDITIONS OF FINITE ELEMENT MODEL AT (A) STEP-1, AND (B) STEP-2.	122
FIGURE 6.5 COMPARISON OF EXPERIMENTAL AND SIMULATED RESULTS: (A) POISSON'S RATIO- TENSILE STRAIN, (B) TENSILE STRESS-TENSILE STRAIN.....	124
FIGURE 6.6 DEFORMATION AND MISES DISTRIBUTION OF 3-D STRUCTURE AT DIFFERENT TENSILE STRAINS IN STEP-1 (ELASTIC WEFT YARN EXTENSION) AND STEP-2 (WARP YARN EXTENSION).....	126
FIGURE 6.7 MISES STRESS DISTRIBUTION IN BINDING YARNS AT A DEFORM STATE.	126
FIGURE 6.8 COMPARISON OF FE SIMULATED AND GEOMETRICALLY CALCULATED PR WITH EXPERIMENTAL PR OF THE 3-D AUXETIC WOVEN STRUCTURE.....	127
FIGURE 6.9 ILLUSTRATION OF THE TOP CROSS-SECTIONAL OF 3-D AUXETIC STRUCTURE: (A) TOP CROSS-SECTION OF WARP AND BINDING YARNS AT INITIAL STATE, (B) ONLY WARP YARNS	

AT INITIALS AND DEFORM STATE (SHOWN AS PARTIALLY TRANSPARENT), AND (C) WARP AND BINDING YARNS UNDER 10 % TENSILE STRAIN.	128
FIGURE 6.10 PR RESULTS OF THREE-DIMENSIONAL AUXETIC STRUCTURE WITH DIFFERENT AXIAL AND RADIAL MODULI OF BINDING YARN.	130
FIGURE 6.11 COMPRESSIVE STRAIN OF BINDING YARN AGAINST THE TENSILE STRAIN OF THE 3-D AUXETIC STRUCTURE.....	132
FIGURE 6.12 MISES STRESS DISTRIBUTION IN BINDING YARN, (A) E_x/E_y 40/10 AND (B) E_x/E_y 70/10.....	132

LIST OF TABLES

TABLE 2.1 SUMMARY OF THE TWO DEVELOPED AUXETIC FABRIC ⁵⁴	32
TABLE 2.2 PARAMETERS OF THE PRODUCED WOVEN FABRICS ⁵⁵	34
TABLE 2.3 PENETRATION AND IMPACT ENERGIES OF CONVENTIONAL AND MODIFIED 3-D SAMPLES ⁵⁸	48
TABLE 3.1 PROPERTIES OF WARP AND WEFT YARNS USED FOR SAMPLE PREPARATION.	64
TABLE 3.2 PARAMETERS OF DEVELOPED THREE-DIMENSIONAL (3-D) AUXETIC WOVEN FABRICS.	69
TABLE 5.1 PROPERTIES OF THE YARNS USED FOR SAMPLE PREPARATION.	92
TABLE 5.2 STRUCTURAL PARAMETERS AND THE CALCULATED POISSON'S RATIO RESULTS OF 3-D AUXETIC WOVEN FABRIC.	105
TABLE 6.1 GEOMETRIC PARAMETERS OF FABRIC STRUCTURE FOR FE MODEL	117
TABLE 6.2 MATERIAL PROPERTIES OF WARP YARN AND BINDING YARN.....	120
TABLE 6.3 MATERIAL LAW PARAMETERS FOR ELASTIC WEFT YARN.	121
TABLE 6.4 AXIAL AND RADIAL MODULI OF BINDING YARN.....	130

CHAPTER 1 INTRODUCTION

1.1 Background and motivation of the study

Auxetic textiles are a group of metamaterials that exhibit an unusual dimensional change in response to applied load. Specifically, the transversal dimension of the material increases under tensile loading and decreases under compressive loading¹. The phenomenon of auxetic and non-auxetic materials under tensile and compressive deformations is presented in Figure 1.1. This unique property of auxetic textiles gives rise to exceptional features such as high surface area under tension, high indentation resistance due to material compaction under compression, and easy shape adoption due to synclastic deformation. As a result, the applications of auxetic textiles are diverse and advanced, ranging from protective textiles and medical textiles to sportswear, fashion textiles, and reinforcement for polymer composite²⁻⁵. Over the last two decades, researchers have gained considerable achievements by implanting auxetic properties in auxetic polymers⁶⁻⁸, auxetic metamaterials⁹⁻¹⁵, auxetic fibers^{16,17}, auxetic yarns¹⁸⁻²⁰, two-dimensional (2-D) auxetic woven fabrics²¹⁻³⁰, 3-D auxetic textiles³¹⁻³³, warp-knitted auxetic fabrics³⁴⁻⁴⁰, weft-knitted auxetic fabrics⁴¹⁻⁴³, non-woven auxetic fabrics⁴⁴⁻⁴⁶ and auxetic composites⁴⁷⁻⁵². However, many researchers are still focusing on auxetic woven fabrics due to their potential applications in clothing, fashion, protective gears, auxetic sensors, etc. However, the development of auxetic woven fabrics still faces challenges that are resulting in relatively slow progress.

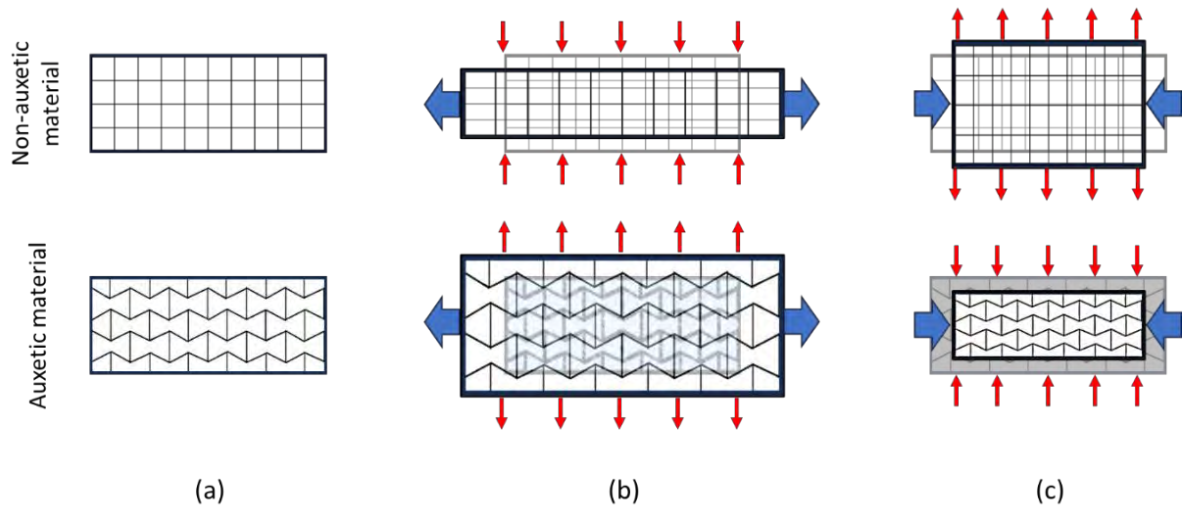


Figure 1.1 Deformation behavior of conventional and auxetic materials: (a) at free state, (b) under tensile deformation, (c) under compressive deformation.

There are two methods of developing woven fabrics with auxetic behavior. One of the two methods of producing auxetic woven fabric is simple and elementary, which involves using auxetic yarns in the warp, weft, or both directions of the fabric. These types of auxetic woven fabrics can be developed with conventional weave patterns such as plain, twill, satin, etc. On the other hand, the second method involves the use of non-auxetic yarns but a visualization of an auxetic geometric structure such as re-entrant hexagonal, rotating squares, etc. By using the first method, typical helical auxetic yarn (HAY) developed by Sloan et al.¹⁹, and double helix yarn (DHY) developed by Miller et al.¹⁸, are utilized to produce auxetic woven fabrics. For instance, numerous studies^{18,19,53,54} have focused on developing auxetic woven fabrics utilizing HAY and DHY in either the warp, weft, or both directions. Miller et al.¹⁸ successfully developed auxetic woven fabric by using a DHY in the weft direction and a meta-aramid yarn in the warp direction. A plain weave design, the simplest among all, is used as an interlacement pattern for the fabric. When tested, the developed fabric showed an out-of-plane NPR caused by the overlapping of DHY yarns in the fabric structure. Other than the use of HAY and DHY,

Ng and Hu⁵⁵ reported a new type of auxetic yarns named “plied auxetic yarns” and used it for the production of auxetic woven fabrics. For fabric making, the plied auxetic yarn and a common non-auxetic elastic yarn were used in the warp and weft directions of the fabric respectively. This study also reported the influence of different design parameters of the plied auxetic yarn (number of plies, diameter of yarns, etc.) and fabric design (plain, twill, satin) on NPR behavior of the woven fabrics. Although developing auxetic woven fabrics using this method is simple, however, these fabrics have drawbacks, including reduced durability in terms of auxetic behavior, the special arrangement of auxetic yarns required in warp or weft direction, incomplete transfer of auxeticity from yarn to fabric, and limited design variation. Therefore, the current focus of many researchers lies in the development of auxetic woven fabrics using non-auxetic yarns. This approach aims to overcome the limitations associated with auxetic yarns, offering opportunities for further advancements in the field.

A uni-stretch (extensible in one direction) and bi-stretch (extensible in both directions) auxetic woven fabrics have been developed using the second and most alluring method^{23,26,56}. This method was first invented by Zulifqar et al.³⁰ when they reported a uni-stretch woven fabric with an in-plane negative Poisson’s ratio (NPR). The principle of differential shrinkage of different types of weaves was used to visualize auxetic patterns, such as foldable structures, rotating rectangles, and re-entrant hexagons. The differential shrinkage property of loose weave (satin) and tight weave (plain) was triggered by using elastic yarn in the weft direction and non-elastic (cotton) yarn in the warp direction. In this study, a maximum of -0.17 NPR was achieved, which is considered insignificant. Therefore, another study²⁶ was conducted on bi-stretch auxetic woven fabrics to improve the NPR. In this study, elastic yarn was used in both warp and weft directions along with non-elastic yarns, resulting in an improved NPR of -0.36. However, auxetic fabrics developed with this method associate some drawbacks, such as low

auxetic effect, high longitudinal deformation, and low mechanical properties due to the use of elastic yarn. Nevertheless, this research gained a lot of attention due to the potential for improvement, such as exploring new auxetic structures and yarns that can offer robust properties.

Over the last few years, there has been an increasing interest in developing three-dimensional (3-D) auxetic structures to address high-profile applications such as protective gears, fiber-reinforced composite structures, safety belts, and impact energy absorption applications. In this regard, Ge et al.⁵⁷ developed the first ever 3-D auxetic textile structure by transforming the conventional multi-layered orthogonal through thickness structure. A combination of knitting and non-weaving techniques was used to fabricate the structure with a specially designed machine. This unique structure exhibits an NPR under compressive load and demonstrates improved indentation resistance and impact energy absorption properties when used as a reinforcement for polymer composite. However, the application of this structure was limited to composite reinforcement only, mainly due to its high thickness and structural instability.

Other authors^{33,58} also reported out-of-plane auxetic effect in 3-D woven fabrics using a different approach. The out-of-plane auxetic effect was achieved by the z-direction arrangement of the binding yarn. The perpendicular crimp of the binding yarns increases the thickness of the structure when stretched longitudinally. The increase in the thickness resulted by pushing the weft yarns by the binding yarn during decrimping under longitudinal deformation. Although these 3-D woven fabrics showed improved impact-resistant properties when used as a reinforcement for polymer composite, their applications are still limited in some cases due to a lack of in-plane NPR effect. Other applications such as automotive seat belts, garment belts, and backpack belts require an in-plane auxetic property since the frequently involved impact pressure in these applications can only be reduced if the contact area of the

belt with the human body is increased⁵⁹. Still, there is currently no available 3-D auxetic woven structure that exhibits an in-plane NPR effect and can be woven using high-performance yarns suitable for applications involving impact pressure. The reason behind this limitation in the existing literature is the considerable challenge involved in achieving an in-plane auxetic effect in 3-D woven fabrics due to the constraints of the weaving process. As a result, the development of a 3-D narrow auxetic woven fabric that exhibits an in-plane NPR and can be utilized in functional belts remains unexplored. The aforementioned drawbacks and the limited scope of applications of previously developed 2-D and 3-D auxetic woven fabrics are the motivation for this study.

1.2 Aims and objectives

This PhD research project aims to study and report the development of a new group of 3-D auxetic woven fabrics with in-plane NPR by using non-auxetic yarns and available conventional weaving machines. Preliminary, we will introduce an in-plane auxetic effect in 3-D woven fabrics using the phenomenon of warp yarn crimp in the weft direction. This study is designed to achieve the following objectives.

1. To design and introduce a new geometrical structure that can be transformed into a 3-D woven fabric capable of producing an in-plane auxetic effect.
2. To convert and fabricate 3-D auxetic woven fabrics based on the above design using commonly available elastic and non-elastic braided yarns and existing weaving machines.
3. To study and optimize the NPR effect of the 3-D woven fabrics by changing different influencing parameters.
4. To develop a geometrical model of the 3-D auxetic woven fabric structure to verify and predict the NPR effect under different geometrical parameters of the 3-D structure.

5. To analyze and simulate the auxetic behavior of 3-D auxetic woven fabrics using the finite element (FE) analysis method.

1.3 Research Methodology

The core objective of this study is to design and develop a new 3-D woven structure that exhibits an in-plane NPR effect by utilizing the commonly available textile yarns and weaving machine. The following research methodology is adopted to achieve this objective.

1.3.1 Designing a three-dimensional auxetic woven structure

Developing 3-D auxetic woven fabric through modification of the existing 3-D structures requires knowledge of both auxetic geometrical patterns and properties and the construction of conventional 3-D woven structures. There, the principle of auxetic behavior generated through different geometric patterns is studied. Then, the three-yarn system in the 3-D woven structures is analyzed to incorporate any possible auxetic geometrical pattern to achieve an in-plane auxetic effect. Finally, a conventional 3-D orthogonal through-the-thickness structure is selected for modification to achieve the auxetic effect. The structure is successfully modified and developed using conventional elastic and non-elastic yarns and a common weave machine. The modification process involved four changes to the conventional structure that are: the use of coarser binding yarn, changing the direction of binding yarn from the warp to the weft direction, using a 2/2 twill weave pattern of binding yarn instead of 1/1 plain, and the use of fine elastic yarn in the weft direction replacing non-elastic yarn. These changes trigger a special geometric arrangement of the warp yarns that resembles re-entrant hexagonal auxetic geometry.

1.3.2 Development of three-dimensional auxetic woven fabrics

A weaving process is set up for the fabrication of the designed 3-D auxetic woven structure on a semi-automated dobby weaving machine. The machine setting, including the number of frames, reed number, drawing-in-draft, etc., was determined based on the technical parameters of the fabric such as interlacing pattern, number of layers, yarn count (diameter), and warp and weft yarn densities.

1.3.3 Characterization and analysis of the auxetic effect

After developing the 3-D auxetic woven fabric, a tensile test was performed to assess the mechanical performance and the auxetic behavior of the fabric sample by calculating its Poisson's ratio. A sample, marked with two longitudinal and two transversal visible dots at a distance of 2.5 mm each, was subjected to a uniaxial tensile test using an Instron tensile testing machine (model 5566) with a separate setup high-resolution camera to record the deformation of the sample. The images at different strain intervals were then extracted from the recorded video for study. The images were analyzed using an open-source screen ruler software to calculate the transverse deformation. The Poisson's ratio of the 3-D woven fabric was then calculated from the longitudinal strain (provided by the machine's head movement) and transverse strain (calculated through image analysis).

1.3.4 Geometrical analysis of the yarns forming the three-dimensional architecture

The developed 3-D auxetic woven fabric possesses a special arrangement of warp and binding yarns that forms an auxetic geometry that triggers the auxetic effect under tensile deformation. As the auxetic effect arises from the geometrical configuration of the yarns, therefore, the behavior of the yarns was studied under tensile deformation to propose a geometric model for the 3-D auxetic woven structure. After analyzing the yarn's behavior, a unit geometric cell of the warp and binding yarns was identified, and a geometric model was proposed. The proposed

model provides a relationship between the tensile deformation and Poisson's ratio of the structure in the form of semi-empirical equations. The geometrical analysis proved as a useful tool to predict the Poisson's ratio of the 3-D auxetic woven structure at different tensile strains by varying the geometrical parameters such as the diameter of warp and binding yarns, the distance between binding yarn, etc.

1.3.5 Finite element analysis of the three-dimensional auxetic woven structure

The experimental study provides the information on development of the 3-D auxetic woven structure and its behavior under tensile deformation while the geometrical analysis proved as tool for predicting its auxetic behavior based on the geometrical parameters of the structure. As the geometric model was based on the geometrical parameters only, therefore, the 3-D auxetic woven structure is further analyzed with the finite element (FE) method that includes both geometrical parameters and material properties. An FE model is first developed and validated with the results obtained from the experimental and geometric study. After validation, the FE model is used to find more concrete reasons for the auxetic behavior at the yarn level. Furthermore, the FE model is also used to predict the Poisson's ratio of the 3-D auxetic structure by varying the yarn properties. The results demonstrate that the FE model is a powerful tool for predicting and designing the required properties of the 3-D auxetic structure for specific applications.

1.4 Significance and values

In recent years, the development of 3-D woven structures has attained special consideration in the area of auxetic fabrics because, in addition to NPR effect, they can offer phenomenal mechanical properties which make them useful for advanced applications. Although many scientists have developed and achieved NPR effect in 3-D woven fabrics, still the auxetic effect of all those fabrics is limited to out-of-plane direction. This study aimed to develop a novel

class of narrow 3-D auxetic woven fabrics that will show an in-plane NPR effect. This breakthrough in the area of 3-D auxetic woven fabrics will further broaden the use of auxetic textiles for more advanced applications. Further, these in-plane auxetic woven fabrics are developed using commonly available elastic and non-elastic braided yarns and a conventional weaving process, which can be produced on an industrial scale. The narrow 3-D auxetic woven fabric is expected to be a useful candidate for applications like automobile seat belts, protective gears, composite reinforcement, etc.

This comprehensive study on the effect of different parameters on the auxetic performance of 3-D woven fabrics can be useful information for further development. Moreover, the geometrical and numerical analysis of the 3-D auxetic woven fabric structure can be useful to engineer and predict the mechanical and auxetic properties prior to production. It could be said that the experimental and numerical data generated in the above-mentioned studies will provide a strong platform for academic researchers to further explore the area of 3-D auxetic woven structures with in-plane auxetic behavior.

1.5 Thesis outline

This thesis consists of 7 chapters, which are summarized as follows:

Chapter 2 reports a review of literature about the previous developments in auxetic textile materials like filaments, yarns, two-dimensional (2-D), and three-dimensional (3-D) fabrics. It also reviews the potential applications of these developed auxetic textiles. In the end, the research gap is identified and explained based on the literature on auxetic textiles.

Chapter 3 explains the design concept, fabrication method, and testing setup of the 3-D auxetic woven fabrics. The theory of 3-D auxetic woven fabrics is described followed by a detailed

manufacturing process. Then, the tensile testing setup is reported for calculating Poisson's ratio values of the 3-D auxetic woven fabrics.

Chapter 4 introduces the experimental results of the study obtained from the deformation behavior of the 3-D auxetic woven fabrics subjected to uni-axial tensile force. The results are presented and discussed in terms of tensile stress versus strain and Poisson's ratio versus strain. This chapter also compares and discusses the results of 3-D auxetic woven fabrics developed with different influencing parameters.

Chapter 5 describes the geometrical modeling of 3-D auxetic woven fabrics. The modeling is based on the geometrical arrangement of warp and binding yarn in longitudinal and lateral directions, respectively. The geometry of the fabric samples is first examined in a free state and under tensile deformation to identify a unit cell of the geometry and to realize the behavior of individual warp and weft yarns. Then, a model is proposed at the meso-level (yarn-level) based on the information gathered about the geometry of the fabric structure. The model transforms the geometry of the structure into semi-empirical equations that establish a relationship between the tensile strain and Poisson's ratio of the 3-D auxetic woven structure. After successful validation, the geometric model is used to predict the auxetic behavior of the structure based on the different geometrical parameters such as yarn diameters, the distance between yarns, etc.

Chapter 6 presents the finite element modeling of the 3-D auxetic woven fabric structure to simulate its Poisson's ratio under tensile deformation. The simulated Poisson's ratio is presented and compared with the experimental Poisson's ratio of the structure for validation. Following, the model is used to study the 3-D auxetic woven structure with different material properties.

Chapter 7 explains the key findings and developments regarding the 3-D auxetic woven fabrics derived from this research. Additionally, the limitations of the study and recommendations for future research are also addressed.

CHAPTER 2 LITERATURE REVIEW

2.1 Introduction

This chapter presents the literature on auxetic textiles including fibers, filaments, yarns, and fabrics. In this review, the raw materials, geometrical structures, and methodology adopted to develop these auxetic textiles are primarily focused. Further, the potential applications recommended by the researchers are also discussed. This literature review will help to understand the concept of incorporating auxetic geometry into textile fabrics. Also, it will be helpful for this study to select suitable materials and effective methods for conducting the experimental work.

2.2 Auxetic fibers and polymers

Up till today, researchers have developed auxetic filaments using different polymers like polytetrafluoroethylene (PTFE), polyethylene (PE), polypropylene (PP), polyurethane (PU), polyester, and high-modulus polyethylene (HMPE). Earlier, the auxetic behavior of materials was first identified by Voigt⁶⁰ in the early 1900s, however, the author did not succeed in coming up with a logical explanation for this unique property. Therefore, for many decades, these materials did not get any attention for further development. Later, auxetic materials were again brought to the attention by Gibson⁶¹ in 1982, when he explained the auxetic behavior of a structure made with polymer rubber-aluminum honeycombs that were able to deform by flexure of the ribs. Since then in 1987, a major breakthrough in the area was claimed by Lakes⁶² when he reported the first manmade auxetic polymeric foam. The inventor successfully converted the commercially available PU form into auxetic foam by passing it through a thermomechanical process where the open-cell PU foam is heated under a triaxial compression

force. After this invention, auxetic materials were investigated in many fields specially in textiles with superior properties and wide applications area.

Following the successful invention of auxetic foam, Caddock and Evens⁸ examined the auxetic effect in an extremely anisotropic form of expanded polytetrafluoroethylene (PTFE). The authors also identified the mechanism of extended PTFE which led them to a very large Poisson's ratio of -12. A commercial-grade sheet and cylindrical PTFE were prepared with a conductive coating to be observed under a scanning electron microscope (SEM). The micrographs in initial and stretch states were taken in x-y directions to measure the Poisson's ratio of PTFE, the schematic diagram of node rotation and lateral expansion is shown in Figure 2.1. The micro-analysis of the structure under deformation concluded this study with a reason that such a large NPR is because of the extreme anisotropy in modulus.

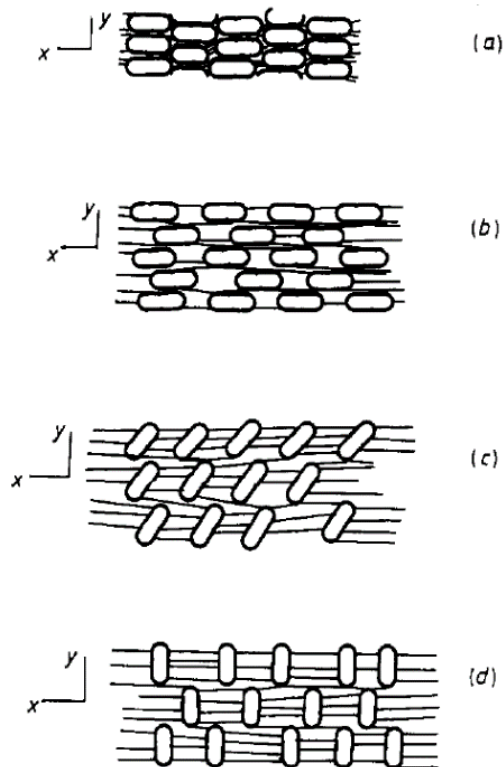


Figure 2.1 Schematic representation of microporous PTFE structure observer under tensile loading in the x-direction, (a) initial state before deformation, (b) tension in a longitudinal

direction causing nodes displacement, (c) rotation of nodes increasing the width, (d) fully expanded state of the nodes⁸.

Alderson et al.⁷ successfully produced auxetic polymer using high-modulus polyethylene (HMPE) powder as raw material and by a novel thermoforming process route. In the reported thermoforming process route, three stages were involved i.e., compaction, sintering, and extrusion. In the first stage, the HMPE powder was converted into a well-formed compacted rod, which was then subjected to different possible sintering and extrusion parameters. Finally, the microporous HMPE fibers were developed at certain parameters of extrusion rig die diameter, extrusion rate, and temperature that showed NPR of as low as -1.2. The SEM image of the developed microstructure HMPE fibers is illustrated in Figure 2.2.

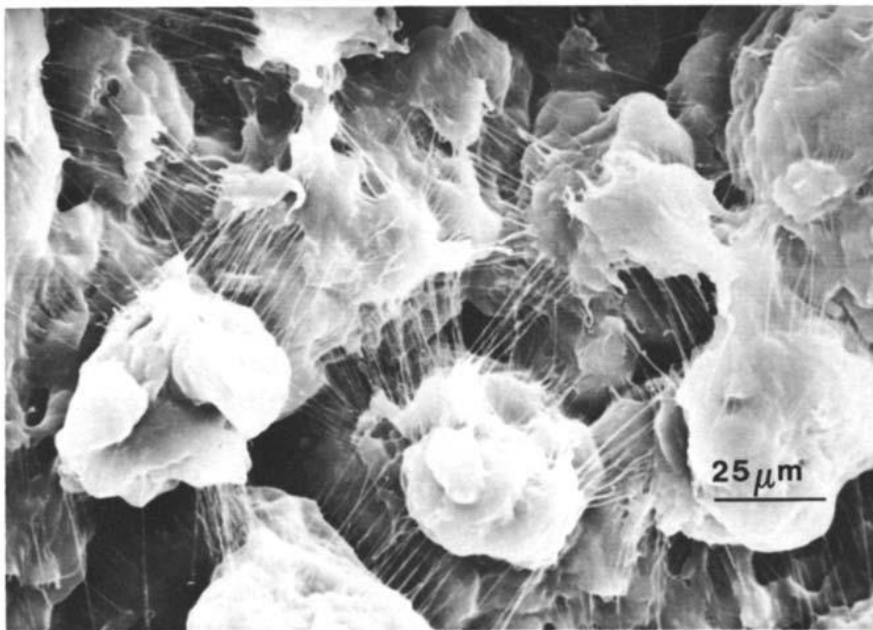


Figure 2.2 SEM image of auxetic HMPE fiber⁷.

Alderson et al.¹⁷ also developed the first polypropylene (PP) auxetic fibers by modifying the conventional melt spinning technique into a novel thermal processing technique. The modification in the existing melt spinning technique was made in terms of process conditions.

This process was able to produce polypropylene (PP) fibers with NPR ($\nu = -0.60 \pm 0.05$) and a diameter of less than 1 mm was achieved. The auxetic behavior of the PP fibers was confirmed by the in-phase length and width data as illustrated in Figure 2.3.

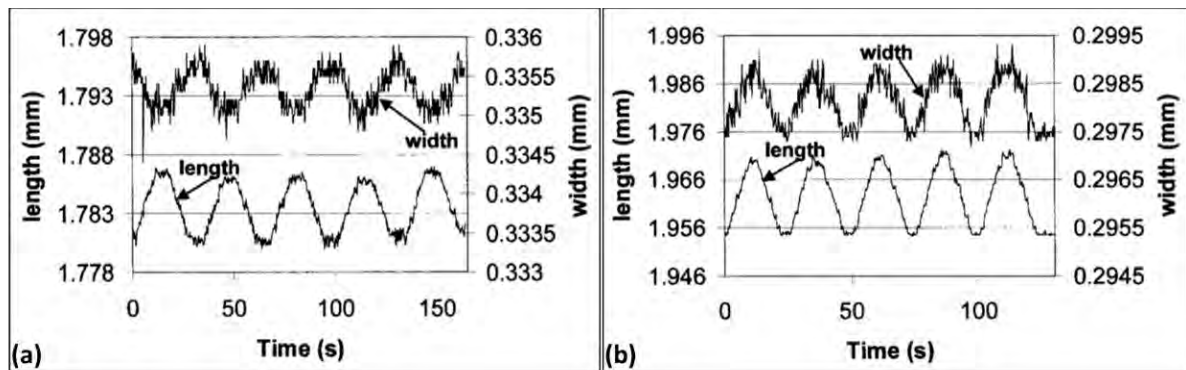


Figure 2.3 Length-width against the time of, (a) conventional polypropylene fibers, (b) auxetic polypropylene fibers¹⁷.

Ravirala et al.¹⁶ manufactured new auxetic polyester fibers using the novel thermal melt-spinning technique, initially developed by Alderson et al.¹⁷ for the production of continuous polypropylene (PP) fibers. First, the thermal properties of granule polyester resin were identified using differential scanning calorimetry (DSC) to find a suitable thermal processing window. Then, before extrusion, the polyester granules were converted into a fine powder of size less than 150 μm , as done previously for the production of auxetic PP fibers. Finally, the auxetic behavior in polyester fiber was achieved by optimizing the following critical process parameters; temperature (225°C), screw speed (0.525 rad/second) and take-up rate (0.075 m/second). The auxetic behavior of the fibers was confirmed by the length and width data noted from the micro-tensile testing and the video extensometer, respectively, as shown in Figure 2.4.

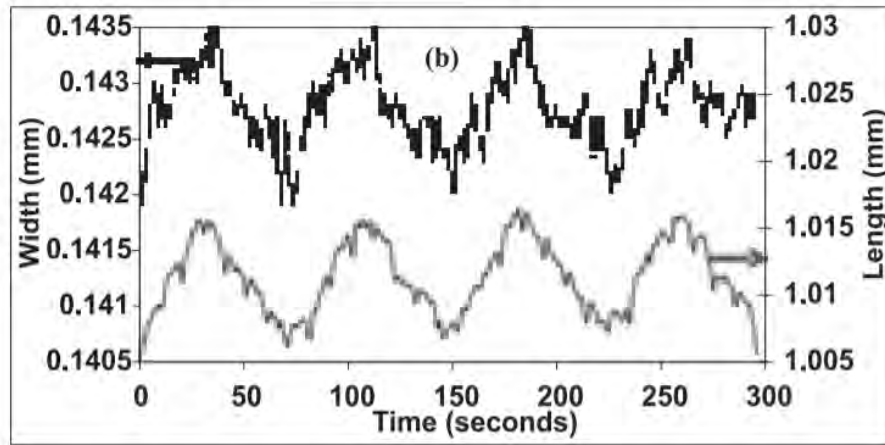


Figure 2.4 the Length-width data against the time of polyester fibers¹⁶.

2.3 Auxetic yarns

Auxetic yarns are composite yarns that are formed using the technique of wrapping two different yarns (i.e., wrapping yarn and core yarn) helically. Although, the technique of wrapping two yarns is simple, however, there are mandatory conditions that must be satisfied to achieve the auxetic effect. The wrapping yarn must be comparatively low thickness but high modulus, while the core yarn must be of high thickness and low modulus. When this assembled helical yarn is stretched length-wise, the high-modulus stiff yarn that is wrapped around tends to become straight and forces the low-modulus coarser yarn to wrap around it. In this way, a net increase in the yarn diameter can be achieved upon stretching in the length direction, which refers to NPR or auxetic effect.

Miller et al.¹⁸ practically invented auxetic yarn by adopting the wrap spinning technology. The auxetic yarns manufactured with this mechanism were called double helix yarn (DHY), because of the double helix geometry. The yarn consisted of two components, where one component (thin and stiffer fiber) is helically wrapped around the other component (thick, elastomeric, and initial straight) as shown in Figure 2.5 (a). High-modulus polyethylene (HMPE) fiber of 0.32 mm (220 dtex) was used as a wrapping yarn whereas polyurethane

elastomer of 0.64 mm diameter yarn as a core yarn with an approximate wrap angle of 70°. Under longitudinal stretching, the high modulus wrap yarn elongates relatively much less than the elastomeric core yarn, and at higher strain, the situation of the wrap and core yarn reverses, i.e., the initial HMPE wrap yarn becomes straight and pushes the elastomeric PU yarn to wrap around, as illustrated in Figure 2.5 (b). The reverse arrangement of the wrap and core yarns under high strain causes an overall increase in the diameter of the DHY yarn. As a result, Poisson's ratio of -2.1 was observed for the developed DHY.

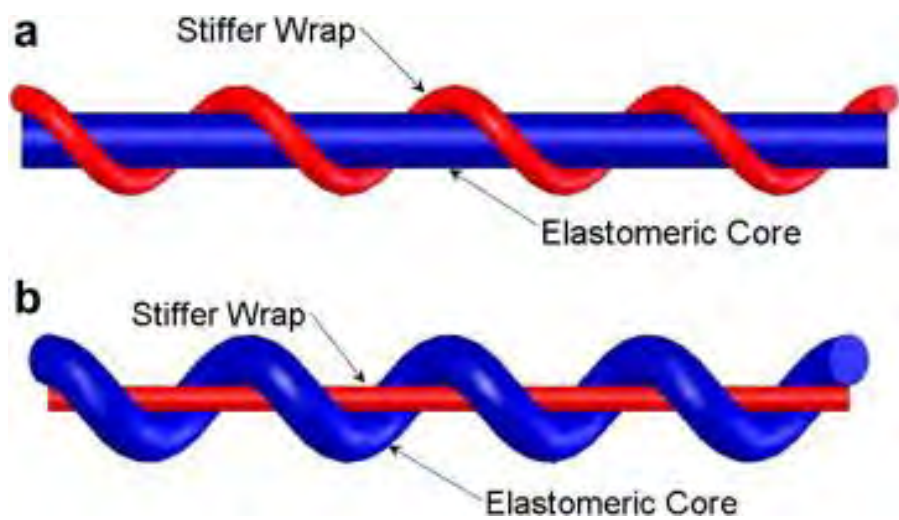


Figure 2.5 Schematic of double helix yarn, (a) relaxed form, (b) under tension¹⁸.

Ge et al.⁶³ introduced a novel approach to develop auxetic yarn, aimed to improve and overcome the drawbacks present in DHY yarns. This approach involves the mechanism of plying four different yarns together. Among the four yarns, two were soft yarns and two were stiff yarns with different diameters. The yarns were placed with an alternate arrangement and twisted together, as shown in Figure 2.6 (a). Initially, the two stiff yarns with smaller diameters are located outside, while the two soft yarns with higher diameters are in contact with each other keeping the soft yarns separate. When plied yarn is stretched along the length, the stiff yarns having low elongation start migrating toward the center. The movement of the stiff yarns

pushes the soft yarns which increases the overall cross-section of the plied yarn, as shown in Figure 2.6 (b).

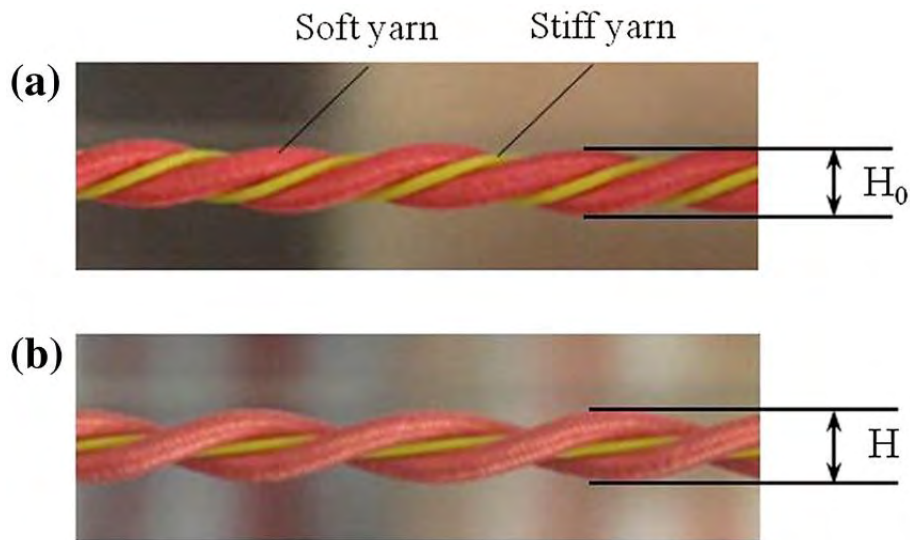


Figure 2.6 Auxetic plied yarn, (a) relax state, (b) stretch state⁶³.

Not long ago, a unique approach was adopted for developing auxetic yarn in order to address the yarn slippage problem that occurs in HAYs. This technique uses a conventional circular braiding technology to develop auxetic yarn⁶⁴. Unlike the conventional HAY, in which a stiff yarn is directly wound on soft core yarn, this technique used three components to develop auxetic yarn. A stiff and a low modulus yarns were used as wrap and a high diameter low modulus yarn was used as a core. The two wrap yarns were interlaced with each other to avoid slippage or misplacement, however, the pattern of stiff yarn was kept helical as shown in Figure 2.7. Based on this design, eight braided auxetic yarns were prepared with different influencing parameters such as the number of stiff yarns used, the arrangement of stiff yarns, and different diameters of yarn. For comparison, a single HAY yarn was also developed with the same stiff and low-modulus core yarn used for developing braided auxetic yarns. The auxetic yarns developed for analysis are shown in Figure 2.8.

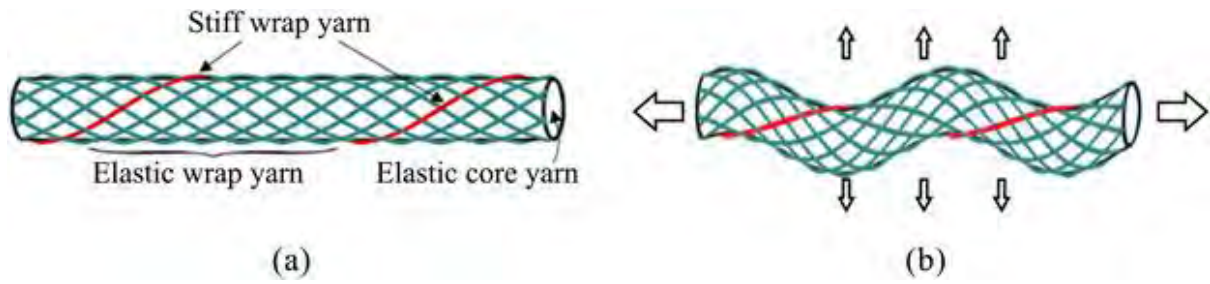


Figure 2.7 Braided auxetic yarn at (a) free state and (b) under tensile deformation⁶⁴.



Figure 2.8 The developed braided auxetic yarns and helical auxetic yarn⁶⁴.

The results show that a significantly higher auxetic effect is achieved with braided yarns as compared to HAY. In addition, the auxetic behavior of braided yarns was more stable than HAY under the cyclic tensile deformation, which confirmed the stability of braided auxetic yarn over HAY. Poisson's ratio curves of BAY 1 and HAY are shown in Figure 2.9. Among the braided auxetic yarn, sample "BAY 1" exhibited the highest NPR of -1.1.

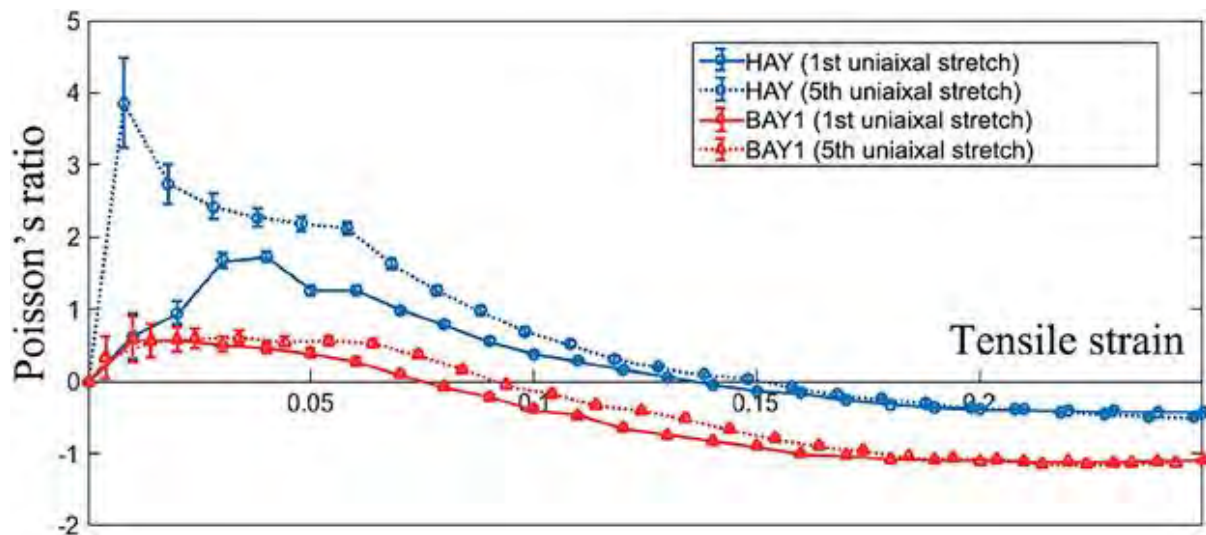


Figure 2.9 Poisson's ratio versus tensile strain curves of braided auxetic yarn and helical auxetic yarn at the first and fifth cycle⁶⁴.

These days, researchers are focusing on the optimization of auxetic behavior of auxetic yarn by studying the effect of various parameters including materials, wrapping angle, diameter of yarns etc^{65,66}. Furthermore, theoretical and numerical studies are also under attention for designing and predicting the NPR as well as the mechanical properties for specific applications^{20,67-70}.

2.4 Auxetic knitted fabrics

Auxetic behavior realization in knitted fabrics was first presented by Starbuck et al.⁷¹ in 2008. The invention claimed auxetic knitted fabric by using a conventional warp knitting mechanism. The auxetic property was implanted by the geometric shapes that can be rotated, deformed, or translated at one or more portions of the auxetic knitted structure. The only reported geometric shape developed in the knitted fabric was a triangular lattice, as illustrated in Figure 2.10.

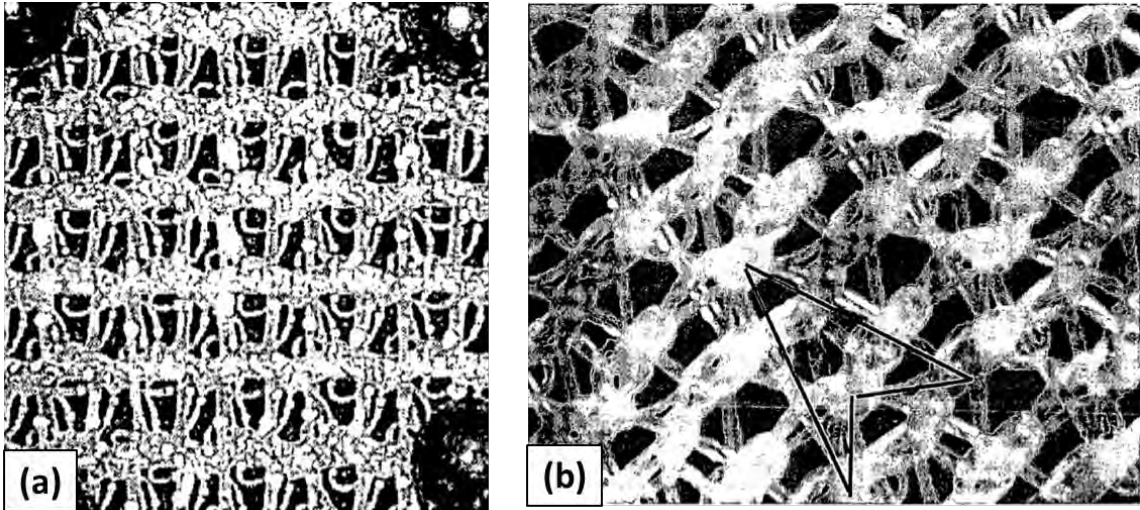


Figure 2.10 Images of developed knitted fabrics in a normal state, (a) microscopic image, (b) more magnified image showing the single repeat unit of triangular lattice geometry⁷¹.

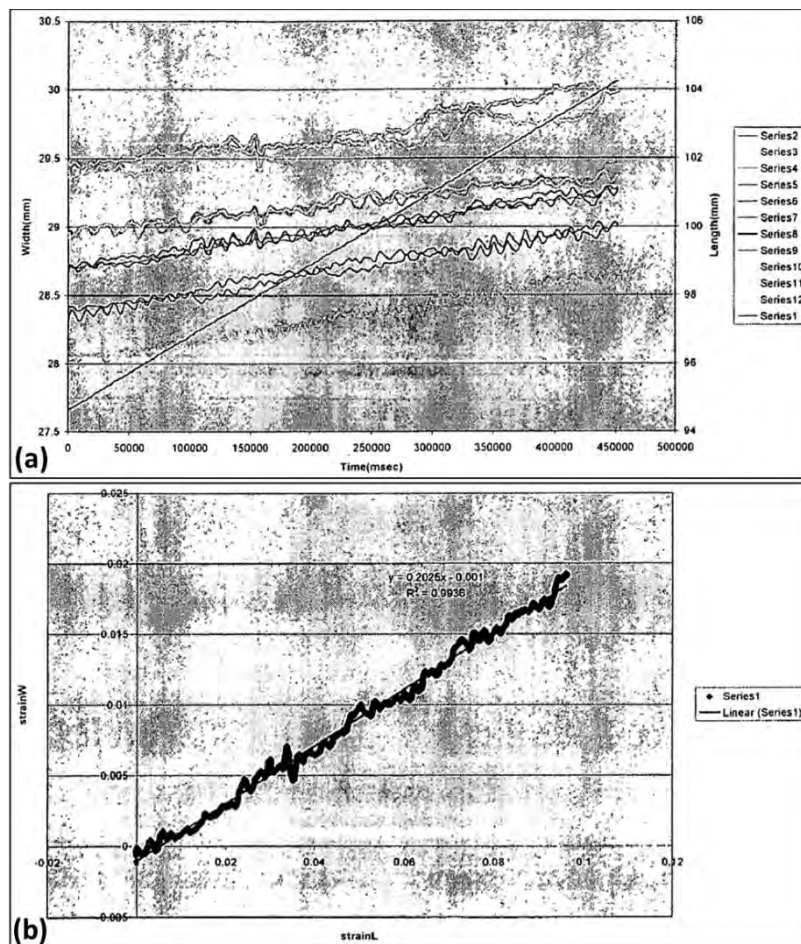


Figure 2.11 (a) Length-width data versus time, (b) transverse strain versus tensile strain⁷¹.

The fabrics were examined with combined tensile testing and video extensometry. The novel finding of auxetic behavior in the knitted fabric was supported by the data plotted, length-width against time and strain in width direction against the strain in length direction, as shown in Figure 2.11 (a) and (b), respectively. Among the 12 developed auxetic knitted samples, fabric 10 showed the maximum NPR ($\nu = -0.22 \pm 0.03$).

Ugbolue et al.⁷² also developed a knitted structure that exhibits NPR. They used two sets of conventional component yarns to impart a re-entrant hexagonal knit structure using the warp knitting technique. To achieve auxetic property through the hexagonal geometry, a chain and filling yarn inlays method was used. An elastic yarn was used in the basic knit structure as a filling. The filling yarn was placed between the stitch wale to confirm structure's recovery upon relaxation. Similarly, the filling yarn was also laid in the nearby wales for wrapping the intersection of ground loops and to improve the overall stability of the structure. The auxetic knitted structure is illustrated in Figure 2.12.

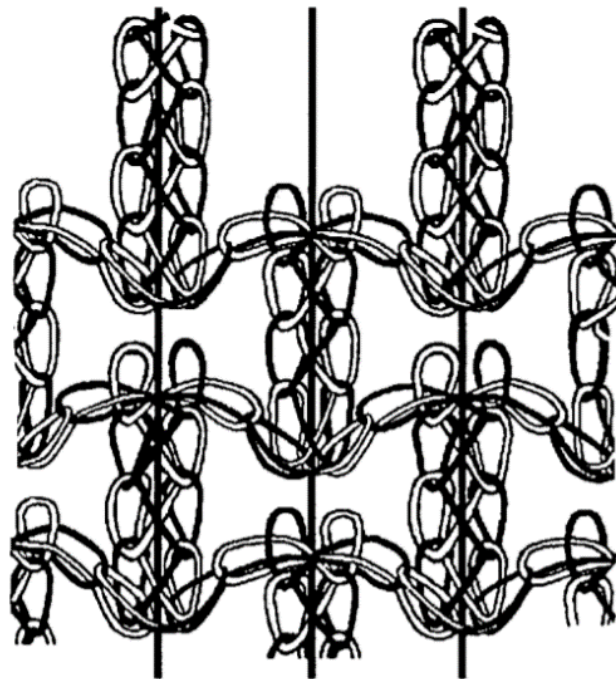


Figure 2.12 Auxetic knitted structure with elastic inlay yarn⁷².

The drawback associated with the above-knitted fabrics^{71,72} was low recovery from the deform state because they used warp knitting technology with open mesh structures. To address this problem, Hu et al. reported multiple different knitted fabrics with auxetic behavior developed by using weft knitting techniques with three different geometrical structures⁴². The three geometries selected and employed were rotating-rectangle, foldable geometry, and re-entrant hexagon. The knitted fabrics with all three geometries were successfully designed and fabricated using programmed flat-knitting machines. For implanting foldable geometries, the mechanism of the face and reverse loop arrangement was used. Two knitted structures with different foldable geometries were fabricated by changing the order of face and reverse loops. For the first structure, the two loops were arranged in rectangular form, while the second structure was formed with horizontal and vertical stripes arrangement, as illustrated in Figure 2.13 (a) and (b), respectively. It is believed that the rotation of many geometric shapes like triangles, rectangles, squares, and parallelograms, shows auxetic effect when they are combined at a certain arrangement⁷³⁻⁷⁶. Auxetic weft-knitted fabric with rotating rectangles was produced based on a similar concept of geometric arrangement⁴². The rectangular knitted structure attached at vertices was fabricated using a special knitting technique of partial-knitting of the programmed flat-knitting machine. This technique can produce the individual rectangle sections continuously in the course direction while connecting each rectangle unit at its vertices. The auxetic fabric made using this process is shown in Figure 2.13 (c). In this common study⁴², auxetic knitted structures designed with re-entrant hexagonal geometry was also explored. The two auxetic knitted fabrics fabricated based on this geometry was real re-entrant hexagonal structure and pseudo-re-entrant hexagonal structure as illustrated in Figure 2.13 (d-e). The real re-entrant structure was produced using racking and intarsia techniques, while the pseudo-re-entrant structure was produced by sectional relief ridges jointly with elastic

yarn. It was found that the fabric developed with real re-entrant hexagonal structure showed the largest PR of -0.6. Further, NPR effect of the knitted sample produced with foldable geometry initially increases and then decreases in response to the axial strain, while all other fabrics showed a decreasing trend of NPR with an increase of the axial strain.

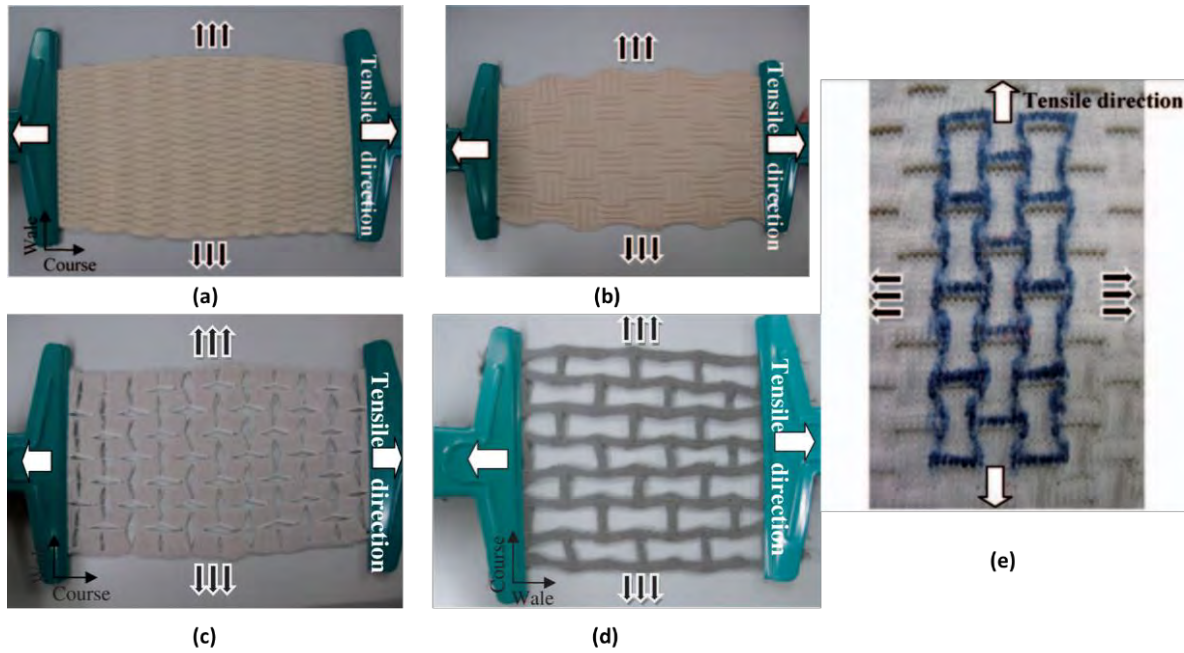


Figure 2.13 Auxetic weft-knitted fabrics: (a) foldable geometry with a rectangular form of the face and reverse loops, (b) foldable geometry with horizontal and vertical stripes form of the face and reverse loops form, (c) rotating rectangles structure, (d) real-re-entrant hexagonal structure, (e) pseudo-re-entrant hexagonal structure⁴².

Zhao et al.³⁹ developed auxetic warp knitted fabrics based on re-entrant hexagonal geometry. They used a novel method of knitting process and special structure design to produce auxetic warp knitted fabric. A tricot warp knitting machine was used to fabricate the samples. An approach of using elastic and non-elastic yarns was adopted to implant an auxetic geometry. A conventional non-auxetic rectangular net structure as shown in Figure 2.14 (a), was converted into a re-entrant by special arrangements of yarns and the lapping movement. A conversion to

re-entrant geometry was done by introducing additional underlaps formed by elastic yarns as demonstrated schematically in Figure 2.14 (b). Evenly distributed elastic and stiff underlaps were formed in an alternate fashion by using stiff yarns and elastomeric yarns respectively. A supplementary yarn guide bar was also used to facilitate the switching of elastic yarns in the loops while keeping them in tension. At free state, elastomeric yarns will shrink along elastic underlaps while the stiff underlaps will support adjacent vertical ribs of rectangular structure. Thus, the rectangular nets were transformed into re-entrant hexagonal nets as illustrated in Figure 2.14 (c).

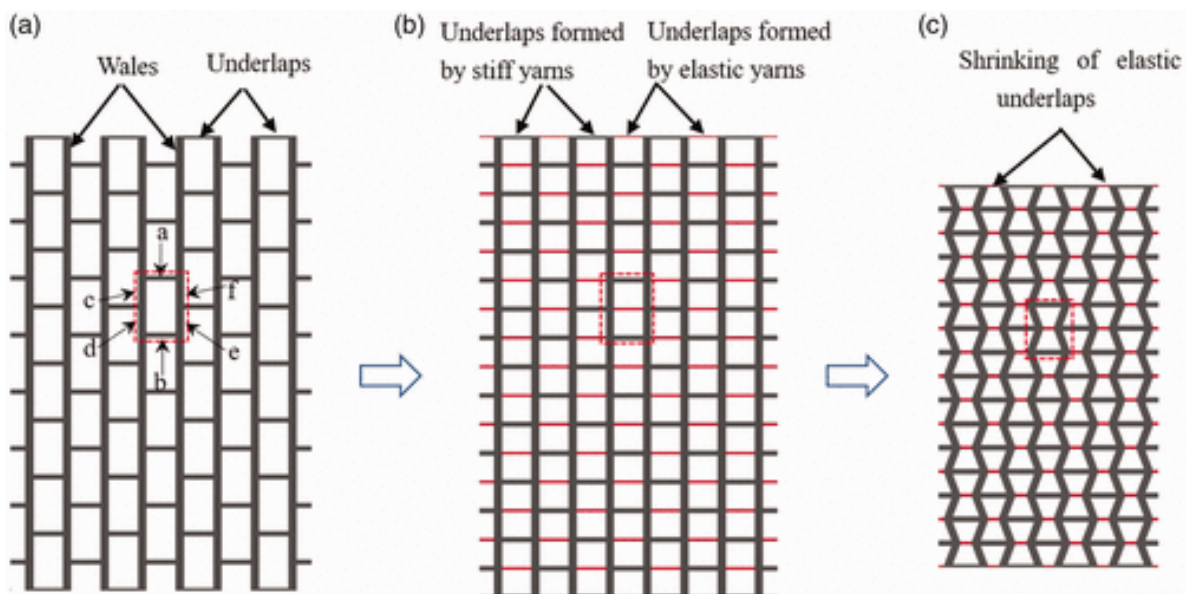


Figure 2.14 Schematic of geometric design of warp-knitted auxetic fabrics: (a) non-auxetic rectangular nets, (b) addition of extra horizontal ribs using elastomeric yarn, (c) formation of re-entrant hexagonal geometry after shrinkage³⁹.

Three auxetic warp-knitted structures with different vertical and horizontal rib sizes were produced to check their influence on the auxetic behavior of fabrics. Three yarn guide bars: GB1, GB2, and GB3 were used to knit the structure with three types of yarn feeding as shown in Figure 2.15. Multifilament polyester yarns were used as binding yarn, and they were

threaded on GB1. The mono-filament polyester and elastomeric yarns were threaded alternatively on GB2 and GB3, which were used to create the horizontal and the vertical ribs. After knitting, the samples were treated to a post-fabrication heat setting process at 160°C for 5 minutes to fix their shape. The shrinking of underlaps resulted from the elastic yarn because of their internal tension, while those made with rigid yarns remained in straight form due to their significant rigidity. Consequently, the fabrics exhibited a re-entrant hexagonal structure. The images of three developed samples with the induced re-entrant hexagon geometry are illustrated in Figure 2.16.

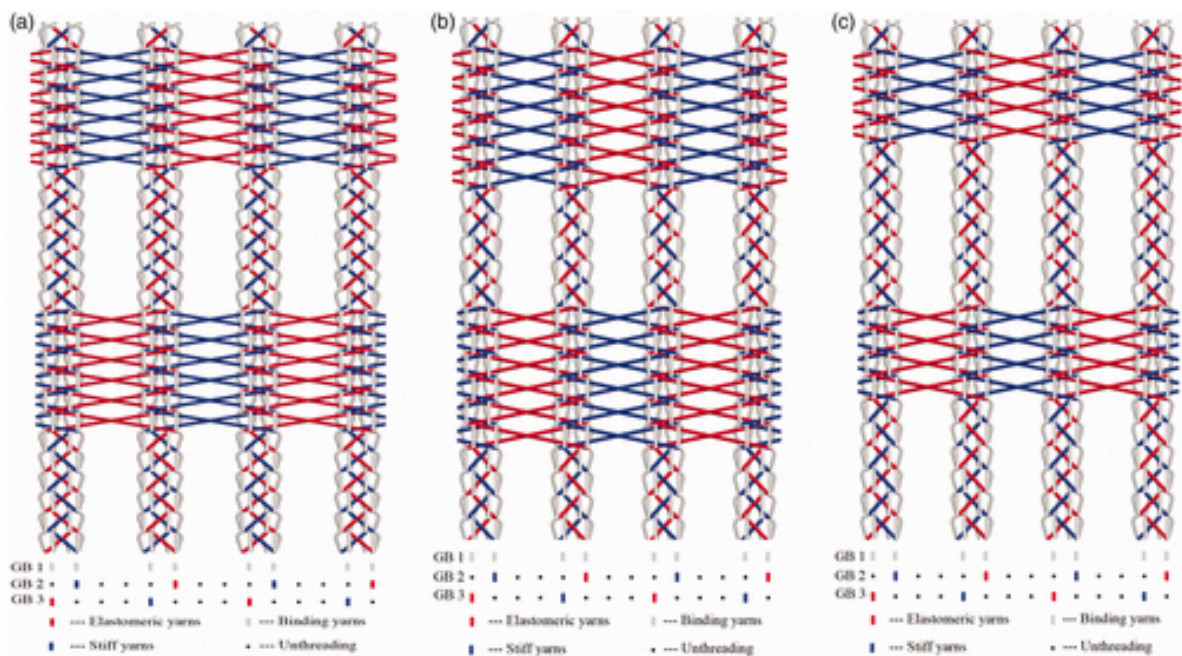


Figure 2.15 Schematic presentation of three fabrics formed with different rib sizes: (a) Fabric 1, (b) Fabric 2, (c) Fabric 3³⁹.

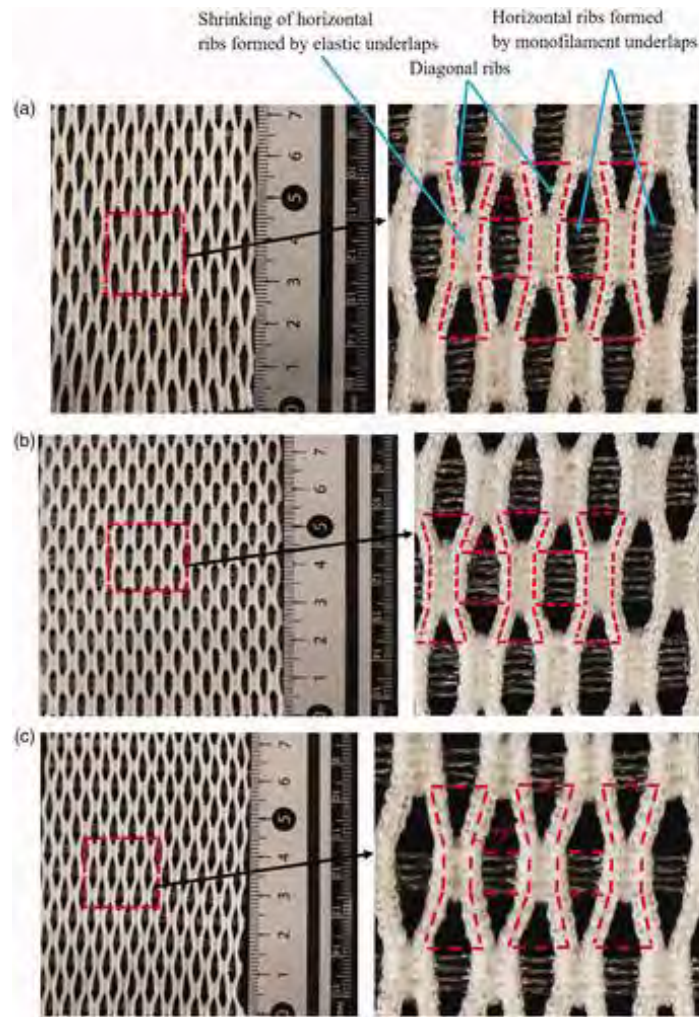


Figure 2.16 Images of the produced knitted auxetic samples: (a) Fabric 1, (b) Fabric 2, (c) Fabric 3³⁹.

After marking horizontal and vertical dots, the samples were tested using an Instron 5566 machine to analyze the auxetic behavior under stretching as demonstrated in Figure 2.17. A camera was installed to record the deformation of a sample during the tensile test, and then the lateral and longitudinal deformation was calculated by the image processing technique. The samples showed auxetic behavior in both principal directions while the NPR in the wale direction was significantly lower than in the course direction as illustrated in Figure 2.18. Furthermore, the size of diagonal and horizontal ribs also affects auxetic behavior of the knitted fabrics.



Figure 2.17 Fabric sample mounted on tensile testing machine³⁹.

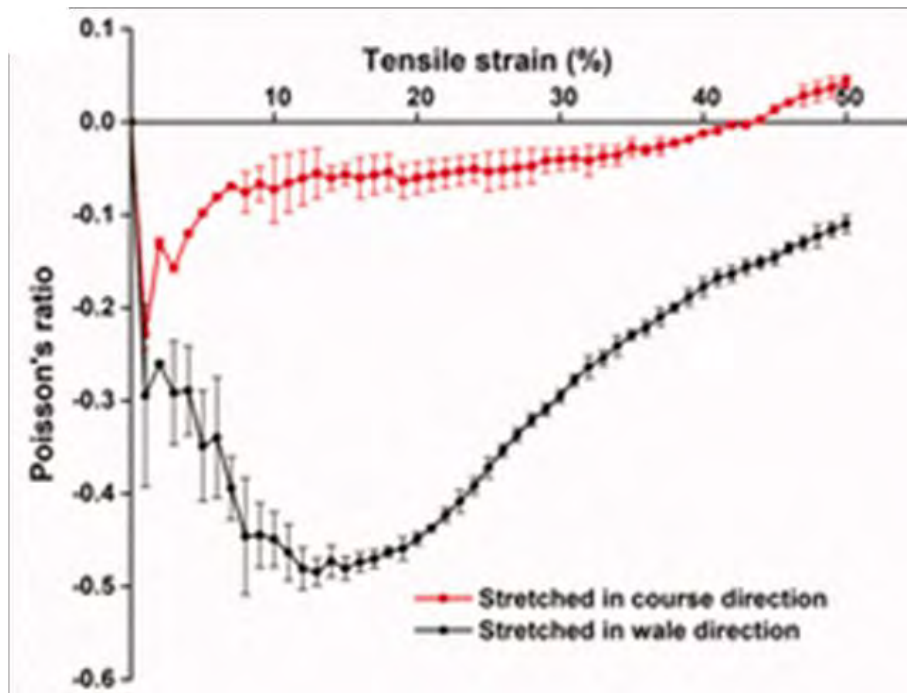


Figure 2.18 Poisson's ratio versus tensile strain curve of Fabric 3³⁹.

A new method of developing auxetic fabrics has been developed and reported that uses lamination of frame fabric (in the form of rotating square geometry) and a base fabric through a hot-melt adhesive membrane⁷⁷. To achieve the best auxetic results, the frame fabric should

be stiff and stable to facilitate the proper rotation of the square geometry. Therefore the material of the frame fabric was 100% polyester with a twill weave fabric design. Differently, the base fabric needs to be soft to facilitate easy deformation and rotation of the frame fabric. So, warp-knitted tricot fabric made of 25% spandex and 75% polyamide, was used as a base fabric. The process of developing the samples is shown in Figure 2.19.

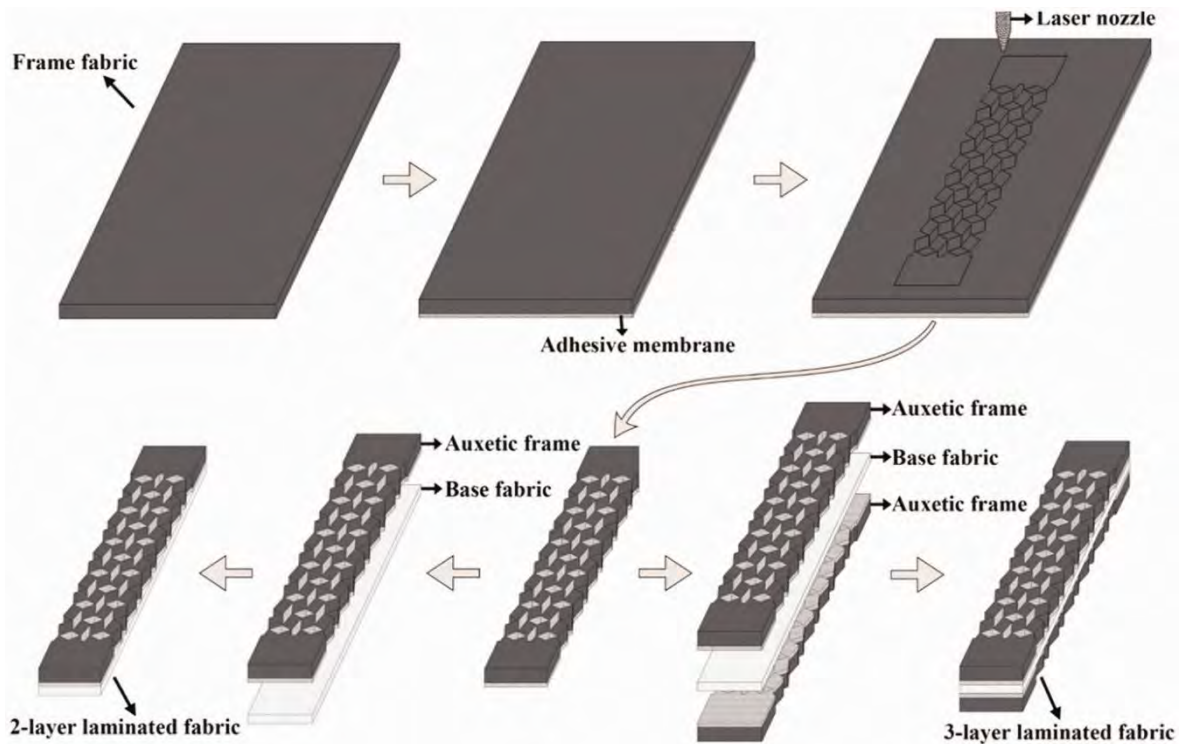


Figure 2.19 Lamination process of frame and base fabrics⁷⁷.

For in depth study, eight (08) samples were produced on the bases of two-layer and three-layer laminations, and the orientation of frame and base fabrics with respect to each other. The samples were then subjected to tensile strain in both warp and weft directions. The fabrics showed the NPR effect when tested in the warp direction, while a positive Poisson's ratio was seen when the test was performed in the weft direction, as shown in Figure 2.20. It was also found that other parameters also affect the auxetic behavior of the laminated fabric. For example, the samples are auxetic when the orientation of the frame fabric is warp and the base

fabric is wale, while the fabric exhibits non-auxetic behavior when the orientation of the frame fabric is warp and the base fabric is course. Similarly, three-layer laminated fabric shows a steady decrease in auxetic effect with an increase in axial strain, while the NPR effect of a two-layer laminated sample reduces rapidly by increasing tensile strain.

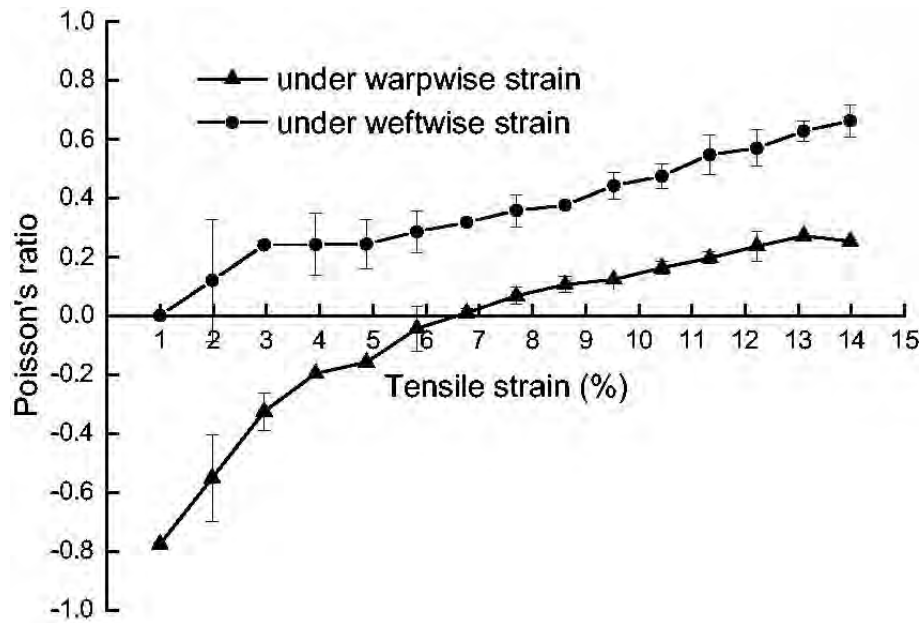


Figure 2.20 Poisson's ratio behavior of laminated fabric under warp and weft tensile strain⁷⁷.

Other studies on auxetic knitted fabrics are also reported to examine different properties and to evaluate their performance for suitable applications^{35,78–80}. In addition, numerical studies are conducted for designing and predicting the Poisson's ratio behavior of knitted fabrics^{38,81}.

2.5 Auxetic woven fabrics

Practically, there are two ways to produce auxetic woven fabrics. Initially, the auxetic effect in woven fabrics was implanted by using auxetic yarns in warp, weft, or in both principal directions. Recently, a new method was introduced to weave an auxetic fabric by realizing auxetic geometry like foldable structure, re-entrant hexagon, rotating squares, etc., and non-auxetic yarns.

2.5.1 Auxetic woven fabrics developed with auxetic yarns

An auxetic woven fabric was first developed by Miller et al.¹⁸ using a double helix yarn (DHY). They produced an auxetic fabric with a plain weave design by using a meta-aramid fiber of count 475 dtex as a warp yarn and DHY as a weft. The utilization of DHY in the weft direction was driven by the objective of achieving an out-of-register arrangement among adjacent DHYs, thereby optimizing the auxetic effect. Under tensile tension, the DHYs overlap each other in the thickness direction, leading to an out-of-plane auxetic effect that increases the thickness of the sample. Simultaneously, the width of the fabric is reduced, as illustrated in Figure 2.21. Therefore, this fabric showed an out-of-plane NPR of -0.1, but an in-plane positive Poisson's ratio of 0.06.

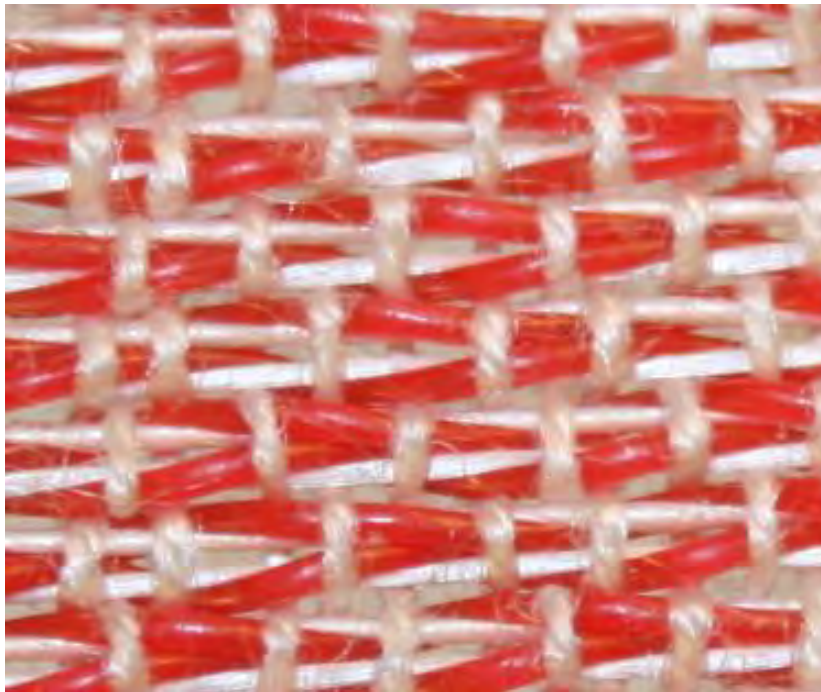


Figure 2.21 Auxetic woven fabric made of double helix yarn (under tension)¹⁸.

Wright et al.⁵⁴ also reported narrow auxetic fabrics using helical auxetic yarn (HAY) as a warp yarn and polyester as a weft. Three different HAYs, named “Yarn-A”, “Yarn-B” and “Yarn-

C”, were produced, of which two were used to develop auxetic fabrics. The specifications of three HAYs employed in two fabric samples are provided in Table 2.1.

Table 2.1 Summary of the two developed auxetic fabric⁵⁴.

Yarn	Fabric
A – 2 mm dia. covered rubber core, 6/110/34 textured nylon wrap, nominal angle 45°	<i>no fabric</i>
B – 1 mm dia. covered rubber core, 16/1 ringspun PET wrap, nominal angle 45°	B – yarn B warp, PET weft
C – 0.18 mm dia. covered rubber core, 2/110/34 textured nylon wrap, nominal angle 45°	C – yarn C warp, PET weft

“Fabric-B” of width 20 mm was developed as shown in Figure 2.22 (a), using “Yarn-B” as a warp yarn with 26 warp ends. A multifilament polyester yarn (PET) of 1100dtex was used as weft yarn with a density of 14picks/inch. Similarly, “Fabric-C” of width 25 mm was developed as shown in Figure 2.22 (b), using “Yarn-C” as a warp yarn with 48 warp ends. The weft yarn used was a 550dtex PET, with a density of 12 picks/inch. A tensile test was performed using Lloyd Instruments’ testing machine. A high-resolution COMS camera was used to capture images at different tensile strains. The images were then analyzed, and the Poisson’s ratio was measured using Image J public domain image processing software. It was found that Fabric B exhibit an in-plane auxetic effect with a maximum PR of -0.1 at about 32% strain. While the

in-plane PR for Fabric C was found positive for all strains. The Fabric C was also analyzed for out-of-plane Poisson's ratio which was found negative. It was found that the auxetic effect changes from in-plane to out-of-plane were associated with the material of the weft yarn and the weave pattern of the fabric, which allows auxetic warp yarns to overlap.

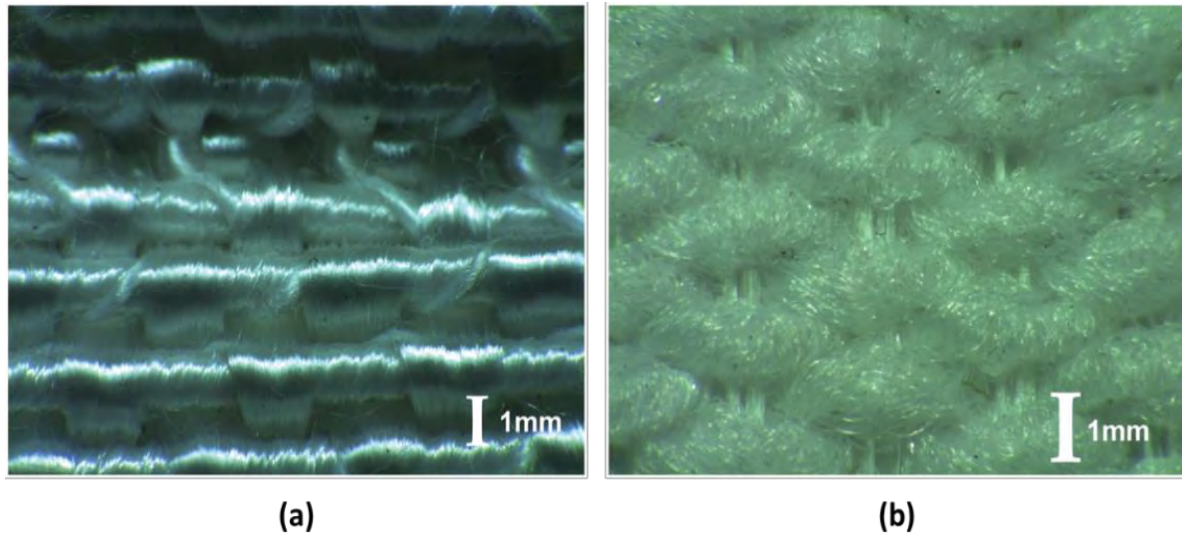


Figure 2.22 Auxetic fabric developed with helical auxetic yarn: (a) Fabric B, (b) Fabric C⁵⁴.

Recently, there has been a development of auxetic woven fabrics using auxetic plied yarns, including 4-ply and 6-ply variations, as well as double-helical yarn (DHY)⁵⁵. For fabric production, auxetic yarns were weaved in the length (warp) direction only, while a conventional elastic yarn was weaved in the width (weft) direction as illustrated in Figure 2.23. This arrangement was used to keep auxetic plied yarn crimp-free inside the fabric construction. Further, an elastic yarn will facilitate the expansion of auxetic plied yarn under tensile stretching.

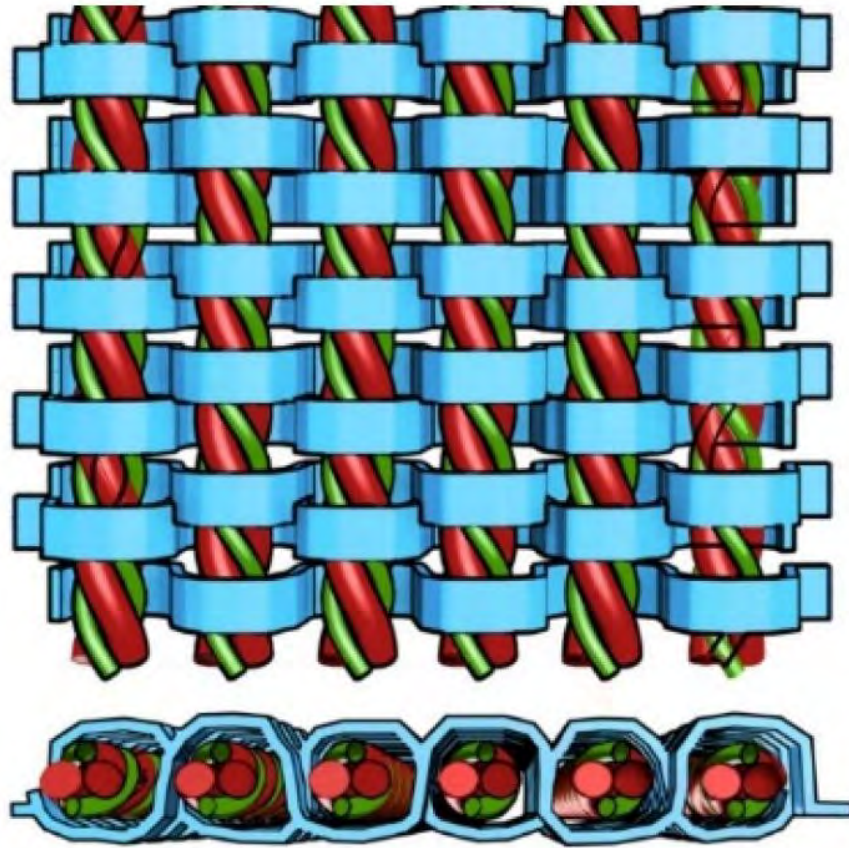


Figure 2.23 Auxetic woven fabric developed with 4-ply auxetic yarn⁵⁵.

12 woven fabrics were produced with six different parameters that include auxetic plied yarn arrangement, direction of twist, type of weft yarn, single component yarn properties, and weave design, to check its effect on the auxetic behavior of the fabric. The four weave designs selected for this study were plain, 2 by 1 twill, 3 by 1 twill, and 5-end satin. The details of all parameters for the woven fabrics are given in Table 2.2. The auxetic behavior of fabrics was evaluated by performing the tensile test and with a post-video/image analysis recorded during the test. The fabric samples were analyzed in terms of PR and percentage open area of fabric structure.

Table 2.2 Parameters of the produced woven fabrics⁵⁵.

Parameter Consideration /Group No.	Fabric Code	Material		Fabric density		Fabric structure
		Warp	Weft	Ends/Inch	Picks/Inch	
G-1 Direction of twist	F1	A-1 (S/Z)	4 mm flat braided polyester elastic band	6.35	6.46	Plain
	F2	A-1 (S/S)				
G-2 Weft type	F1	A-1 (S/Z)	4 mm flat braided polyester elastic band	6.35	6.46	Plain
	F3	A-1 (S/Z)	100 D polyester-covered spandex yarn		6.10	
G-3 4-ply auxetic yarn properties: diameter of the soft yarn	F3	A-1 (S/Z)	100 D polyester-covered spandex yarn	6.35	6.10	Plain
	F4	B-1 (S/Z)		8.63		
	F5	C-1 (S/Z)		9.03		
G-4 4-ply auxetic yarn properties: tensile modulus of stiff yarn	F3	A-1 (S/Z)	100 D polyester-covered spandex yarn	6.35	6.10	Plain
	F6	A-3 (S/Z)				
	F7	A-4 (S/Z)				
G-5 Weave	F1	A-1 (S/Z)	4 mm flat braided polyester elastic band	6.35	6.46	Plain
	F8					2x1 Twill
	F9					3x1 Twill
	F10					5-end Satin
G-6 Helical structure of yarn	F11	A-1-D (S/Z)	100 D polyester-covered spandex yarn	9.14	6.10	Plain
	F3	A-1 (S/Z)		6.35		
	F12	A-1-T (S/Z)		5.59		

2.5.2 Auxetic woven fabrics developed with non-auxetic yarns

A. Zulfiqar et al.³⁰ first time developed single and multi-layered woven auxetic fabrics using common weaving technology and non-auxetic yarns. Auxetic effect was integrated into fabrics through foldable geometry, re-entrant hexagon structure, and rotating rectangle structures. The

core mechanism responsible for the auxetic effect was the different shrinkage properties of different weave designs. The tightness and looseness of weave designs are responsible for governing different shrinkages. Differential shrinkages are also induced by using stiff and elastic yarns simultaneously. The auxetic behavior has been described concerning the longitudinal strain, tensile deformation, and transverse strain. The unfolding of the developed folded structures governs negative or zero Poisson's ratio during tensile loading. While it is possible to achieve a rotating rectangular geometry in uni-stretch woven fabrics, the true rotating rectangle effect cannot be fully attained due to the restriction imposed on the free rotation of rectangular units by the continuous warp and weft yarns. In contrast, a re-entrant hexagonal structure is relatively easy to fabricate, which utilizes the alternate placement of long float and tight weave. The auxetic deformation of different geometries is given in Figure 2.24. It can be observed that the auxetic honeycomb geometry shows the NPR and high strains, which can essentially provide a lower stiffness. Overall, the maximum NPR of the fabrics was recorded to be -0.15 for zig-zag folded stripes. Fabrics having convexities exhibit almost zero Poisson's ratio.

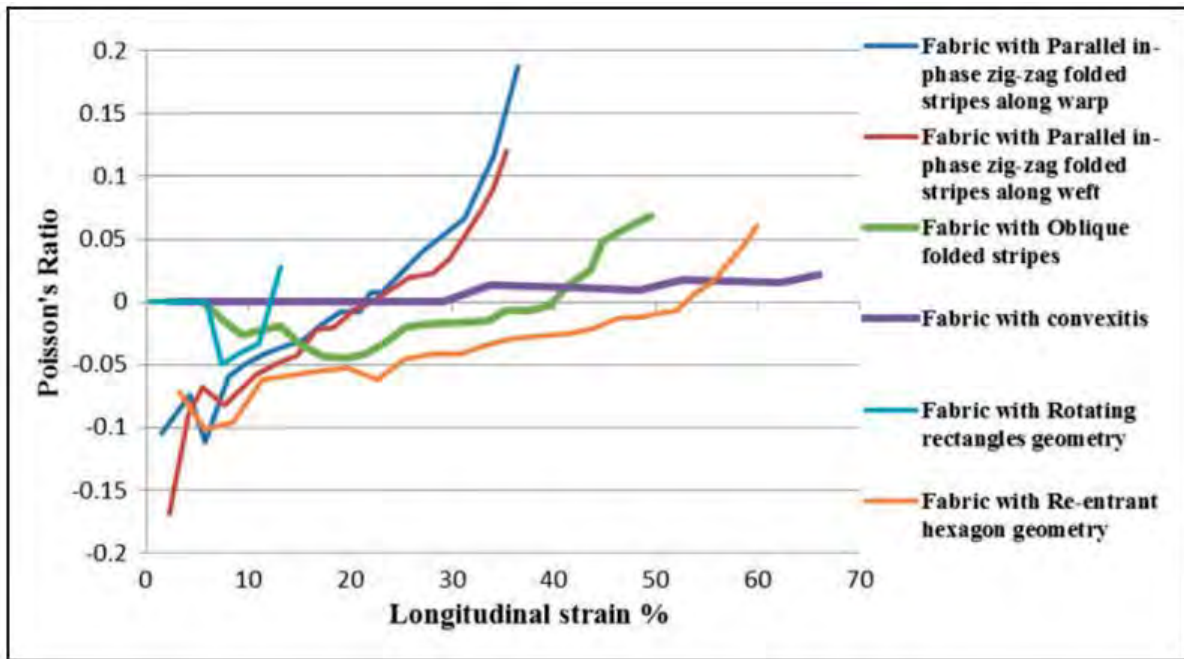
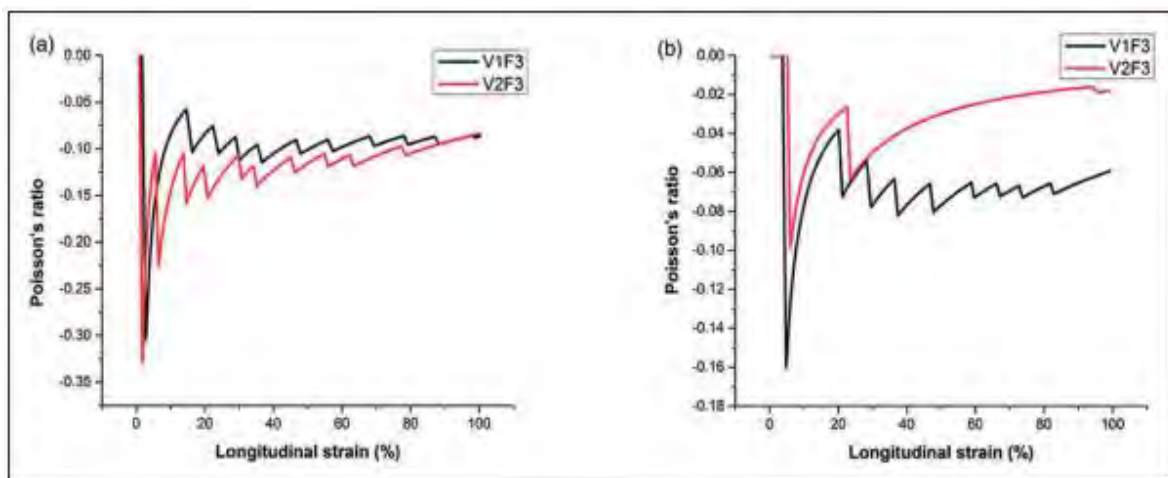


Figure 2.24 PR-longitudinal strain curves of the different auxetic geometries visualized in uni-stretch woven auxetic fabrics³⁰.

The previous work was extended through the development of bi-stretch auxetic woven fabrics, which were achieved using conventional weaving techniques with non-auxetic yarns. The differential shrinkage behavior of different weaves was used to achieve a parallel zig-zag (in-phase) geometry progressing in the warp in the fabric architecture²⁶. Such fabrics exhibit NPR even at high strain values in the warp and weft directions. Simultaneous use of the tight (short float length) and loose (long float length) woven structures with elastic and stiff yarns produce fabrics with special geometry that exhibit auxetic effects in both principal directions. The amount of yarn floats in loose weave is responsible for governing folded geometries in fabric, more number yarn floats result in more regular folded geometries. The shrinkage difference between elastic and stiff yarns is responsible for the difference in auxetic behaviors of the fabric in two directions. More shrinkage is experienced in the weft direction while a higher Poisson's ratio is obtained in the warp direction. Float length influences the PR value of auxetic fabrics,

but it does not imply that an increase in float length will increase NPR. Fabric having 3 float length exhibited the highest NPR values. While the arrangement of elastic weft yarn can increase the NPR effect if stretched along the warp direction. The optimized sample with the highest auxetic effect showed NPR of -0.33 in the warp direction and -0.16 as shown in Figure 2.25 (a-b).

Similarly, Poisson's ratio of bi-stretch fabrics developed with re-entrant auxetic geometry was also tested⁵⁶. The structure was modeled, and different geometrical parameters were studied for the auxetic effect. The development of auxetic geometry was supported by combining tight and loose weave designs with elastic and stiff yarns on rapier weaving loom. Two different fabrics were produced using different arrangements of weft yarns. The designed auxetic geometries were achieved after the removal of sizing material due to differential contraction within the auxetic unit cell of the structure. The deformation behavior in lateral and longitudinal directions confirmed that the fabrics exhibited NPR in the weft and warp directions over a wide range of tensile strains. This high strain is not only because of the elastane yarn used in warp but also because of the orientation of warp and weft yarns in the auxetic geometry, as illustrated in Figure 2.25 (c-d).



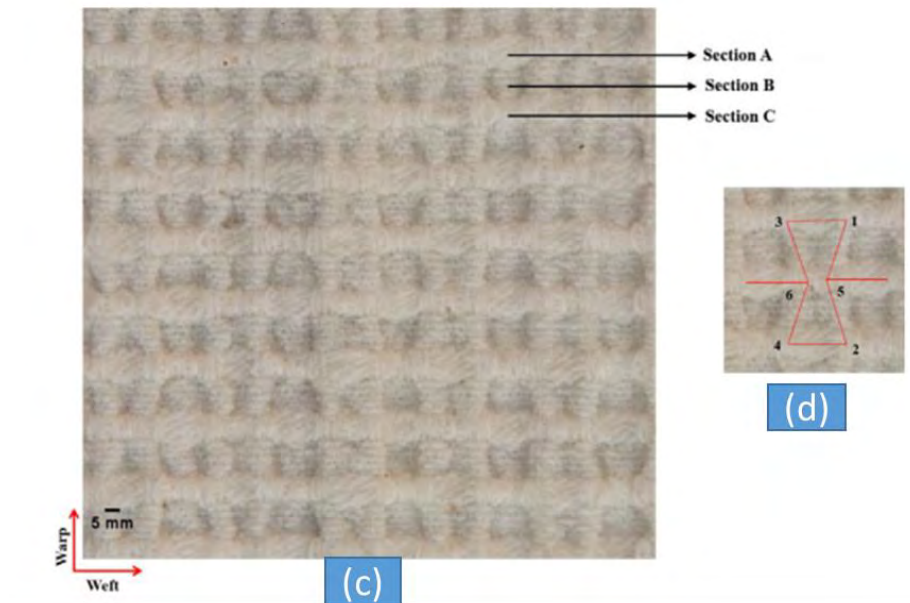


Figure 2.25 The auxetic behavior in the zig-zag geometry-based bi-stretch woven fabrics tested: (a) along the warp, (b) along the weft, (c) The bi-stretch auxetic fabric, (d) unit cell of re-entrant hexagonal geometry^{26,56}.

2.6 Auxetic non-woven fabrics

Besides woven fabrics, the auxetic property is also visualized in non-woven textiles. Verma et al.⁴⁶ induced an auxetic effect in the out-of-plane direction of non-woven fabrics by post-processing commercially produced needle-punched non-woven fabrics. The idea of studying auxetic behavior in non-woven fabrics came when the research team found an auxetic behavior in a commercial wooden-based paper⁸². During the study of the paper at a micro level, they came to the conclusion that the cellulose fiber network structure, as shown in Figure 2.26, of the paper triggers the out-of-plane NPR behavior. It was further suggested that strong bonding among the fibers at junctions and interwoven patterns of the fibers leads to the NPR.

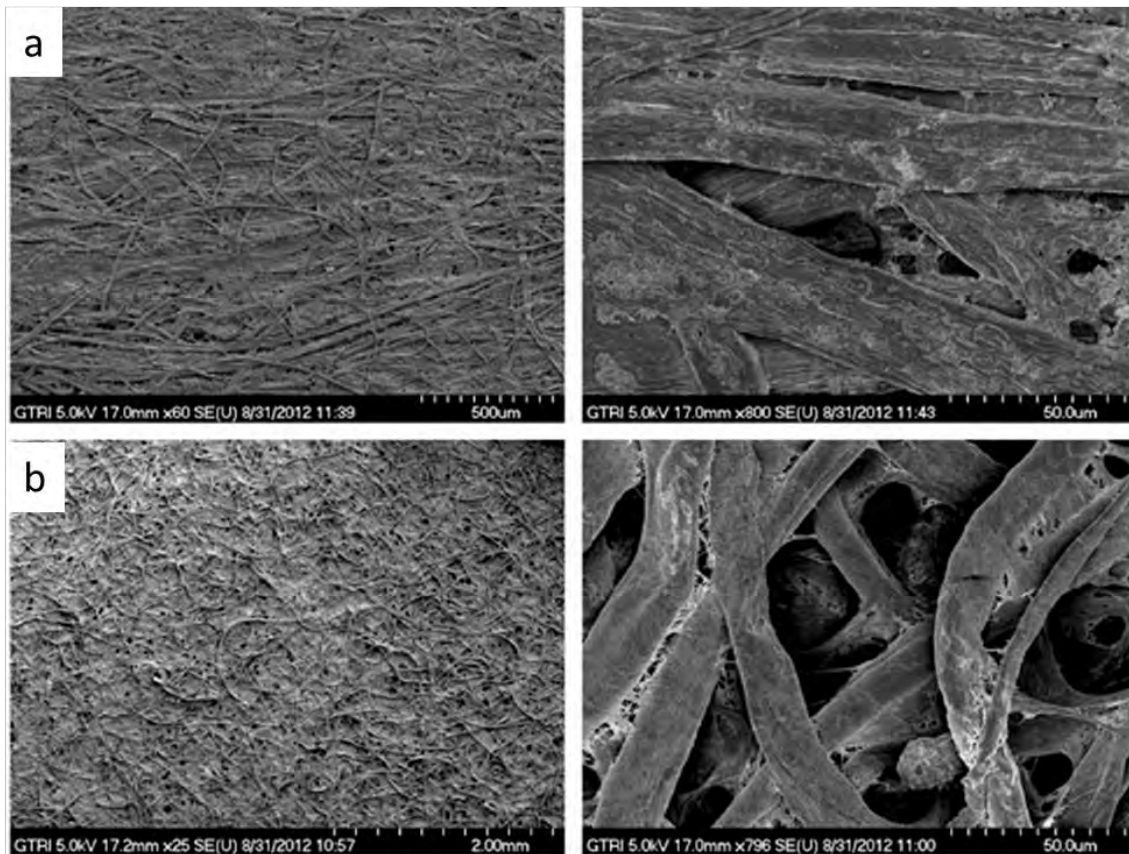


Figure 2.26 SEM micrographs the cellulose fiber network structure of paper at two given magnifications for each sample: (a) copy paper, (b) filter paper⁸².

Based on the principle of auxeticity found in wooden paper, the team studied needle-punched non-woven fabrics and developed a method of inducing an out-of-plane auxetic effect on a similar principle. In this research, two types of readymade non-woven fabrics named NW1 and NW2 were used. From the two types of fabrics, three distinct sets of samples were prepared for testing auxetic behavior. The first set of fabrics was without any modifications and referred to as “As-received”. The second and third sets were a modified form of the “as-received” non-woven fabrics with a heat-compression protocol and only compression protocol, respectively. In the heat-compression protocol, the two fabric samples, 20 cm square in dimensions, were subjected to a 2.45 MPa compression pressure in the thickness direction for 20 h at 70 °C temperature. The temperature was decided based on the glass transition temperature (T_g) of the

material forming non-woven fabric. After completion of 20 h, the sample was left to cool however the compression remained effective for the next 4 h. The heat-compressed samples were removed after completing a total of 24 hours. The third set of samples was also made ready by repeating the same procedure of compression for 24 h, but without using heating. The two types of treated samples were then prepared for two types of analysis i.e., thickness recovery and Poisson's ratio. The modification and experimental process of the non-woven fabrics is illustrated in Figure 2.27.

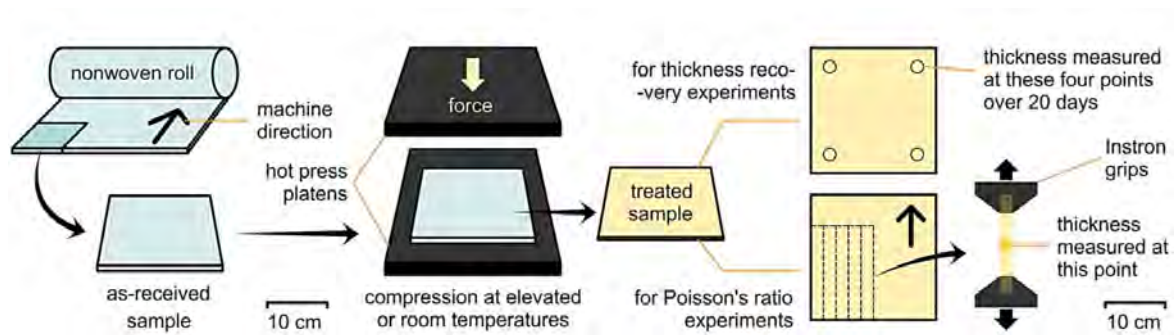


Figure 2.27 Schematic representation of heat-compression processing treatment of non-woven fabric samples⁴⁶.

The three types of samples were subjected to a uni-axial tensile load using a universal testing machine at a constant strain rate (10 mm/min). However, the testing program was modified to take a pause at regular intervals to manually note the change in thickness. Thus, the out-of-plane Poisson's ratio of the fabric was calculated from the longitudinal strain provided by the machine and the change in thickness (out-of-plane strain) of the sample. The calculated Poisson's ratio of the fabrics is plotted against the axial strain in Figure 2.28.

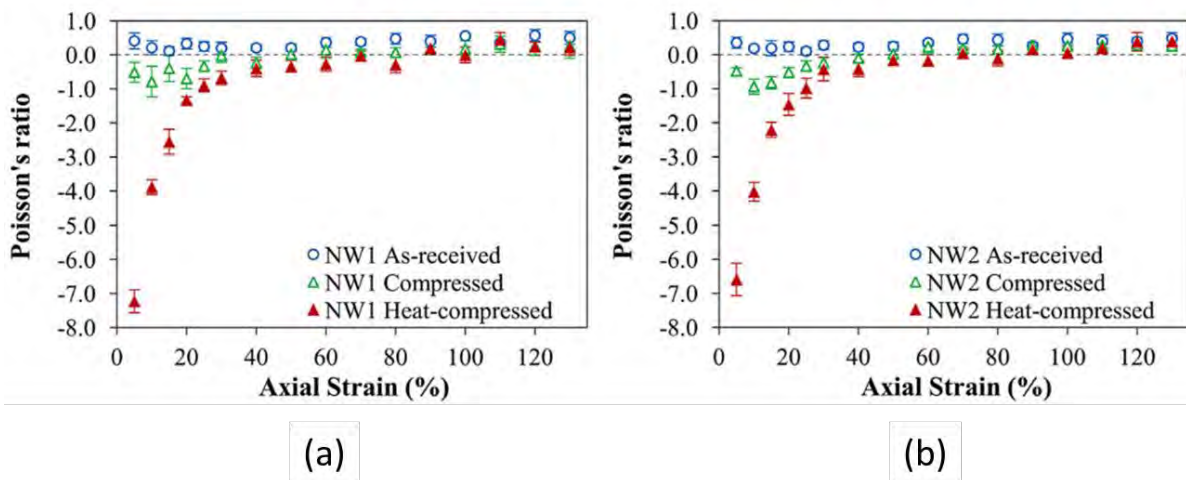


Figure 2.28 The Poisson's ratio against the axial strain of the sample as-received, compression, and heat-compressed: (a) fabric type NW1 and, (b) fabric type NW2⁴⁶.

In Figure 2.28, it can be seen that both the as-received non-woven fabrics exhibited a positive Poisson's ratio ranging from 0.1 to 0.5, throughout the tensile strain. The positive Poisson's ratio (PPR) means that as the axial strain increases, the thickness of the material decreases. While in the case of compressed samples, the samples have an increase in thickness for up to 40% axial strain exhibiting a lowest of -0.9 Poisson's ratio, followed by a decrease in thickness beyond 40% strain. Notably, the heat-compressed fabrics showed an abrupt increase in thickness at the initial strain of 5%, exhibiting -7.2 and -6.6 Poisson's ratio for samples NW1 and NW2, respectively. The samples retain their NPR until 80% axial strain.

The higher auxetic response of heat-compressed non-woven fabrics as compared to compressed non-woven is due to the heating of fabrics to the T_g which makes the fibers flexible and helps in bending, leading to the reconfiguration of fiber-to-fiber contacts. This generates a lock-in effect in the fibers when the fabric is cooled down while staying under compression. The fiber arrangement in the as-received and heat-compressed non-woven fabrics is illustrated in Figure 2.29 (a-b) and (c-d), respectively.

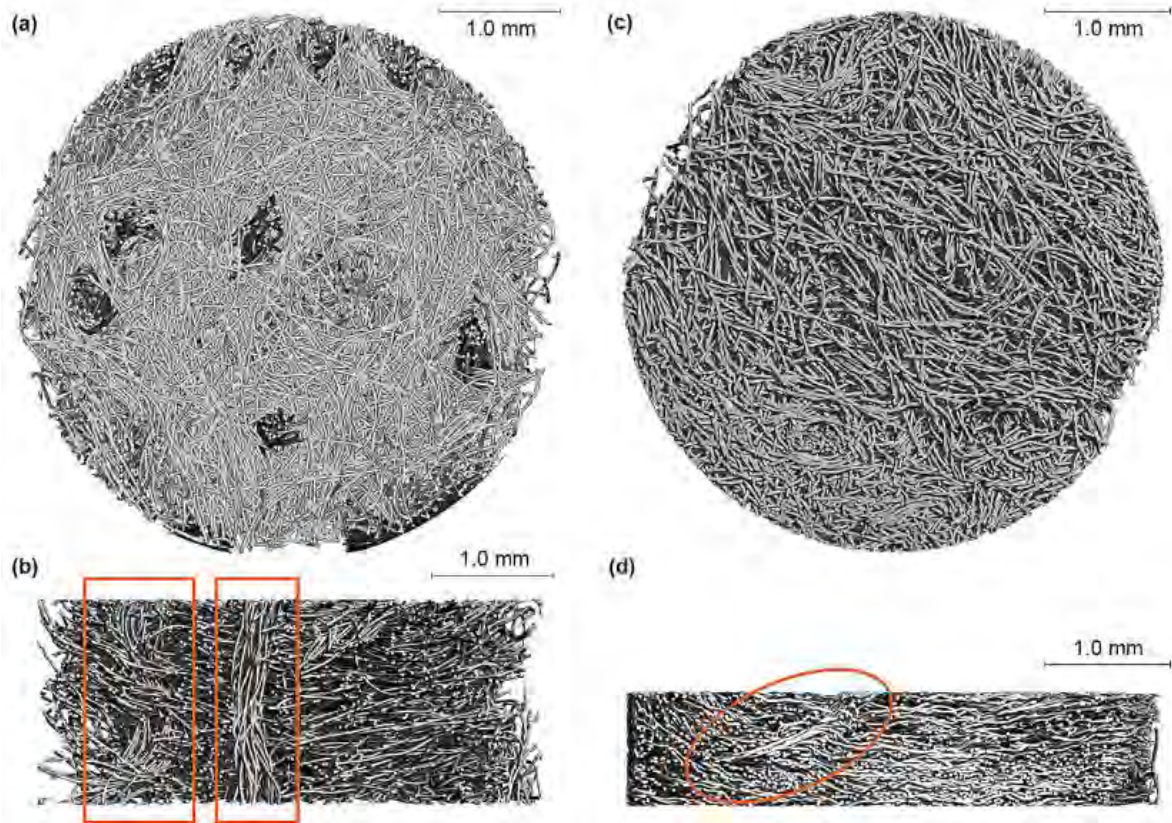


Figure 2.29 Micro-CT images of as-received sample: (a) top-view and (b) section view, and heat-compressed sample: (c) top view, and (d) section view⁴⁶.

Other than the development and processing of non-woven auxetic fabrics, the same research team has recently studied the out-of-plane auxetic behavior of needle-punched non-woven fabrics under cyclic tensile deformation⁶⁴. The non-woven auxetic fabrics processed with the heat-compress method were subjected to cyclic strains ranging from 1% to 3% (within the axial elastic extension). They found that the auxetic effect was completely reversible for 1% strain while irreversible changes were observed for 2% and 3% cyclic strains.

2.7 Three-dimensional auxetic fabrics

2.7.1 Three-dimensional auxetic knitted fabrics

The first ever weft-knitted fabric that exhibited NPR was produced by Liu et al.⁸³. A special knit pattern was designed based on a three-dimensional (3-D) arrangement of parallelogram planes in a zigzag folded form. This knit pattern is shown in Figure 2.30 (a) while the 3-D zigzag geometry is shown in Figure 2.30 (b). The structure shows the NPR effect upon stretching in any principal direction because the parallelogram planes of the structure that formed the 3-D arrangements by inclining at different positions started to become flattened. Thereby, the folded structure opens and becomes two-dimensional (2-D), resulting in a net increase in the surface area. For sample preparation, conventional 100% wool (2/28 Nm) yarn and a 14-gauge programmed flat-knitting machine were used. The developed knitted fabric in relaxed and stretched form are illustrated in Figure 2.30 (c) and (d), respectively.

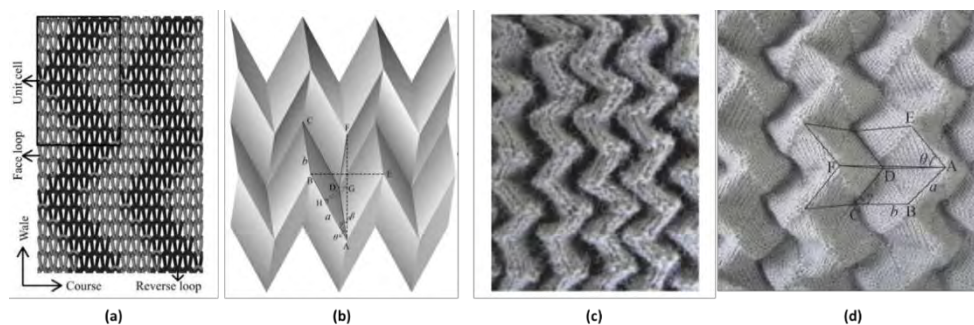


Figure 2.30 Three-dimensional knitted fabric: (a) fabric knit pattern, (b) schematic of parallelogram planes of zigzag pattern, (c) knitted fabric in relaxed form, (d) knitted fabric in stretch form⁸³.

A novel three-dimensional (3-D) auxetic warp-knitted spacer fabric was designed and developed by Wang and Hu⁸⁴. An approach of using conventional non-auxetic yarns and an auxetic geometry was adopted for producing auxetic fabric. The geometry realized is based on rotation parallelograms of the same size. The 3-D spacer fabric consists of three layers, where

the two face layers made with polyester multifilament yarn are joined by a polyester monofilament spacer yarn as a middle layer. The multifilament polyester yarn used for the two faces was 400D/96F and the diameter of monofilament polyester spacer yarn was 0.12mm. A double warp knitting machine equipped with six yarn-guide bars was used for sample preparation. The two face layers of the fabric are designed with a geometrical structure based on parallelograms of the same size and shape connected in a way to form a V, as illustrated in Figure 2.31. After fabrication, the samples were heat-treated to fix the designed geometrical arrangement. The fabric stretching in either direction causes rotation of the parallelograms around the connecting points which results in an overall auxetic effect.

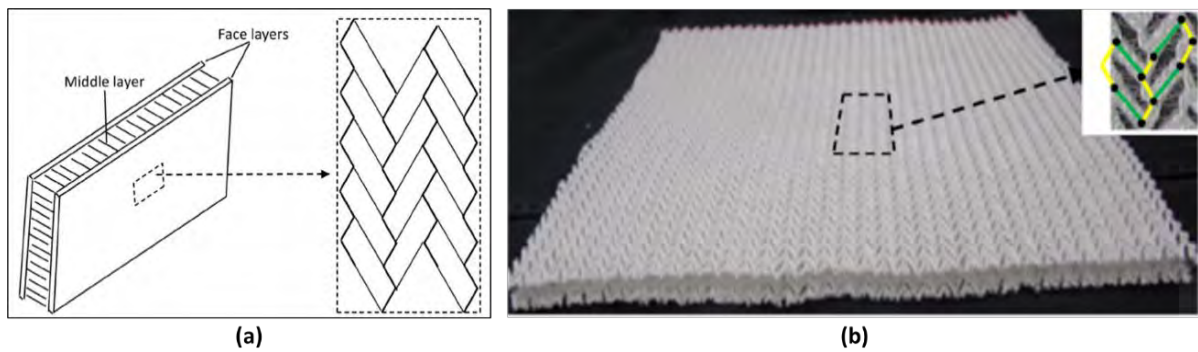


Figure 2.31 Three-dimensional auxetic knitted spacer fabric: (a) schematic representation, (b) produced fabric⁸⁴.

Recently, a more comprehensive study was carried out by the same research group to produce 3-D warp-knitted spacer fabrics based on two geometries, i.e. rotating squares and re-entrant hexagon⁴⁰. In the 3-D knitted spacer fabric, the re-entrant hexagonal geometry was realized by incorporating an elastic yarn (stretch form) into a rectangle mesh. The elastic yarn then converted the rectangle net into an auxetic geometry (re-entrant hexagon) upon shrinkage as depicted in Figure 2.32 (a). A monofilament polyester spacer yarn was alternately knitted on the two faces in the wale direction without lateral movement, to avoid its effect on the z-

direction deformation of the face fabric structure. The designed fabric samples were produced using an RD7 Raschel machine (double-needle) equipped with seven (07) guide bars for the yarns. A 3-D knitted spacer fabric was also produced with rotating square geometry on the face layers. The geometry was formed by the rotating square framework made with stiff yarn and with an elastic base as shown in Figure 2.32 (b). During the fabric design, some important features were ensured to achieve the auxetic effect. Those points include enough stiffness of the rotating square framework, stretchability in both (length-wise and width-wise) directions of the base fabric, and minimizing the restricted deformation of the rotating squares. The fabric samples were produced using an RDPJ4/2 jacquard machine with two (02) bars for base yarn and four jacquard guide bars.

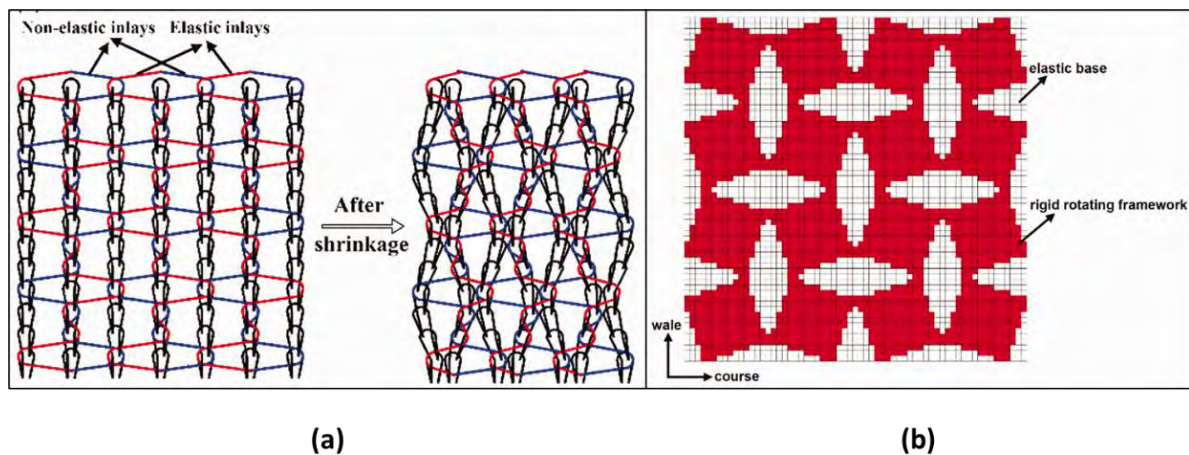


Figure 2.32 Three-dimensional auxetic warp-knitted spacer fabric design: (a) loop diagram of re-entrant hexagon, (b) jacquard pattern of rotating square⁴⁰.

2.7.2 Three-dimensional auxetic fabrics made by using non-weaving and knitting technology

The innovative three-dimensional (3-D) non-woven and knitted structures were developed by Ge and Hu⁵⁷. Unlike most of the 3-D fabric structures, these novel structures exhibit NPR effect under compressional stress. A combination of knitting and non-woven techniques was used to

develop 3-D structures having different warp yarn diameters. Poisson's ratio of the samples under compression stress was evaluated along with fabric thickness. Increasing yarn's fineness ratio between warp and weft yarns can increase the NPR of developed structures keeping other parameters constant. It is important to note that the yarn arrangements in the proposed structure are the most important reason for the auxetic behavior of the composite structure. There is an alternate placement of the non-woven weft yarns, hence under compression the spaces between the yarns are removed, and NPR is observed, as shown schematically in Figure 2.33. The auxetic effect increases at higher compression strain. Also, a geometrical model was developed for predicting the NPR effect with known structural parameters. Strong agreement was observed between the theoretical model and actual results obtained from the auxetic structure. A 3-D NPR fabric structure was recommended as a suitable candidate for the composite reinforcement⁵⁰, which has soft or compressible resins. Such composites have the ability to concentrate in compressive loading which makes these favorable for various applications e.g., automobile, defense, sports equipment, and aerospace where impact resistance is a highly desirable property.

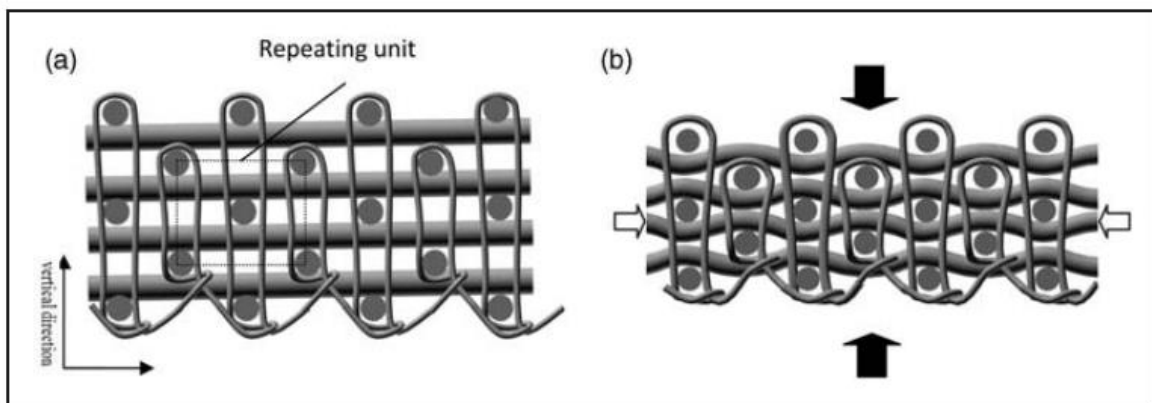


Figure 2.33 Structure of innovative 3-D non-weaving and knitted auxetic structure, (a), relax state, (b) under compression⁵⁷.

2.7.3 Three-dimensional auxetic fabrics made by using weaving technology

The three-dimensional (3-D) auxetic structures were successfully developed using the differential modulus of the yarns. Through thickness yarns with high modulus are placed in such a fashion that the layer to stitched 3-D woven fabric will be pushed and the thickness of the 3-D fabric will be increased⁵⁸, as illustrated in Figure 2.34. Conventional four-layered fabric with thickness in structure exhibited positive Poisson's ratio, whereas modified 3-D woven four-layered thick fabric structure exhibited NPR which makes modified 3-D woven fabric an auxetic structure. The auxetic composite showed 6.7% better energy absorption compared to the non-auxetic composite as shown in Table 2.3. Auxetic composites exhibit ductile failures while brittle failure is usually experienced in conventional composites. The projected modified four-layer thick structure has the potential to be used in impact-resistance applications.

Table 2.3 Penetration and impact energies of conventional and modified 3-D samples⁵⁸.

Sample	Penetrating force (N)	Energy dissipation (J)
Conventional 3-D sample (warp)	1068.61 ± 208.33	40.44 ± 0.392
Conventional 3-D sample (weft)	-	40.44 ± 0.392
Modified 3-D sample (warp)	802.97 ± 172.07	43.16 ± 0.392
Modified 3-D sample (weft-)	-	42.03 ± 0.001

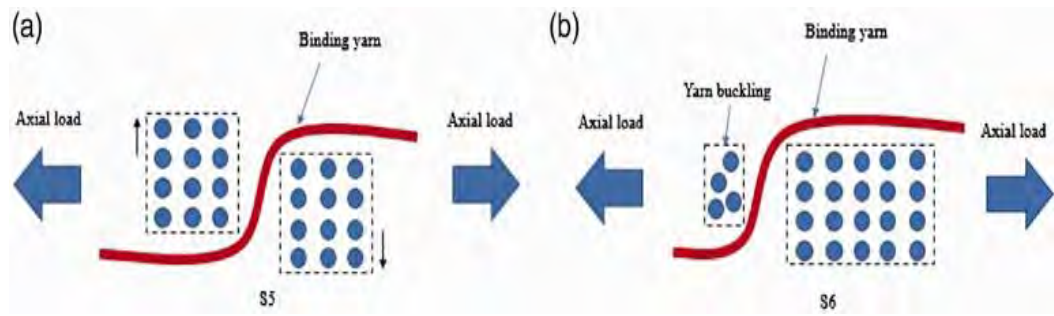
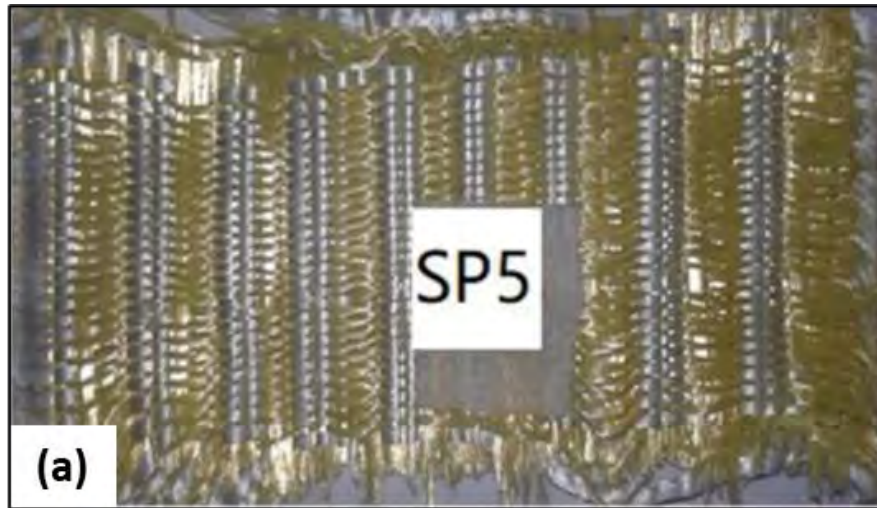


Figure 2.34 Mechanism of auxetic behavior in the 3-D woven fabrics⁵⁸.

Later, the same group reported the influence of float length and Poisson's ratio for the auxetic composites³³. Para-aramid filament yarn was utilized in both the warp and weft directions, with high-modulus polyethylene (HMPE) yarn employed as a binding yarn, as shown in Figure 2.35 (a). It was found that a direct relationship exists between Poisson's ratio and the float length of the warp and binder yarn in the fabric. The Poisson's ratio of the 3-D auxetic fabric samples ranged from -0.9 to -2.98, as shown in Figure 2.35 (b). The impact test results of the composites demonstrate that utilizing auxetic reinforcements leads to higher energy absorption. The energy absorption is also influenced by the float length of the warp and binder yarn. The impact test revealed that composites with a longer float length exhibited superior energy absorption. The composite structure with a long float auxetic fabric demonstrated the highest impact strength of 158.46 kJ/m². As the float length of the warp and binder yarn increases, the energy absorption improves due to the enhanced mobility of the binder and warp yarn within the reinforcement. The ductile nature of auxetic composites contributes to superior impact resistance compared to conventional composite reinforcements.



(b)

Figure 2.35 (a) 3-D auxetic pre-form developed with para-aramid yarn (yellow) and UHMWPE yarn (white), (b) Poisson's ratio values of developed samples³³.

2.8 Auxetic composites

Similar to other auxetic textile materials, researchers are also focused on the development of auxetic composites for structural applications because of their outstanding specific strength, high modulus, and other properties^{85,86}. In general, there are two basic approaches for developing auxetic composites⁸⁷. The first approach uses normal manufacturing techniques by using non-auxetic reinforcement and a polymer matrix. As an alternative, the special lamination technique is used at a certain angle to achieve an auxetic effect^{88,89}. The second

approach to developing auxetic composite involves the use of auxetic reinforcements such as auxetic yarns^{51,90}, auxetic fabrics^{58,91}, and auxetic inclusions⁹²⁻⁹⁴. The second approach is based on the use of auxetic textiles, therefore, developments made in this field are further reported here.

The 3-D auxetic fabric structure developed by Ge et al.⁵⁷, was redeveloped by the same research group and used for the production of composite structure⁹⁵. The 3-D auxetic structure developed with non-auxetic yarns and modified non-weaving and knitting techniques was used as a reinforcement and a soft polyurethane (PU) foam as a matrix system. The two components forming the polyurethane formulation were industrialized MDI Wannate PM-400 and a mixture of eight (08) other chemicals. The two components were mixed and injected into a metal mold containing the 3-D auxetic fabric reinforcement using the hand injection molding technique. The composite structure was cured for 2 h at 90 °C in a lab-scale oven. The composite structure was then de-molded and prepared with specified dimensions for a compression test. Two controlled samples, 100% pure PU matrix, and non-auxetic 3-D fabric structure composites were also prepared using the same procedure as illustrated in Figure 2.36 (a-c).

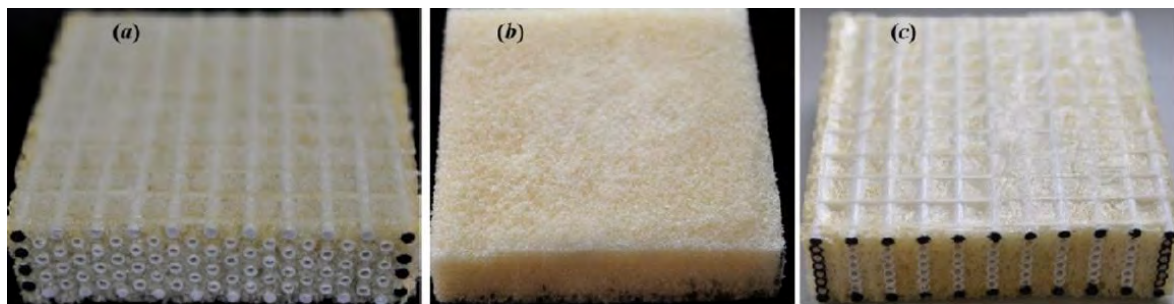


Figure 2.36 Composite samples: (a) auxetic fabric reinforced composite, (b) 100% pure matrix, and (c) non-auxetic fabric reinforced composite⁹⁵.

The three samples were tested with a uni-axial compression test to analyze the compression properties and most importantly the NPR behavior. For evaluating the Poisson's ratio, the

samples were marked vertically and horizontally with black dots to identify the change in dimension in the lateral and axial directions. The Poisson's ratio was calculated from the negative ratio of the lateral change in dimension to the axial change in dimension.

The two composite samples, with auxetic and non-auxetic reinforcements, under compressive deformation are shown in Figure 2.37 (a) and (b) respectively. It can be observed that the composite samples made with auxetic reinforcement contract in the lateral direction under compressive load, proving the auxetic behavior of the composite structure. In addition, the contraction is made at the center of the structure because the top and bottom surfaces are restrained by the compression plates. The auxetic behavior can be attributed to the alternate placement of warp yarns on the weft yarns forming empty spaces that allow the warp yarns to crimp in the z-direction of the structure and the overall lateral length of the warp yarn decreases and eventually the structure shrinks. On the other hand, the composite made with non-auxetic reinforcement collapses (to the right side) under compressive load because the weft yarns were placed in the form of a vertical column. From the compression test, as shown in Figure 2.38, it was found that the values of specific stress of the auxetic composite and pure PU foam are almost the same until 33.48 % of compressive strain, after which the compressive stress of auxetic composite increases at a higher rate. This unique response enables the auxetic composite to absorb more energy than the PU form. At the same time, it displays enhanced mechanical properties.

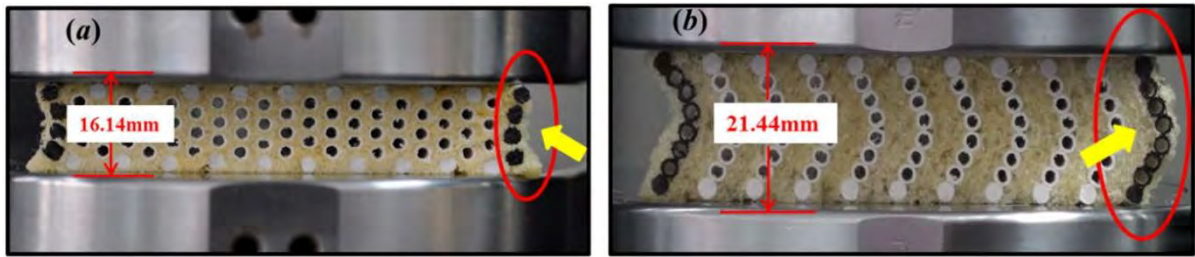


Figure 2.37 (a) auxetic and (b) non-auxetic fabric reinforced composites under compressive load⁹⁵.

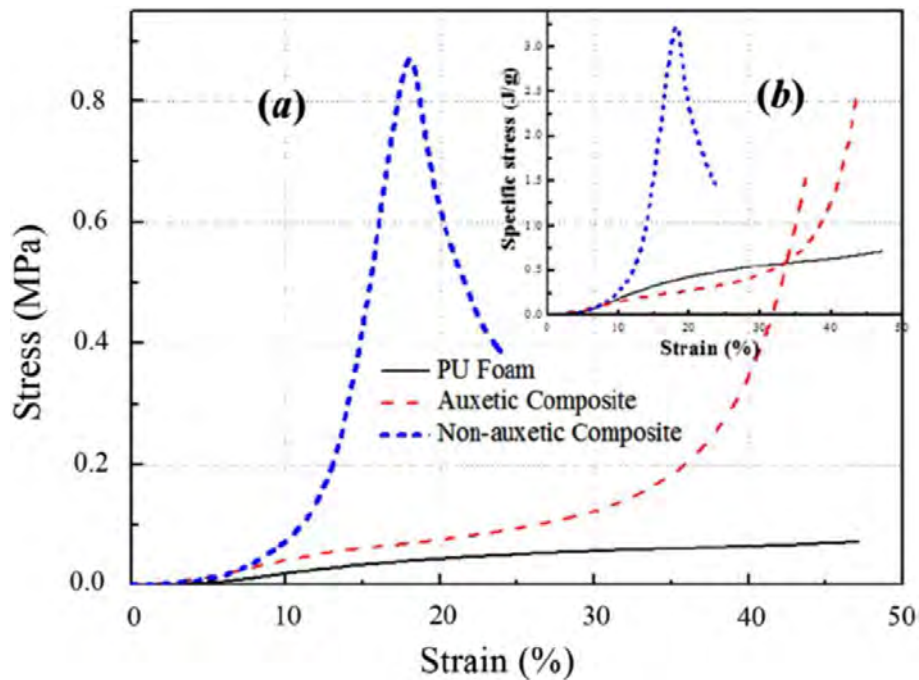


Figure 2.38 Comparison of compression curves of the three samples: (a) compressive stress-strain, (b) compressive specific stress-strain⁹⁵.

Due to the extraordinary response of the auxetic composites to the compressive deformation, the study was extended to analyze the low-velocity impact response of the composite reinforced with 3-D auxetic fabric structure⁸⁵. Auxetic and non-auxetic composites were subjected to a low-velocity test with different energy levels (from 12.7 to 25.5J). As expected, it was found that the auxetic composite structure absorbs a higher amount of impact energy compared to the non-auxetic composite structure when tested at an impact energy of 19.1J. The auxetic

composite absorbs 14.3J while the non-auxetic composite absorbs 12.8J. However, due to the soft nature of the PU form, it absorbs the highest impact energy of 14.5J. The energy-time curves of the samples are illustrated in Figure 2.39.

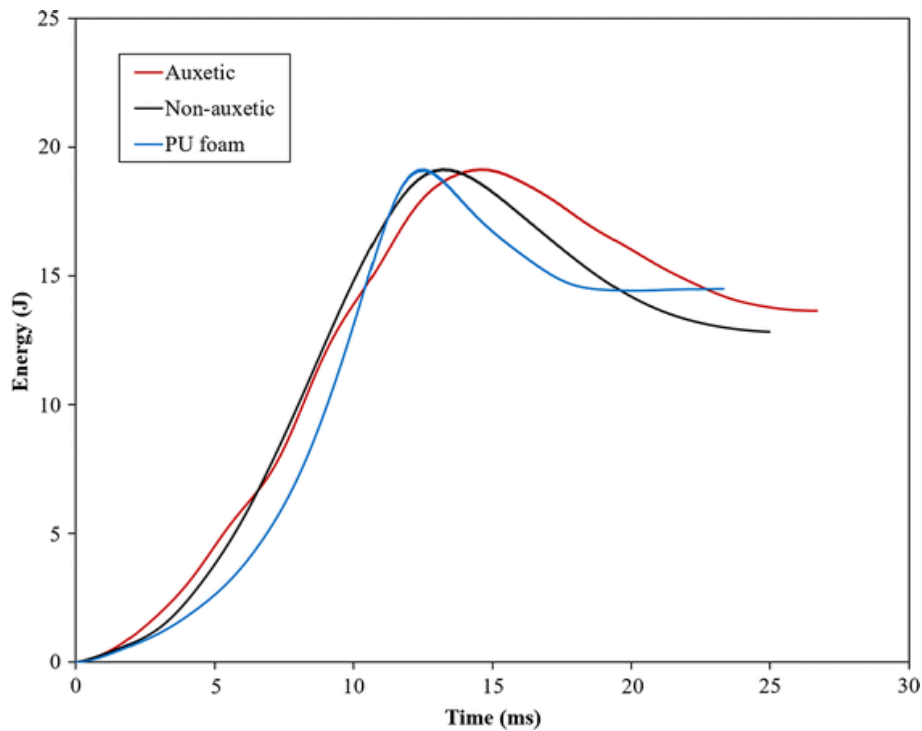


Figure 2.39 Energy-time curves of auxetic composite, non-auxetic composite, and PU form⁸⁵.

These studies also inspired other researchers to develop and analyze the energy absorption abilities of composites developed by using auxetic fabrics as a reinforcement. For example, Xu et al.⁹⁶ studied the low-velocity impact response of a composite structure reinforced with warp-knitted auxetic spacer fabric. A similar study is also conducted on enhancing the energy absorption of composites reinforced with weft-knitted auxetic structures⁴⁹. Interestingly, the property enhancement of auxetic composites is not limited to impact energy absorption, but it also enhances the indentation resistance, as studied by Li et al.⁹⁷.

2.9 Potential applications of auxetic textiles

Unlike conventional materials, the unusual deformation behavior and response to external force enhanced the physical and mechanical properties of auxetic textiles. Those enhanced properties include indentation resistance, high surface area under tension, synclastic curvature property, high energy absorption, fracture toughness and crack resistance, and variable permeability. With all those properties, auxetic textiles are highly recommended for applications in clothing, medical, protection, filtration, and automotive⁹⁸.

As discussed previously, auxetic knitted fabrics and auxetic woven fabrics are developed with in-plane auxetic behavior which means that these fabrics expand laterally when stretched. Therefore, such auxetic fabrics are useful for making garments because they will show size expansion in both directions. With this property, these garments can be useful in many situations like size fitting and size growing in people such as children and pregnant women^{99,100}. Parents need to buy new clothes for their children very frequently because their body growth is very fast at an early age up to 3 years. This problem can be overcome by using garments made with auxetic fabric. Auxetic fabrics made with foldable geometries can expand in both directions which is a suitable choice for making children's clothes that can adapt to the changes in body size. Hence, these garments can be used to save money, reduce waste, and enhance shape fit, and comfort. Furthermore, maternity dresses made with auxetic fabric can improve the shape adaptation which can provide more comfort during the pregnancy period.

The pore opening effect and expansion in both directions under tension of auxetic textiles can be utilized for biomedical applications. Auxetic fabric can be used to develop smart bandages that can be expanded in response to the swelling of a wound. In addition, the expansion will also facilitate the permeability of the bandage for gaseous exchange. By using a smart auxetic bandage, the drug release and the speed of drug release can be controlled due to the pore

opening effect. Other than smart bandages, auxetic yarns can be used to manufacture dental floss which can be more effective than conventional floss which becomes thinner under tension^{101,102}.

Auxetic textiles have great potential to be considered as a candidate for personal protection because of their superior properties like indentation resistance, energy absorption and dissipation, and increased fracture toughness^{98,99,103}. Many developments including auxetic foams, auxetic knitted structures made with high-performance fiber, and three-dimensional (3-D) auxetic fiber-reinforced composites have shown exceptional improvement in properties like mechanical properties and energy absorption ability. Therefore, auxetic fabrics, foams, and composites can be used as a single or in combination to develop protective clothing, blast-proof curtains, bullet-proof vests, sports equipment etc^{86,95}.

Auxetic textiles have one possible application in automobiles, that is a seat belt. The seat belt is one of the most important safety devices of automobiles which serves driver and passenger all the time during a ride⁵⁹. Conventional seat belts are made from high-tenacity, multifilament polyester, and nylon fibers. These seat belts have been in service for many years because they can offer excellent load carry capacity, high abrasion resistance, lightweight, and resistance to sunlight. Besides many advantages, there is a problem associated with these seat belts. A seat belt should be fastened constantly during the journey, which makes passengers feel uncomfortable, specially when it applies and releases pressure during acceleration and deceleration. Sometimes the situation becomes more severe under sudden deacceleration or when an accident occurs. This is because the human body will be exposed to a huge amount of pressure which can cause serious injuries like breakage of ribs. This problem can be overcome if the seat belt is made of auxetic fabric using high-performance fibers. Auxetic seat belts will be capable of expanding and increasing the contact area between the belt and the human body.

This phenomenon will reduce the amount of pressure applied by the seat belt on the human body.

2.10 Conclusions

This chapter reviewed the developments made over the past three decades in the field of auxetic textiles. Due to the high interest of researchers, significant discoveries have been made to implant auxetic behavior in every component of textiles, for example, auxetic filaments, auxetic yarns, 2-D auxetic knitted fabrics, 3-D auxetic knitted fabrics, 2-D auxetic woven fabrics, and 3-D auxetic structure for composite reinforcements. From the literature, it was found that auxetic fabrics are developed using knitting, weaving, and non-weaving technologies. Auxetic knitted fabrics have some drawbacks which make them unsuitable for several applications like protective textiles etc. The drawbacks associated with auxetic knitted fabrics are low structural stability and low elastic recovery. On the other hand, using weaving technology, only 2-D in-plane auxetic woven fabrics have been developed so far. The 2-D auxetic woven fabrics that have been developed show the potential for applications in areas such as clothing and fashion garments. However, their usage in high-performance applications is limited due to their relatively low thickness, higher longitudinal deformation under tension, low auxetic behavior, and abrupt decrease in NPR at higher strain. The developed 3-D auxetic structures that are made using non-weaving and knitting technology or weaving technology (for out-of-plane auxetic effect), are only suitable for composite reinforcements. Developing an auxetic fabric that could be used for high-performance applications is still missing in the literature. Furthermore, up till today, introducing in-plane auxetic effect in 3-D woven fabrics is a real challenge and hence unaddressed.

Thus, this study aims to develop a novel class of 3-D auxetic woven fabrics made of non-auxetic yarns. The developed 3-D auxetic woven structure will exhibit an in-plane NPR effect

that will show a potential to be considered for high-performance applications. The design and manufacturing process of the new 3-D auxetic woven structure will be first introduced. Then, its auxetic behavior and mechanical properties will be studied by performing a uni-axial tensile test combined with a video recording setup. Furthermore, geometrical and finite element models of the 3-D auxetic woven structure will be proposed for a deeper understating of the auxetic behavior of the structure and to provide a platform for predicting a engineering the properties of the structure prior to production. Detailed research methodology will be discussed in the next chapter.

CHAPTER 3 MATERIALS AND METHODS

3.1 Introduction

This chapter reports the selection of conventional three-dimensional (3-D) structures for modification, the selection of materials, and the methodology adapted to develop 3-D auxetic woven fabrics. The methodology adapted for approaching the auxetic effect in the 3-D woven fabric is based on realizing an auxetic geometry (in resemblance to a re-entrant hexagonal structure) by inducing an unusual in-plane crimp in warp yarns. This chapter first explains the concept of realizing an auxetic geometry in conventional 3-D woven fabric and its subsequent transformation. Next, the methodology adapted to fabricate the transformed 3-D auxetic structural design into a woven fabric is reported. Then, the tensile testing setup and the procedure for measuring Poisson's ratio are described. Finally, the auxetic behavior of the 3-D auxetic woven fabric is analyzed and discussed.

3.2 Development of three-dimensional auxetic woven fabrics

3.2.1 Structure design

Woven fabrics are considered 3-D if they have considerable thickness¹⁰⁴. The two basic 3-D multilayer fabric designs are orthogonal interlock structure and angle interlock structure¹⁰⁵. Orthogonal through-thickness is a type of 3-D woven fabric, in which the warp and weft yarns run in all three dimensions, i.e. X (along the length), Y (along the width), and Z (through-thickness)¹⁰⁶. In this type of 3-D woven structure, the warp and weft yarns are arranged in the x, y, and z-directions as shown in Figure 3.1. As usual, the x-direction yarns are warp yarns and y-direction yarns are weft yarns, however, the z-direction yarns may be either warp or weft yarns, which is also called binding or stitching yarn. If the weft yarns are interlaced by the warp yarns through the thickness to form the z-direction, such an arrangement is called a warp

interlock. Whereas, the interlacement of warp yarns by the weft yarns is called weft interlock 3-D structure¹⁰⁷.

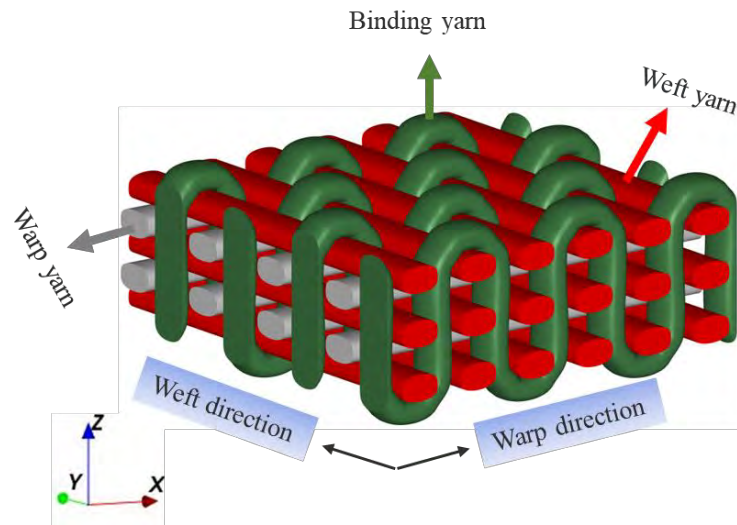


Figure 3.1 Conventional three-dimensional orthogonal through thickness structure.

Typically, within the multilayer 3-D woven structures, the orthogonal through-the-thickness structure is regarded as the most compact structure due to the presence of three yarn systems in all three directions, as illustrated schematically in Figure 3.2 (a). This study introduces three significant modifications to transform the conventional non-auxetic orthogonal through-the-thickness structure into an auxetic structure exhibiting an in-plane NPR effect. In the first modification, the conventional warp direction for binding yarn (warp interlock) was replaced by the weft direction (weft interlock). Second, the conventional 1 by 1 plain weave pattern of binding yarn was changed to 2 by 2 twill weave. These two modifications lead the structure to create an alternate spacing in the x-(warp) and y-(weft) directions, as illustrated in Figure 3.2 (b). In the final modification, a fine elastic yarn was used instead of non-elastic yarn, as depicted in Figure 3.2 (c).

After each insertion of the binding yarn, multiple repeats of elastic yarns were inserted in stretched form as weft. These fine elastic yarns serve three functions: 1) holding the warp yarns

to enhance the structure's stability, 2) shrinking the structure widthwise to fill the voids left by the coarse binding yarn, and 3) acting as a return spring, restoring the structure to its original position after deformation. Thus, in a relaxed state, the shrinking of the structure compels the warp yarns to crimp laterally and fill the voids as shown in Figure 3.2 (d). This induction of unusual lateral crimp to the warp yarns forms a unique structure that resembles a re-entrant hexagon, as shown in Figure 3.3 (a). Nevertheless, when the structure is subjected to a tensile extension, the warp yarns will try to decrimp and straighten by exerting a lateral force on the binding yarns, as shown in Figure 3.3 (b). As a result, an in-plane (width direction of fabric) auxetic effect will be achieved.

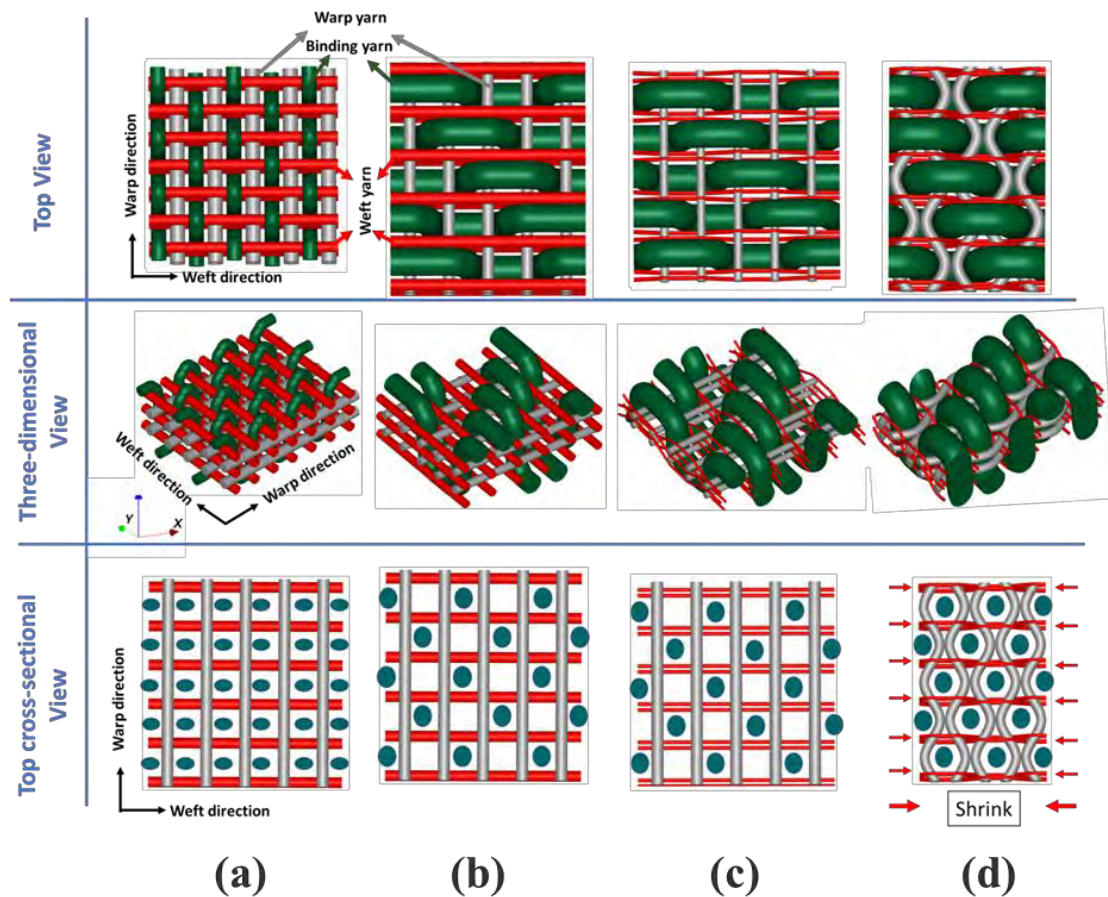


Figure 3.2 Schematic representation of side view and top view: (a) conventional 3-D orthogonal structure with 1/1 plain pattern of binding yarn, (b) changing weave pattern of

binding yarn by 2/2 twill pattern in weft interlock manner, (c) introduction of fine elastic yarn in the weft direction, (d) modified 3-D orthogonal structure with auxetic geometry in a relaxed state.

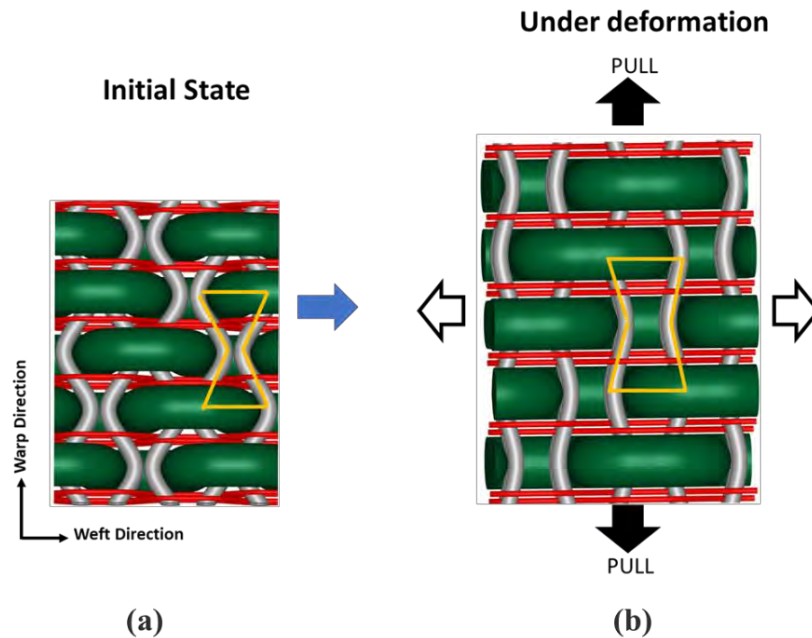


Figure 3.3 Schematic of 3-D Auxetic woven structure (a) initial state, (b) under tensile tension in the warp direction.

3.2.2 Fabric manufacturing

To develop the samples, a single yarn system was utilized for the warp, while the weft comprised a two-yarn system consisting of a fine elastic yarn and a coarse binding yarn, based on the design specifications. The three yarns were procured from the local market, possessing essential properties necessary to achieve the desired auxetic structure and a significant auxetic effect. The first crucial requirement was to select appropriate diameters for the warp, elastic weft, and binding yarns. In this regard, a diameter of 0.7 mm for the warp yarn and 0.62 mm for the elastic weft yarn were chosen consistently across all samples. However, the binding yarn's diameter varied among the samples, as the ratio of binding yarn diameter to warp yarn

diameter directly influences the auxetic behavior⁵⁷. The variation in diameter among the three binding yarns is attributed to the core yarn i.e., a finer core yarn corresponds to a smaller diameter binding yarn and vice versa. For the warp direction, a stable and high-strength yarn was chosen as it directly experiences tensile loads. Similarly, an elastic yarn with a low modulus and high tensile deformation was selected as the weft yarn. This elastic yarn provides an elastic restoring force, enabling the structure to shrink in a relaxed state. In contrast, the binding yarn was chosen to have a coarser diameter compared to the warp and elastic weft yarns. This coarser diameter helps increase the void area within the fabric, ultimately causing sufficient lateral crimping in the warp yarns upon shrinkage. Additionally, besides the coarser diameter, it is important to note that the binding yarn should be easy to bend (facilitating the weaving process and adopting an orthogonal U-shape) but resistant to compression (from the forces exerted by the elastic yarns and warp yarns during stretching). To fulfill these requirements, a polyester wrapper polyurethane (PU) based coarse braided yarn was chosen. The PU-based core enhances the flexibility and bending capability of the yarn, while the polyester wrapping maintains the solidity of the core and making it resistant to compression. Additionally, a binding yarn with a 2.5 mm diameter and high bending stiffness was also selected to evaluate its impact on the auxetic behavior. The difference in braiding angle between the two yarns of the same diameter (2.5 mm) results in varying bending stiffness. A yarn with a higher braiding angle demonstrates higher bending stiffness but reduced axial stiffness (tensile modulus)^{108,109}. These statements are supported by the tensile load-strain curve of the yarns shown in Figure 3.5. Real images of all the different yarn types used in sample fabrication are presented in Figure 3.4. Furthermore, a summary of the properties of the various yarn types can be found in Table 3.1.

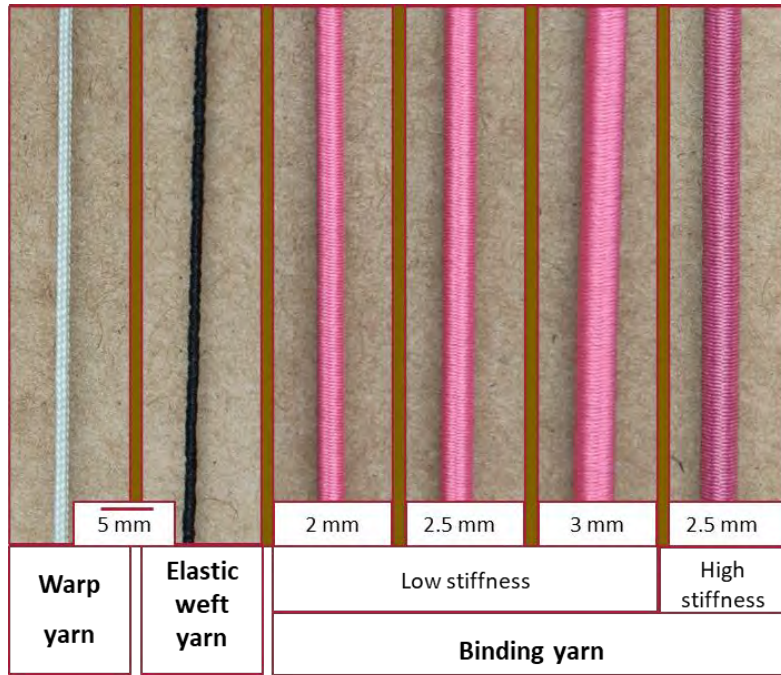


Figure 3.4 Images of warp yarn, elastic weft yarn, and binding yarns used for producing three-dimensional (3-D) auxetic woven structure.

Table 3.1 Properties of warp and weft yarns used for sample preparation.

Yarn	Type	Diameter (mm)	Tensile Modulus (MPa)	Tensile strength (N)	Bending stiffness (μPa) 108
Warp yarn	Braided	0.7	1645.8	106.32	-
Binding yarn	Low stiff (LS)	2	61.2	202.96	0.66
	braided yarn	2.5	39.7	208.47	0.38
		3	29.8	275.88	1.11
	High stiff (HS)	2.5	44.5	200.73	2.29
	braided yarn				
Weft yarn	Braided yarn	0.62	11.2	14.36	-

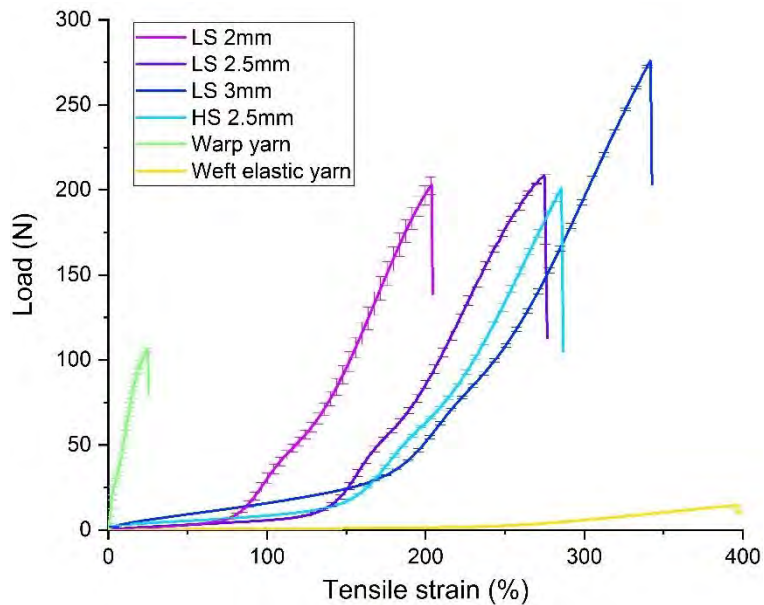


Figure 3.5 Tensile load versus strain curves of the warp, elastic weft, and binding yarns.

In order to develop 3-D auxetic woven samples, we choose the least number of layers (two) for the 3-D structure to reduce the required time for weaving preparation. Furthermore, developing a two-layer fabric ensures that the structure can accommodate an increased number of layers if desired. The initial stage in fabric development involves creating the interlacing patterns for the warp and weft yarns. When compared to the interlacing pattern of a 2-D structure, the presentation of the interlacing pattern for a 3-D woven structure is considerably more intricate and complex. Therefore, various approaches^{110,111} are reported to enhance the presentation of the interlacing pattern for 3-D woven fabrics. In our specific case, the two layers are designated as the top layer (referred to as "face" or F) and the bottom layer (referred to as "back" or B). To facilitate the depiction of the interlacing pattern, alphanumeric characters such as F1, F2, F3, and F4 are assigned to the warp and weft yarns of the face layer, while B1, B2, B3, and B4 are used for the warp and weft yarns of the back layer. The binding/stitching weft yarns are denoted as S1, S2, S3, and S4. Figure 3.6 (a) illustrates a schematic representation of the warp and weft yarns for both layers, while Figure 3.6 (b) represents the interlacing pattern of the 3-

D auxetic woven fabric with one repeat of elastic weft yarn. Additionally, Figure 3.6 (c) provides a schematic illustration of the top layer of the auxetic woven structure.

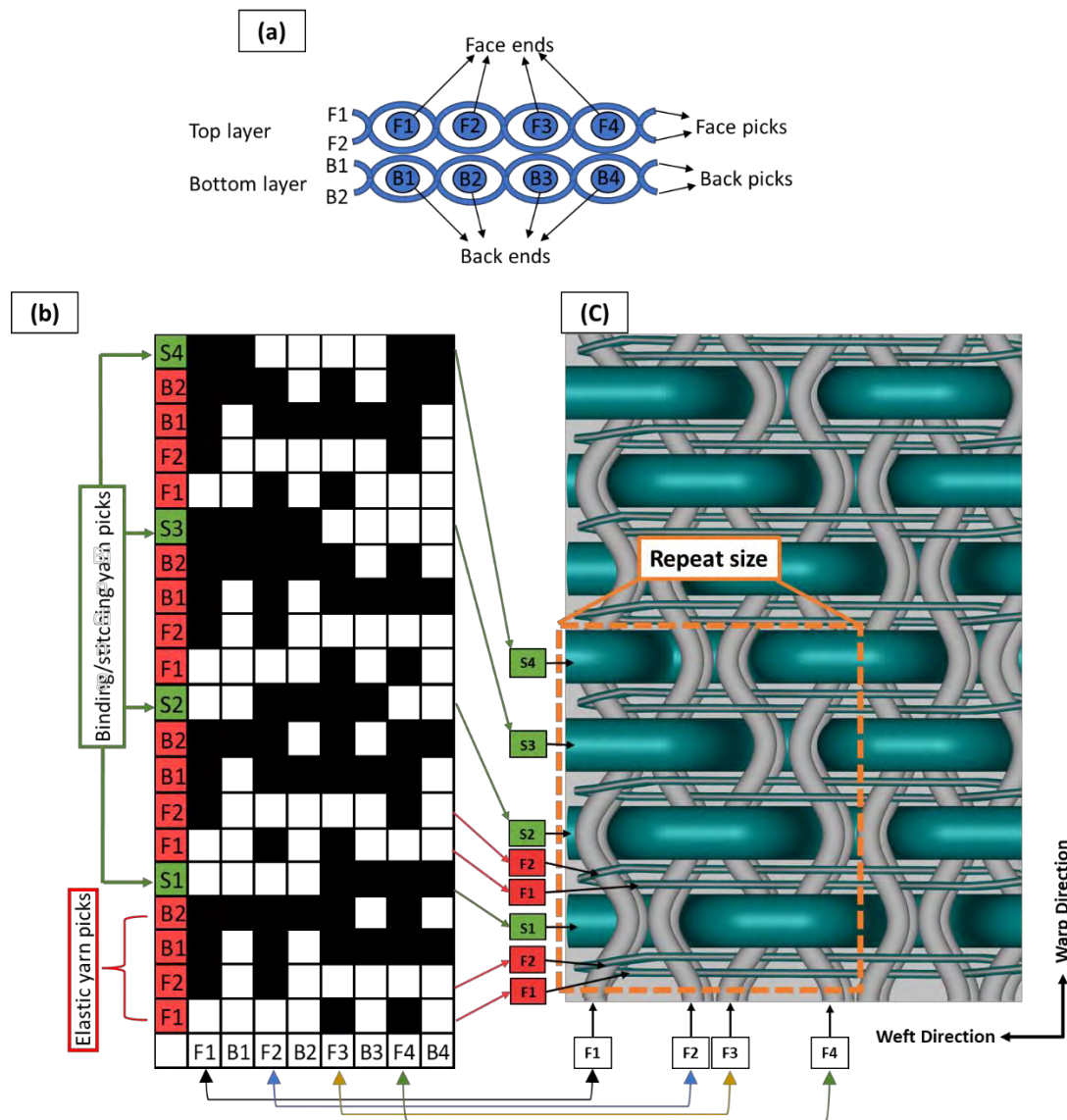


Figure 3.6 (a) Schematic illustration of warp and weft yarns of the two layers of 3-D woven fabric, (b) the interlacing pattern of 3-D auxetic woven fabric, (c) top layer of the orthogonal through-the-thickness auxetic woven structure.

To produce the narrow-woven fabric samples, a commonly used semi-automatic weaving machine equipped with a dobby shedding mechanism was employed, as shown in Figure 3.7.

To accommodate the total number of warp yarns (40), a customized weaving beam with a

narrow width was prepared. It was ensured that the total number of ends remained consistent across all samples to enable a comparison of their tensile properties. For the weaving process, a total of 8 harnesses were utilized with a straight drawing-in draft approach. To facilitate smooth insertion and accommodate the additional length of the binding yarn, a specific reed plan was implemented. This plan involved a sequence of two yarns per dent, followed by zero yarns per dent. Moreover, it was necessary to insert the elastic yarn in a stretched form during the weaving process. This allowed the structure to shrink to a relaxed state after weaving was completed and the fabric was cut off the loom.



Figure 3.7 Semi-automatic weaving machine used for fabrication.

During the fabrication process, it was observed that certain crucial parameters could significantly impact the weaving process, the physical properties of the structure, and ultimately the auxetic behavior of the fabric. Therefore, these parameters were carefully considered for a detailed examination to assess their influence on the performance of the novel 3-D auxetic woven structure. The four selected parameters were as follows: the diameter of the

binding yarn, the number of repeats of the elastic weft yarn, the bending stiffness of the binding yarn, and the stretching of the elastic yarn during insertion. Based on these four parameters, a total of nine (09) distinctive sample types were developed, as outlined in Table 3.2. Since the samples were created using various binding yarn diameters and different numbers of elastic yarn repeats, the weft yarn densities (expressed in terms of binding yarn) varied among all the samples. Theoretically, it is expected that the spacing between the binding yarns will impact the auxetic behavior of the fabric. A decrease in spacing between the binding yarns is anticipated to increase the lateral crimp in the warp yarns over a specific length. The measured picks per inch (PPI) of the binding weft yarn are provided in Table 3.2 to further illustrate these variations.

To design the experiment, a specific approach was employed, where the least dependent parameter was optimized first. Afterward, the remaining samples were produced using the parameter that had been previously optimized. For example, the first set of samples (Fabric 1) was developed using three different binding yarns with diameters of 2 mm, 2.5 mm, and 3 mm. Based on the feasibility and auxetic behavior observed in these three samples, the yarn with a diameter of 2.5 mm was selected as the optimal choice for producing the subsequent sets of samples. The other three sets of samples were as follows: Fabric 2, which involved altering the repeat size of the elastic weft yarn; Fabric 3, which used a high bending stiffness of the binding yarn; and Fabric 4, which involved weaving with a high stretch percentage of the elastic weft yarn. The bending stiffness of the binding yarns was determined using the beam deflection method described in the study by Msalilwa et al¹⁰⁸. Additionally, the stretch percentage of the elastic weft yarn was calculated using Equation (3.1). To calculate the stretch percentage (%) of the elastic yarn, the original length of the yarn was indirectly determined by cutting the developed sample along the width direction and obtaining a specific number of picks (n). The

length of the obtained yarn (in relaxed form) provides the original length (L_o) of an elastic weft yarn. While the length in stretched form (L) was directly calculated by multiplying the specific number of picks (n) by the width of the fabric.

$$\text{Stretch percentage (\%)} = \frac{L - L_o}{L_o} \times 100 \quad (3.1)$$

Where L_o is the length of elastic yarn in a relaxed state, while L is the length under a stretch state.

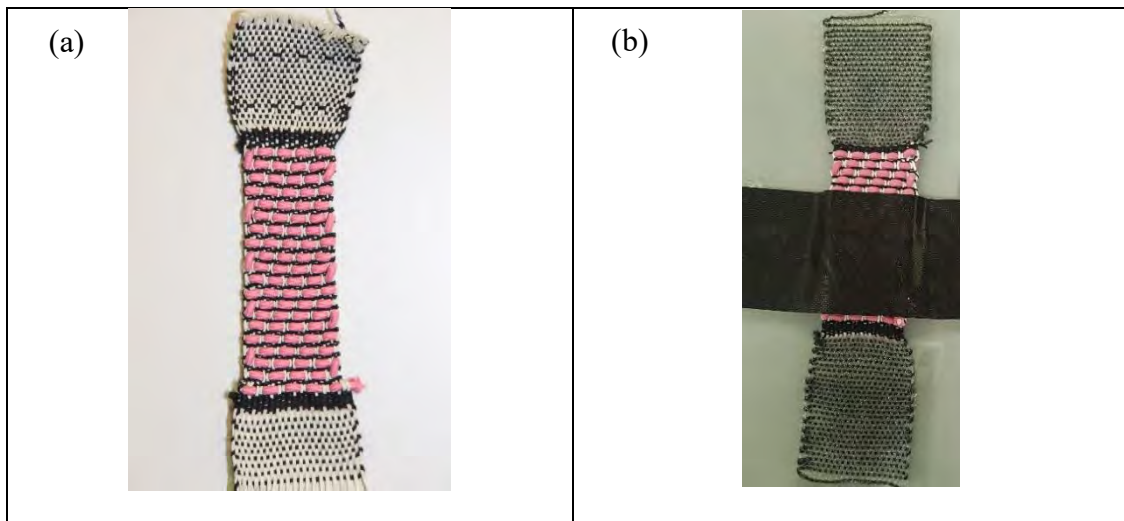
Table 3.2 Parameters of developed three-dimensional (3-D) auxetic woven fabrics.

Woven fabric made	Parameters considered				Properties		
	Sample Code	Binding yarn diameter (mm)	Number of weft repeats (elastic yarn)	Bending stiffness of binding yarn	Stretch percentage of elastic yarn (%)	Thickness of fabric sample (mm)	Weft density (PPI) of binding yarn
Fabric 1 (F1)	F1-S1	2	2	Low	14.8±3	4.5±0.2	8.5
	F1-S2	2.5	2	Low	14.8±3	5.5±0.3	7
	F1-S3	3	2	Low	14.8±3	6.3±0.3	5
Fabric 2 (F2)	F2-S1	2.5	1	Low	14.8±3	5.5±0.3	8
	F2-S2	2.5	3	Low	14.8±3	5.5±0.3	6
Fabric 3 (F3)	F3-S1	2.5	2	High	14.8±3	5.5±0.3	7
	F3-S2	2.5	3	High	14.8±3	5.5±0.3	6
Fabric 4 (F4)	F4-S1	2.5	2	Low	49.8±5	5.5±0.3	7
	F4-S2	2.5	3	Low	49.8±5	5.5±0.3	6

3.3 Experimental testing for auxetic effect

Since there is currently no existing standard for evaluating the auxetic performance of textile fabrics, the procedure utilized in previous studies⁴⁰ was adopted in this research. To ensure reliability, the narrow specimens were fabricated following the dimensions recommended by

the tensile standard ASTM D5035-11. During the initial tensile testing, sample slippage occurred within the grips due to the high strength of the warp yarns. To address this issue and enable accurate tensile testing, additional measures were taken. Firstly, the 3-D auxetic woven structure, as previously described, was developed only up to a length of 75 mm out of the total 150 mm. This covered the central gauge length portion, while the remaining length on each side was plain-woven specifically for machine clamping, as shown in Figure 3.8 (a). Secondly, the plain-woven sections of the samples intended for machine clamping were transformed into reinforced composites using an EL2 epoxy and AT30 slow hardener system as the matrix, as illustrated in Figure 3.8 (b). Lastly, aluminum tabs were glued to the plain-woven areas of the samples to prevent slippage or breakage during testing, as shown in Figure 3.8 (d). These tabs were manually applied using a two-part Scotch-Weld epoxy adhesive 2216, followed by a negative pressure vacuum compression molding process lasting 24 hours, as demonstrated in Figure 3.8 (c). To ensure statistical validity, a set of three replicate samples was prepared for the tensile test from each sample group to calculate average results.



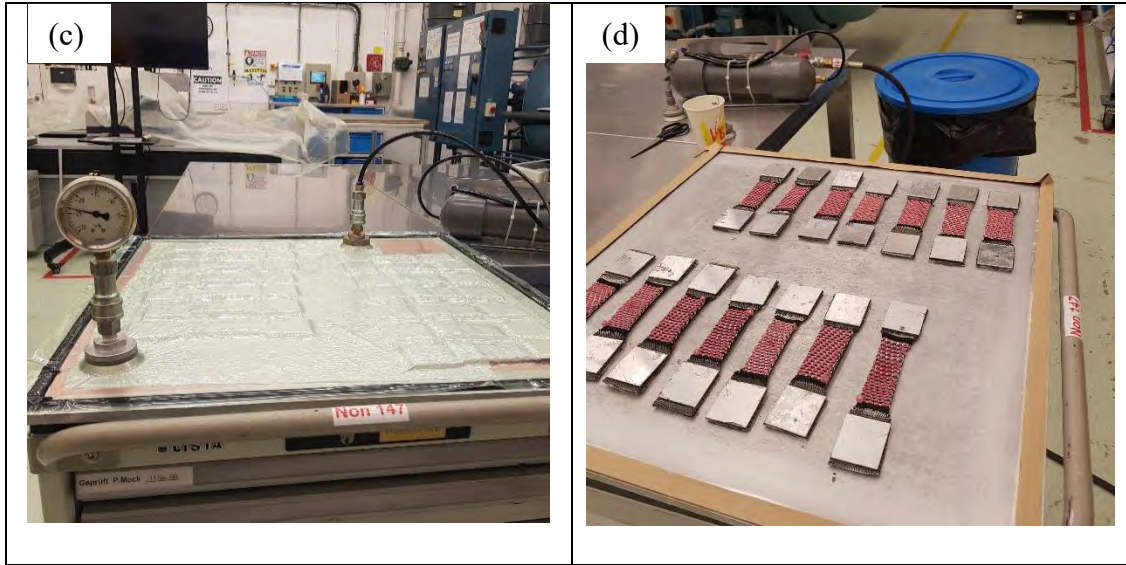


Figure 3.8 Process of preparing samples for tensile test; (a) 3-D woven sample, (b) application of epoxy to the clamping area, (c) application of tabs under negative pressure, (d) Samples with aluminum tabs.

Since all the samples were manufactured with a narrow width, the tensile test focused only on the length (warp) direction. After sample preparation, four dots were marked on each sample at 25 mm distance along both the length and width directions. These dotted visuals were used to measure longitudinal and lateral changes during the tensile test. The tensile test was conducted using an Instron 5982 universal tensile testing machine, which has a maximum capacity of 100 kN. To capture the deformation behavior of the samples during the test, a digital camera (Canon EOS 800D) was positioned approximately 30 cm in front of the fabric. The real testing environment and a schematic representation of the setup can be seen in Figures 3.9 (a) and (b), respectively. The tensile test was performed at a speed of 30 mm/minute. Images were extracted from the recorded video at intervals of 3 seconds, corresponding to 1.5 mm or 2% extension. Using screen ruler software, the distances between the two longitudinal and two lateral marks were measured in each image. Subsequently, the longitudinal and lateral strains

were calculated based on these measurements. By utilizing the formula provided in Equation (3.2), the PR could be determined from these lengthwise and crosswise strains.

$$\nu_{xy} = -\frac{\varepsilon_y}{\varepsilon_x} = -\frac{(Y' - Y_0)/Y_0}{(X' - X_0)/X_0} = -\frac{(Y' - Y_0)X_0}{(X' - X_0)Y_0} \quad (3.2)$$

Where ε_x is the strain in the longitudinal direction and ε_y is the strain in the lateral direction; Y_0 and X_0 are the initial width and length; Y' and X' are width and length under stretch state, respectively.

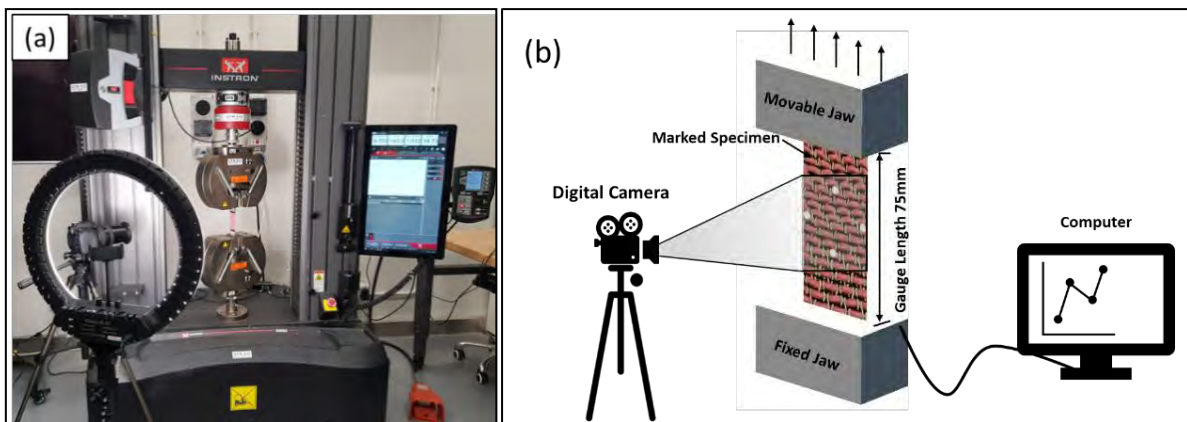


Figure 3.9 Poisson's ratio evaluation of three-dimensional auxetic woven fabric: (a) Tensile testing setup on UTM machine, (b) Schematic representation testing process.

3.4 Geometrical analysis

As mentioned earlier in the chapter, the modified auxetic structure of the 3-D woven fabric has a unique arrangement of warp and binding yarns that helps the structure to possess a negative Poisson's ratio (NPR) effect under deformation. Therefore, a unit cell representing the geometrical arrangement of warp and binding yarns within the structure is selected for geometrical analysis. From experimental testing, the change in geometry of the structure under tensile deformation was first observed. Then, a geometrical model was proposed based on the geometrical parameters of warp and binding yarns, the deformation behavior of the structure,

and the behavior of warp and binding yarns during deformation. Finally, the proposed geometrical model, based on semi-empirical equations, was validated by comparing Poisson's ratio results calculated through the developed model and the experimental results obtained from the 3-D auxetic woven fabrics. After successful validation, the model will be used to calculate and discuss critical parameters that affect the auxetic behavior of the structure. Thus, the geometrical analysis is believed to be helpful in predicting the auxetic behavior of 3-D woven fabrics with different geometrical parameters of the structure.

3.5 Finite element analysis

A finite element (FE) 3-D model of the auxetic woven fabric was developed to simulate the Poisson's ratio of the structure. For this purpose, the geometry of the structure, based on the real dimensions and arrangement of each yarn, was built in TexGen software. The geometry was then imported into Abaqus CAE for further simulation. The model was fed/guided with the practical scenario of the real fabric properties and conditions. For example, each yarn of the structure was defined with actual material properties, the interaction between the yarns was defined based on their behavior toward each other, etc. Then, a uni-axial tensile test was performed to simulate the Poisson's ratio of the structure. The model was then validated by comparing simulated and experimental results. The structure will be studied with different binding yarn properties once a good agreement is found between simulated and experimental results. The FE analysis can provide new insights and uncover fresh discussions regarding the auxetic behavior of the 3-D woven structure. Because the FE model provides an advantage over the geometrical model as it also considers the material properties along with the geometrical parameters.

3.6 Conclusions

This chapter explained the methodology adopted to design a novel 3-D auxetic woven fabric by modification of the existing conventional multi-layer through-the-thickness fabric structure. The process of modification is first outlined and then the concept of achieving auxetic effect in a modified 3-D structure is discussed. The development process of the designed auxetic structure using conventional non-auxetic yarns and a common weaving machine is described. The designed 3-D auxetic woven structure was successfully weaved into fabric form as it was intended to achieve an auxetic effect. For example, the developed fabrics possess a special unusual lateral crimp in the warp yarns that are expected to cause in-plane auxetic behavior when stretched longitudinally.

The preparation of fabric samples for conducting experimental tests is also explained, which includes Poisson's ratio analysis test and mechanical performance test. During the tensile testing, the deformation of the fabric was closely monitored to analyze the deformation of structural geometry and behavior of individual warp and binding yarn. The analysis was used to propose a geometrical model based on the pattern of warp and binding yarn forming unit cell of the geometry. In addition to fabric analysis, the warp, weft, and binding yarns were also tested to measure their properties that can be used as a reference for the material property setup in a finite element (FE) simulation. A 3-D FE model was then developed based on the geometry formed by the yarns defined with individual yarn properties. The geometrical and FE models developed for simulating the auxetic effect of the 3-D auxetic woven fabric are introduced in this chapter.

CHAPTER 4 DEFORMATION BEHAVIOR OF THREE-DIMENSIONAL AUXETIC WOVEN FABRICS

4.1 Introduction

The 3-D woven fabrics with auxetic property reported previously only exhibited a negative Poisson's ratio (NPR) in the out-of-plane direction (thickness direction). Because achieving an in-plane (width direction) auxetic behavior is challenging due to the complex architecture of the yarns in conventional 3-D woven fabrics. So, a novel approach, reported in the previous chapter, was employed to modify the conventional 3-D orthogonal through-the-thickness structure for visualizing auxetic geometry that could be able to produce an in-plane auxetic effect. The newly modified design of a 3-D woven structure was then developed using conventional yarns and a common weaving machine. In addition, a total of nine fabric samples, consisting of four types of fabrics, were produced to study the influence of different parameters on the auxetic behavior of the 3-D auxetic woven structure.

This chapter reports the evaluation of auxetic performance of the developed three-dimensional (3-D) auxetic woven fabrics. The samples based on the four parameters are tested and presented. The deformation behavior of samples and resistance to deformation is measured by performing a uni-axial constant strain-rate tensile test. Because of the narrow width of the woven fabrics, the tensile test was performed in the warp direction only. Further, the Poisson's ratio (PR) values of the samples are calculated from the deformation behavior under tension. The stress-strain curves and the PR-strain values are presented and discussed in detail here.

4.2 Typical deformation behavior

The geometry, number of ends, and material of the warp, weft, and binding yarns remained consistent across all developed samples. Based on this condition, it is expected that the tensile deformation behavior would be comparable among the samples. Therefore, sample F2-S2, which exhibited the maximum auxetic effect of $\nu = -1.61$, has been selected for discussion in order to understand the general tensile deformation and auxetic behavior of the 3-D narrow woven fabrics. Figure 4.1 shows the tensile stress, lateral strain, and Poisson's ratio as a function of tensile strain for this particular sample. Specifically, Figure 4.1 (a) showcases the tensile stress, Figure 4.1 (b) displays the lateral strain, and Figure 4.1 (c) illustrates the Poisson's ratio.

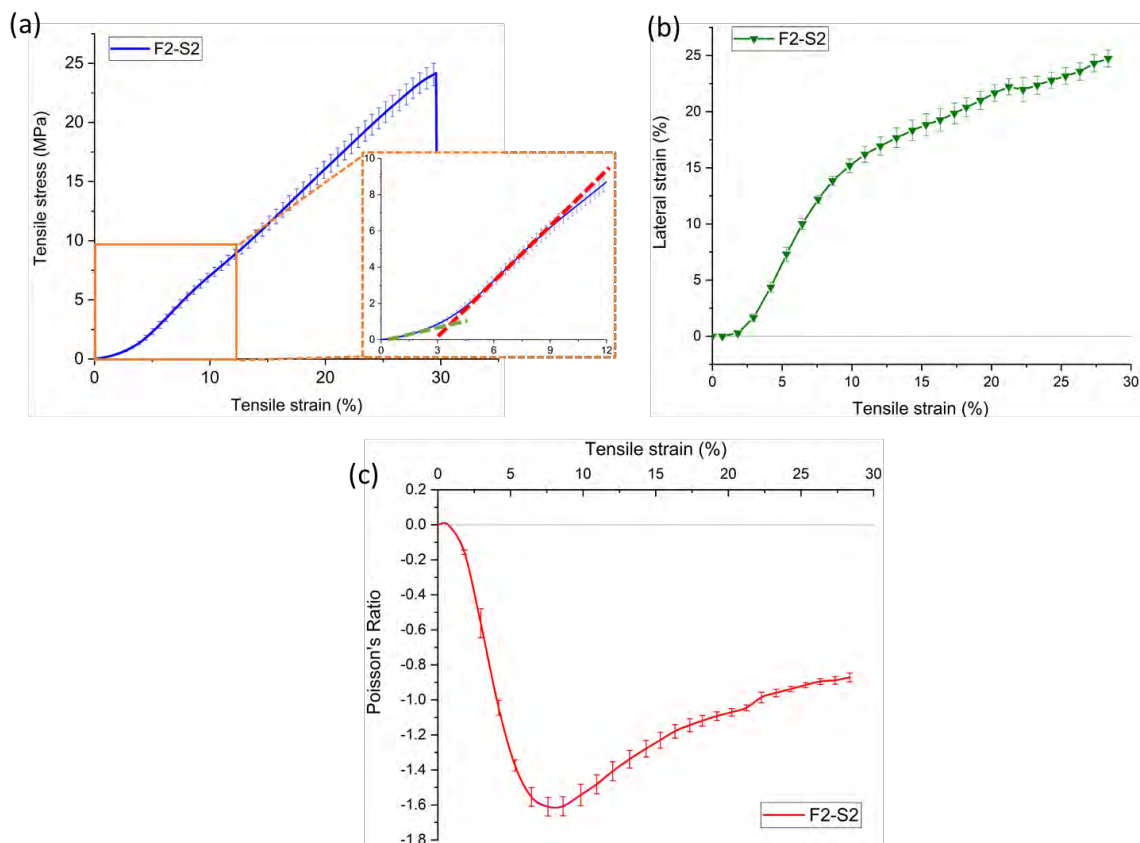


Figure 4.1 The deformation behavior of fabric F2-S2: (a) tensile stress-strain curve, (b) lateral-tensile strain curve, (c) Poisson's ratio-tensile strain curve.

From Figure 4.1 (a), it can be seen that the initial deformation behavior is nonlinear until reaching a 10% tensile strain, after which it transitions into linear deformation before eventual rupture. The initial nonlinear behavior can be further divided and explained into two distinct regions. Firstly, there is a low tensile modulus, resulting in the first nonlinear region ranging from 0% to 3% strain (indicated by the green dotted line). Then, the tensile modulus increases by approximately 3% to 10% tensile strain, leading to the second nonlinear region (indicated by the red dotted line). The initial low modulus is attributed to the adjustment of the warp yarns in the direction of tensile force. On the other hand, the second nonlinear region with a higher tensile modulus between 3% and 10% strain is caused by the decrimping of the warp yarns. This can be observed in Figure 4.2 (a-f), which displays the decrimping of warp yarns at various tensile strains. The images clearly indicate that the maximum decrimping occurs up to a 10% tensile strain. In addition to warp yarn decrimping, the resistance to deformation of the warp yarns also contributes to the high tensile modulus between 3% and 10% tensile strain. This is supported by the tensile load-strain curve of the warp yarn shown in Figure 4.3. Due to the braided structure of the warp yarn, the load-strain curve exhibits a steeper slope of up to 5% strain, followed by a lower slope. Similarly, the woven fabric demonstrates comparable deformation behavior to that of the warp yarn beyond a 3% tensile strain.

Since this study reports on the in-plane auxetic behavior of the fabric, which is independent of its thickness (out-of-plane). Therefore, the impact of tensile stretching on through-the-thickness property has not been evaluated. The lateral deformation of the fabric during tensile stretching directly correlates with its auxetic behavior. In Figure 4.1 (b), it is evident that the lateral strain increases as the tensile strain increases. Furthermore, the lateral strain demonstrates a more pronounced increase during the initial 8% of tensile strain. Afterward, the tensile strain is dominant, although the lateral strain continues to gradually increase. Figure 4.1

(c) demonstrates that the 3-D woven narrow fabric structure exhibits a noticeable NPR effect. However, the NPR is not constant. It initially increases until a tensile strain of 8% and then gradually decreases. Nevertheless, the Poisson's ratio remains largely negative until the fabric breaks. At the onset of tensile strain (up to approximately 2.5%), the Poisson's ratio is positive or zero due to the adjustment of the warp and elastic weft yarns, as explained in the tensile deformation behavior. However, beyond 2.5% tensile strain, the warp yarns start to decrimp, resulting in lateral deformation and an increase in fabric width. Consequently, the NPR effect increases with increasing tensile strain. When the tensile strain reaches approximately 8%, the warp yarns nearly straighten, and the fabric attains its highest NPR value of -1.61. It is worth noting that the maximum NPR is achieved at 8% tensile strain, whereas Figure 4.2 illustrates the decrimping phenomenon up to 10% tensile strain. By careful observation of the decrimping phenomenon, it can be assumed that more effective decrimping occurs during the initial 8% of tensile strain. Therefore, the lateral expansion of the fabric surpasses tensile stretching, resulting in a stronger NPR effect. However, beyond 8% tensile strain, decrimping continues at a reduced rate. As a result, tensile strain becomes the dominant factor over lateral expansion, leading to a decrease in NPR. Similarly, the decrease in NPR persists until the fabric breaks due to consistent tensile deformation, while experiencing less lateral expansion.

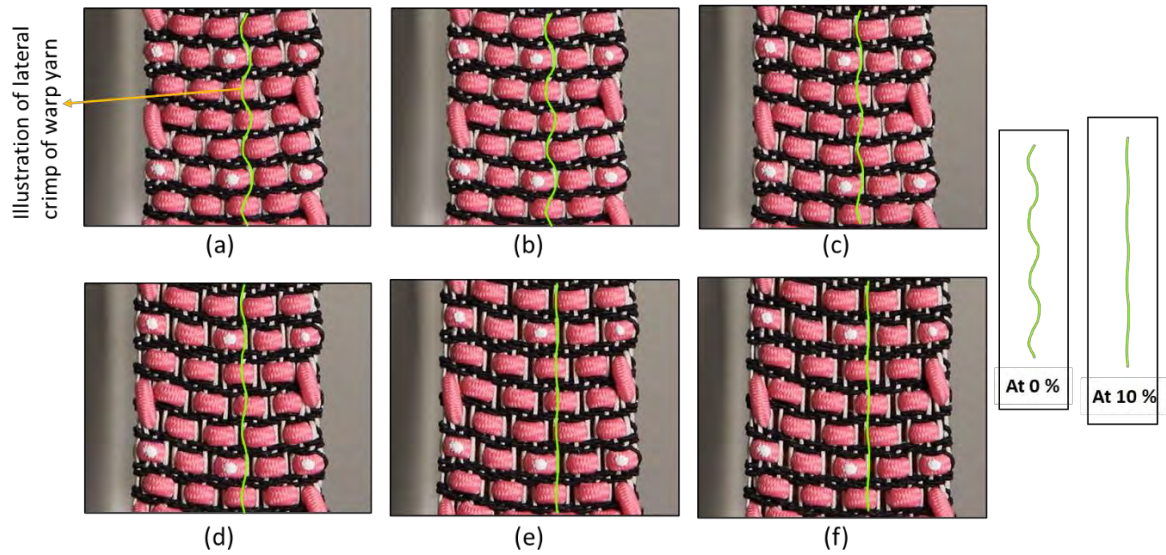


Figure 4.2 Decrimping of warp yarns under tensile tension at, (a) 0%, (b) 2%, (c) 4%, (d) 6%, (e) 8%, (f) 10%.

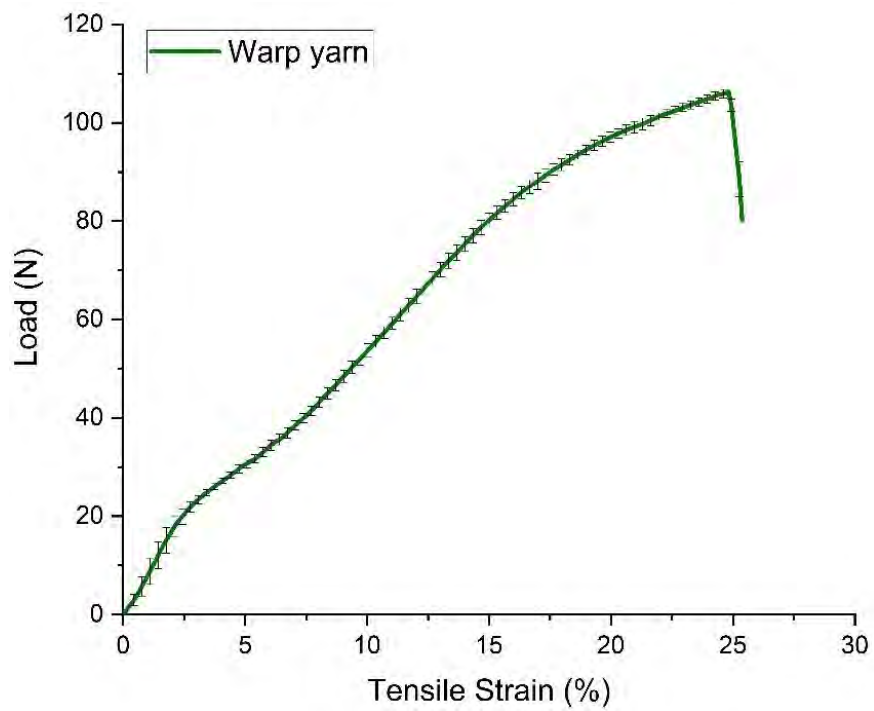


Figure 4.3 Tensile load-strain curve of single warp yarn.

4.2.1 Effect of binding yarn diameter on negative Poisson's ratio

To investigate the impact of binding yarn diameter on the structural appearance and auxetic performance of 3-D woven fabrics, three samples were developed. The binding yarn diameters used were 2 mm, 2.5 mm, and 3 mm. Physical analysis was conducted during and after the weaving process of all three samples. Sample F1-S3, with a binding yarn diameter of 3 mm, proved challenging to weave due to its higher bending stiffness¹¹². Consequently, it resulted in an irregular structure with unwanted gaps and increased width. Similarly, sample F1-S1, fabricated using a 2 mm binding yarn diameter, was evaluated. The smaller diameter of the binding yarn introduced less lateral crimp in the warp yarns. As a result, the low crimp in the warp yarns led to a smaller increase in lateral expansion when stretched longitudinally, resulting in a lower NPR. On the other hand, sample F1-S2, woven with a 2.5 mm binding yarn diameter, was found to be suitable in terms of the warp and elastic weft yarn diameters, as well as the overall structure. The fabric structure achieved using the 2.5 mm diameter yarn closely resembled the intended 3-D auxetic woven structure. Based on this experimental analysis, it is concluded that selecting an appropriate binding yarn diameter, considering the elastic weft and warp yarn diameters is crucial for achieving the desired results.

Interestingly, contrary to the general principle reported by other researchers⁵⁷, where increasing the binding yarn diameter should increase the NPR ratio by enhancing lateral crimp in the warp yarns, our findings showed a significant decrease in the NPR for the sample with a larger diameter (3 mm). This contrasting phenomenon can be attributed to the bending stiffness of the binding yarn, which also increases with diameter. Therefore, to achieve NPR results consistent with the aforementioned principle, it is essential to ensure that the bending stiffness of the yarn is comparable. Further evaluation of other parameters was carried out using a 2.5

mm diameter binding yarn, as sample F1-S2 exhibited a notable auxetic effect, as shown in Figure 4.4.

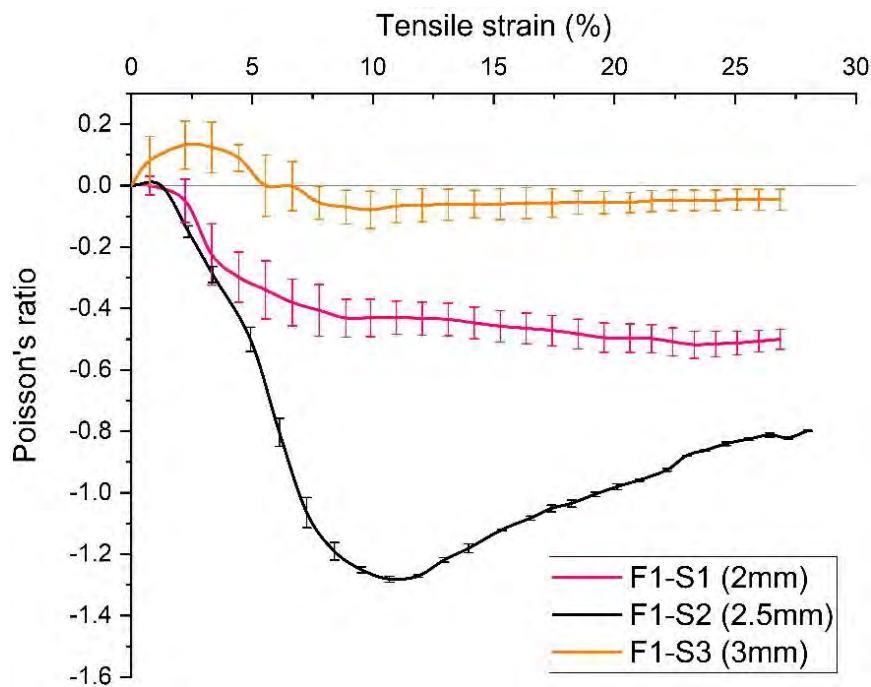


Figure 4.4 Poisson's ratio versus tensile strain curves by varying the diameter of the binding yarn.

4.2.2 Effect of repeat size of elastic yarn on negative Poisson's ratio

In order to investigate the influence of elastic weft yarn density on the auxetic behavior of the 3-D woven structure, two additional samples were created, each with a different repeat size of fine elastic yarn (single-repeat and three-repeats). For comparison, a fabric sample (F1-S2) from the initial set of fabrics was also included, which had two elastic weft yarn repeats. Thus, now the three fabric samples with repeat sizes of one (F2-S1), two (F1-S2), and three (F2-S2). The stress-strain curves and Poisson's ratio-tensile strain curves of these three samples are shown in Figure 4.5 (a) and (b), respectively. This analysis allows for a comprehensive examination of their mechanical behavior and the relationship between Poisson's ratio and tensile strain.

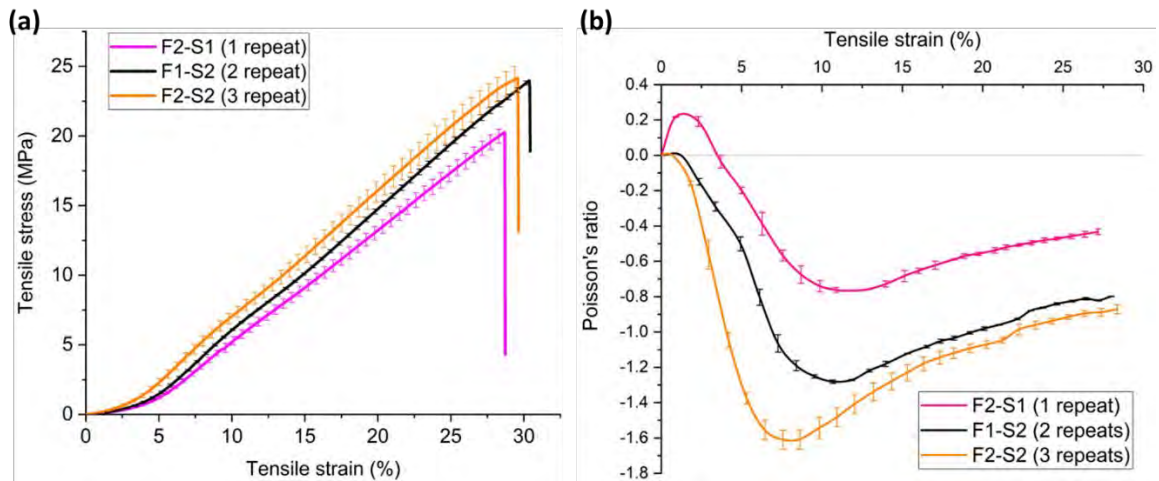


Figure 4.5 Tensile behavior of three-dimensional auxetic woven fabric: (a) stress-strain curves of woven fabric, (b) Poisson's ratio-tensile strain curves of woven fabric.

The tensile behavior of the three samples exhibits a similar trend, consistent with the typical deformation behavior of fabric. However, the magnitude of tensile strength varies depending on the elastic weft yarn density. Increasing the repeat size of the elastic yarn leads to an increase in tensile strength. Fabric F2-S2 demonstrates the highest tensile strength, followed by fabric F1-S2, and then fabric F2-S1. This increase in tensile strength can be attributed to the narrowing of the fabric during fabrication, which is a result of the higher restoring force exerted by the elastic yarns. Consequently, the cross-sectional area of the fabric sample decreases, resulting in an increased warp yarn density.

The NPR values of the three samples follow a similar trend of initially increasing and then decreasing, as observed in the typical deformation behavior. Among the three samples, F2-S2 and F1-S2 exhibit significantly higher NPR values compared to F2-S1. The lower NPR of F2-S1 may be due to the insufficient restoring force of the elastic weft yarn to induce enough crimp in the warp yarns. It is important to note that the elastic weft yarn in fabric F2-S1 was inserted with a higher stretch compared to F1-S2 and F2-S2. The intention was to achieve maximum

crimp in the warp yarns, but a single elastic weft repeat proved to be insufficient. The high-stretch insertion of the elastic yarn generates an inward force during the adjustment of the warp yarns at an initial tensile strain of up to 3%. This inward force leads to the formation of an initial positive Poisson's ratio spike in fabric F2-S1, which is not observed in fabric F1-S2 and F2-S2.

4.2.3 Effect of bending stiffness of coarse binding yarn on negative Poisson's ratio

The Poisson's ratio-tensile strain curves of the two samples developed with high stiffness (HS) binding yarn are plotted and compared with the Poisson's ratio-tensile strain curves of low stiffness (LS) binding yarn samples, as shown in Figure 4.6. The two samples made with HS binding yarn have different weft repeats of elastic yarn: two repeats (F3-S1) and three repeats (F3-S2). Both samples are compared with previously developed samples (F1-S2 and F2-S2) having similar configurations but only different binding yarn (low stiffness).

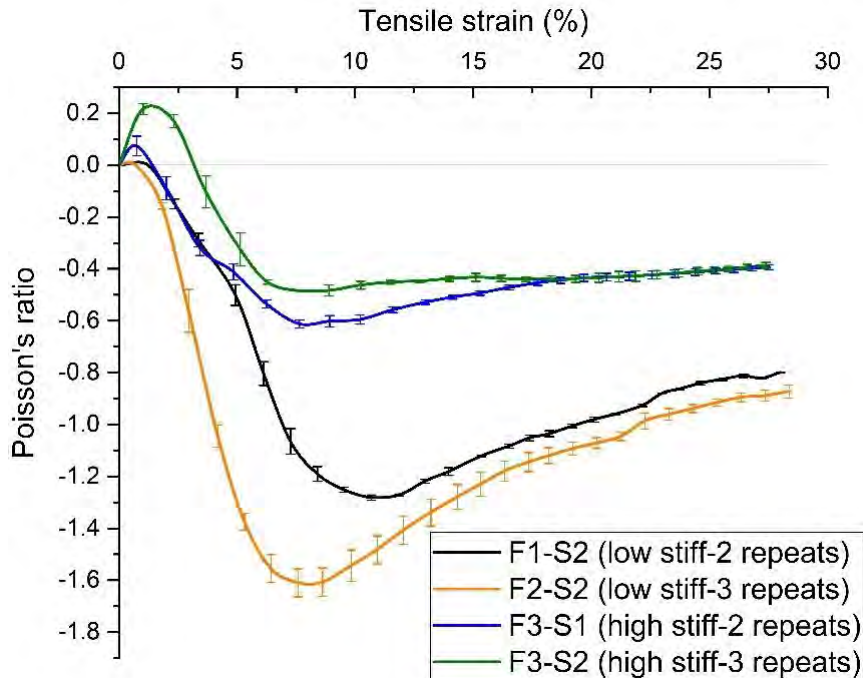


Figure 4.6 Comparison of Poisson's ratio-tensile strain curves of fabric with high-stiff and low-stiff binding yarn.

Figure 4.6 demonstrates the significant influence of the bending stiffness of the binding yarn on Poisson's ratio of auxetic woven fabrics. Samples constructed with low stiffness (LS) binding yarn exhibit an NPR approximately three times higher than those made with high stiffness (HS) binding yarn. This difference in NPR values can be attributed to the higher bending stiffness of the HS binding yarn, which cancels or resists the restoring force exerted by the elastic yarn during fabrication. Consequently, the induction of lateral crimp in the warp yarns is minimized, leading to a reduced auxetic effect. Additionally, in an attempt to overcome the resistance caused by the high bending stiffness of the binding yarn, an elastic weft yarn was inserted with a high stretch. Interestingly, due to the high-stretch insertion, the initial auxetic behavior of fabric F3-S2 (with three repeats of elastic yarn) is lower than that of fabric F3-S1 (with two repeats of elastic yarn), which contrasts with the auxetic behavior observed in fabric F1-S2 and F2-S2. The inclusion of three high-stretch elastic yarn repeats induces greater lateral shrinkage during the initial tensile strain, resulting in a reduced auxetic effect compared to the fabric with two repeats.

4.2.4 Effect of weft stretch (elastic yarn) during insertion

Based on the previous experimental findings, it is evident that the stretch percentage of the elastic weft yarn significantly influences the auxetic behavior of 3-D woven fabrics. Therefore, two additional samples (F4-S1 and F4-S2) were created, using high-stretch elastic weft yarn during the insertion process. The objective of this development was to further investigate the impact of the stretching percentage of the elastic weft yarn on the auxetic performance and deformation behavior of the 3-D woven fabric. Figure 4.7 (b) presents the tensile load versus strain curve of the elastic yarn. In addition, the Poisson's ratio versus tensile strain is plotted and compared with samples having a low-stretched elastic yarn, as shown in Figure 4.7 (a).

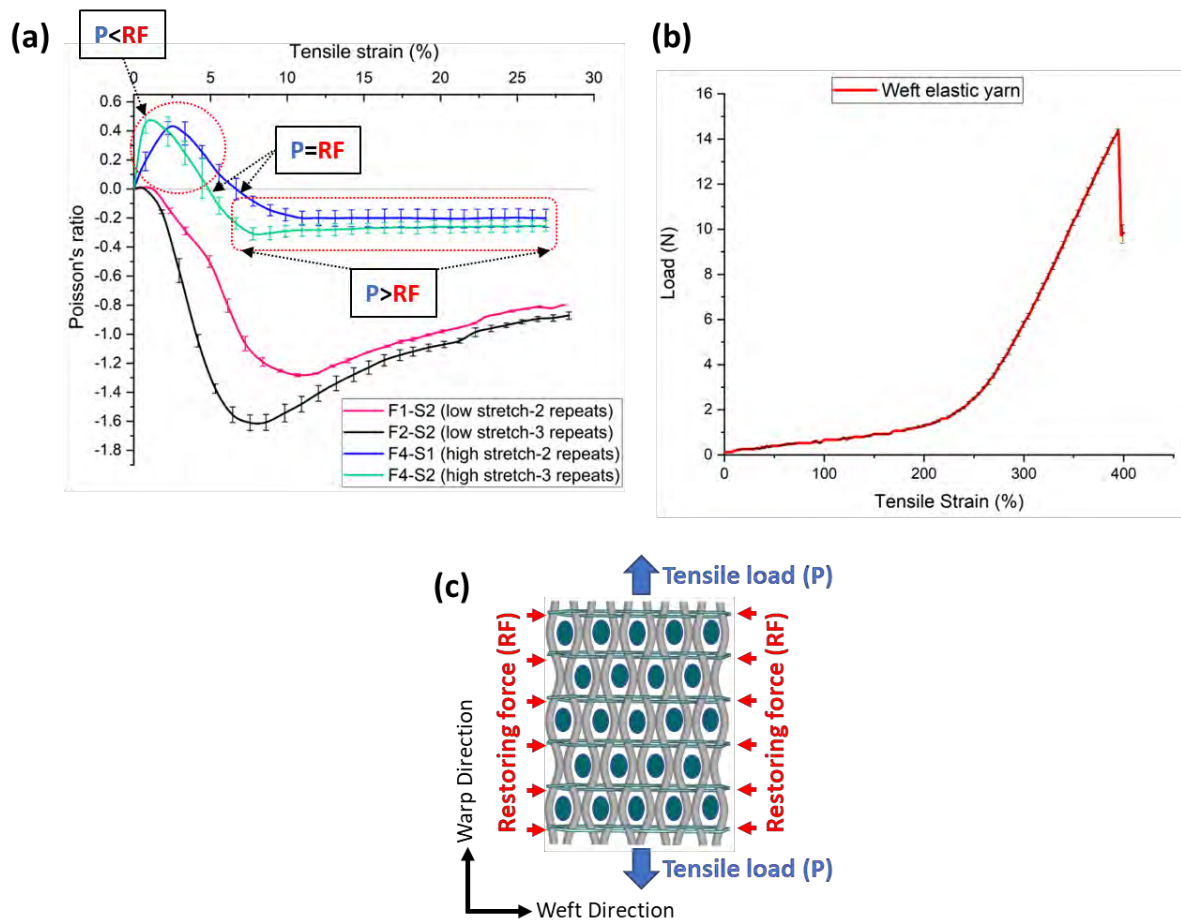


Figure 4.7 (a) Comparison of Poisson's ratio-tensile strain curves of fabric with high-stretch and low-stretch elastic weft insertion, (b) tensile load-strain curve of elastic weft yarn, (c) mechanism of tensile force and restoring force during deformation.

The influence of the stretch percentage and expansion of the elastic weft yarn on the NPR value of the 3-D woven fabric is shown in Figure 4.7 (a). Notably, samples F4-S1 and F4-S2, which were developed using a high-stretch percentage of elastic weft yarn (49.8%), exhibit significantly lesser auxetic behavior compared to samples created with a low-stretch percentage (14.8%). This difference can be attributed to the continuous restoring force exerted by the elastic weft yarns along the width direction of the fabric, as illustrated schematically in Figure 4.7 (c). Moreover, the restoring force increases with a higher stretching percentage of the elastic yarn, as observed in samples F4-S1 and F4-S2 where the elastic weft yarn is in a stretched state.

While the warp yarns try to decrimp and straighten under tension, the coarse binding yarns experience compression due to the elevated restoring force, rather than undergoing thorough decrimping to facilitate lateral expansion. As a result, a lower auxetic effect is achieved. Additionally, the initial positive Poisson's ratio region is wider and continues up to 5% and 7% axial strains for F4-S2 and F4-S1, respectively. This behavior can be attributed to the tensile load that is less effective than the elastic restoring force applied by the weft elastic yarns. However, beyond 5% and 7% axial strains, the tensile load becomes more effective than the elastic restoring force. Furthermore, the initial adjustment of the warp yarns allows the elastic restoring force of the weft yarns to shrink the fabric structure, resulting in a positive Poisson's ratio. A previous study also examined the impact of weft yarn type on the auxetic behavior of woven fabric and found that it significantly affects the NPR, particularly at low strains. They associated this observation with the expansion behavior of the elastic weft yarn⁵⁵.

4.3 Conclusions

In this chapter, the auxetic behavior of the 3-D woven fabrics developed by using conventional yarns and weaving machines was analyzed and discussed. The 3-D auxetic structure was comprised of the yarn system in x-(warp yarn), y-(weft yarn), and z-(binding yarn) directions. The auxetic property mainly comes from the unusual crimp of warp yarn in the lateral direction which triggers lateral expansion under longitudinal deformation. Due to the complicated design of the structure, many factors play an important role in its auxetic behavior. The effect of those design parameters was analyzed, including binding yarn diameter, repeat size of elastic weft yarn, bending stiffness of binding yarn, and stretch percentage of elastic weft yarn. Based on the tensile testing and Poisson's ratio results, the following conclusions can be drawn:

- The 3-D woven fabrics produced with non-auxetic warp, weft, and binding yarn exhibited an in-plane NPR effect. It was observed that under tensile deformation, the

warp yarns decrimp its lateral crimp and push the binding yarn in a lateral direction resulting in an auxetic effect.

- There is an abrupt increase in the auxetic behavior at the initial tensile strain, and then starts decreasing at the strain of 8% and later, but at a slower pace. The initial higher auxetic behavior is caused by the lateral decrimping process of warp yarns, climbing the NPR to its highest value of -1.6, however, at this point, the warp yarn is fully decrimped resulting in a decrease in NPR value.
- The initial higher auxetic behavior is considered important from the application point of view. For example, impact pressure involved in automotive seat belts requires an instantaneous response to the applied force to overcome the pressure.
- The use of an appropriate diameter for the binding yarn to the warp yarn was found critical. It is determined that a higher diameter of binding yarn can create problems during weaving while using less coarse binding yarn can only induce low lateral crimp to the warp yarns which produces a low auxetic effect.
- The role of elastic weft yarn is observed important because it provides a restoring force to the structure and thus keeps it shrink in a relaxed state. The number of elastic weft yarn repeats changes the magnitude of the restoring force. Therefore, to achieve auxetic behavior, the number of repeats should be enough to provide sufficient restoring force. Fabric with a single elastic weft repeat produced a less auxetic effect as compared to two repeats and three repeats. In addition, the stretching of elastic weft yarn during insertion highly affects the deformation behavior of fabric under tension. High stretch can reduce the auxetic effect of the 3-D auxetic woven fabrics.
- The bending stiffness of the binding yarn also affects the auxetic property. For example, the low bending stiffness of the binding yarn can produce a higher auxetic effect.

The analysis and discussion on the influential parameters of the structure give a strong understanding of the structure and its auxetic behavior. To explore more information on the fundamental geometrical analytics of structure, a geometrical model is developed based on a unit cell representing warp and binding yarn arrangement. The model will be explained in the next chapter.

CHAPTER 5 GEOMETRICAL ANALYSIS OF THREE-DIMENSIONAL AUXETIC WOVEN FABRICS

5.1 Introduction

In the previous chapter, the deformation behavior of the three-dimensional (3-D) auxetic woven fabrics under tensile stretching was analyzed and discussed. The fabric exhibited an auxetic effect in the in-plane direction due to the special geometrical configuration of the warp, weft, and binding yarns. The placement of binding yarns and the restoring force of elastic weft yarns crimp the warp yarns in the lateral direction which upon stretching causes lateral expansion and NPR effect is observed in the structure.

This chapter reports a geometrical analysis of the 3-D auxetic woven structure based on the geometrical arrangement of yarns that causes the NPR effect. After studying the deformation behavior of the structure in the previous chapter, a two-dimensional (2-D) unit cell that represents the whole structure in an in-plane (width and length) direction is selected for geometrical analysis. Based on the unit cell, a geometrical model is proposed by establishing a relationship between longitudinal and lateral deformations. The geometrical model (in the form of semi-empirical equations) will be used to calculate the Poisson's ratio against the longitudinal strain of the structure, and it will be validated by comparing it with the experimental results reported in the previous chapter. Furthermore, after validation, the model will also be used to predict the Poisson's ratio of the structure under different geometrical parameters of the structure.

5.2 Geometrical analysis

5.2.1 The architecture of a three-dimensional auxetic woven structure

A novel 3-D woven structure with in-plane negative Poisson's ratio (NPR) was developed by converting a conventional 3-D structure. The introduction of the auxetic effect involved a unique alteration to the binding yarn, warp yarns, and weft yarns, creating a distinctive geometry similar to a re-entrant hexagon, as shown in Figure 5.1(a). This modification was achieved by inducing lateral crimping in the warp yarns through the use of two weft yarn systems: a fine elastic yarn and a coarser binding yarn. In the weft direction, a coarser yarn with a 2 by 2 twill design was inserted as a binder, resulting in alternating voids within the warp yarns. Simultaneously, the fine elastic yarn was inserted multiple times in a stretched state. This caused the structure to shrink in a relaxed state, compelling the warp yarns to crimp laterally and fill those voids created by binding yarn. Consequently, the warp yarns exhibited an unusual crimp in the lateral direction. During longitudinal stretching of this structure, the warp yarns endeavored to straighten, thereby exerting a lateral force on the binding yarns. As a result, the structure expands in the lateral direction under tensile extension, leading to an in-plane auxetic effect.

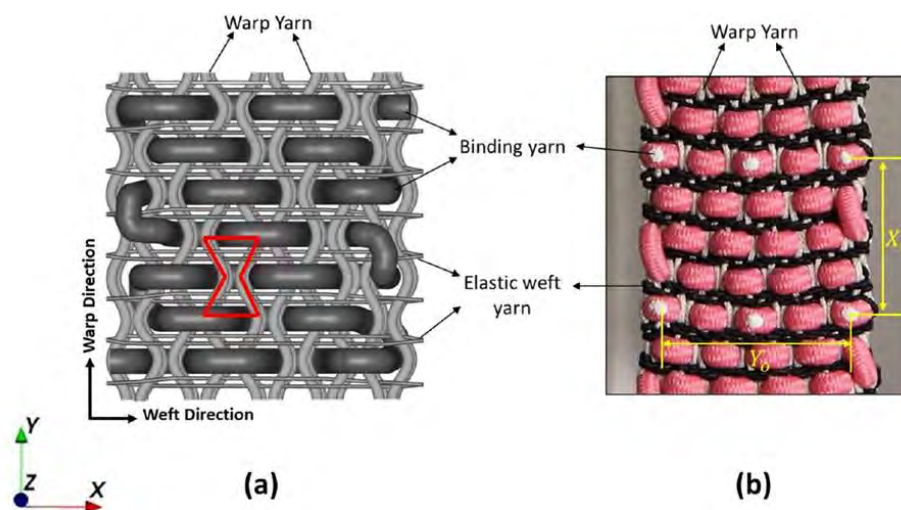


Figure 5.1 Three-dimensional auxetic woven structure: (a) schematic representation, (b) real

To fabricate the samples, a specific type of yarn was chosen for the warp, consisting of multi-filament polyester with a diameter of 0.7 mm. As for the weft, two types of yarn were selected: coarse binding yarn and fine elastic yarn. The coarse binding yarn was made of polyester-wrapped polyurethane (PU) and had a diameter of 2.28 mm, while the elastic yarn had a diameter of 0.62 mm. The selection of the warp yarn was based on its stability and strength since it would bear the tensile loading. Similarly, the coarse binding yarn was chosen to be solid yet flexible enough to facilitate orthogonal shaping during the weaving process. For the fabrication of the fabric samples, a semi-automatic weaving machine equipped with a dobby shedding mechanism and capable of accommodating up to 16 heald frames was utilized. During the fabrication process, the elastic yarn was inserted in a stretched form to induce shrinkage along the width direction when the sample was cut off from the loom. Figure 5.1(b) shows the developed fabric sample that was produced as a result of these modification steps.

In the previous chapter, the investigation of the 3-D auxetic woven structure focused on four highly influential parameters. It was observed that the NPR effect of the 3-D woven fabrics depends on the properties of the yarns, which pose limitations during the weaving process. For instance, achieving a favorable 3-D auxetic structure was challenging when using binding yarns with higher diameter and stiffness. Therefore, it is preferable to select fabric samples with optimized parameters that exhibit maximum auxetic effect. This selection facilitates the validation of the geometric model of the structure, as a sample demonstrating maximum auxetic behavior indicates the best formation of the auxetic geometry. Table 5.1 provides the physical properties of the three types of yarns used in the development of the samples. The bending stiffness of the binding yarn was determined using the beam deflection process, as reported by Msalilwa et al¹⁰⁸.

Table 5.1 Properties of the yarns used for sample preparation.

Yarn	Material	Type	Diameter (mm)
Warp yarn	Polyester multi-filament	Braided yarn	0.70
Binding yarn	Polyester-wrapped PU	Braided yarn	2.28
Elastic weft yarn	Polyester-wrapped PU	Braided yarn	0.25

5.2.2 Yarn analysis

During the experimental testing, it was observed that the auxetic effect of the 3-D woven fabric is closely linked to the extension of the elastic weft yarn and the compression of the binding yarn during tensile deformation. Therefore, incorporating these two yarn characteristics is crucial for developing an accurate geometric model.

To characterize the elongation of the elastic yarn, a simple tensile test was conducted using an Instron 5566 machine. The yarn was tightly clamped between the jaws with a gauge length of 100 mm between them. The lower jaw was stationary and the upper jaw moved at a constant strain rate of 30 mm/minute. The compression test on a binding yarn was performed to determine its compressive behavior. However, a conventional flat compression method could not be applied in this case since the compression of the binding yarn occurred due to the warp yarns. To address this, a customized assembly, as illustrated in Figure 5.2, was prepared for conducting the test. The assembly was designed in a manner that two pins, whose diameter matched that of the warp yarn, exerted compressive force on the binding yarn. The binding yarn was positioned perpendicular to the pins between the upper and lower parts of the assembly. Subsequently, the assembly was placed between the two platens of the Instron 5566 machine. For the compression test, the upper platen moved downward at a constant velocity of

1 mm/min while the lower platen remained fixed. Precise results were obtained using a higher sensitive load cell with a capacity of 50 N and an accuracy class of 0.5 %.

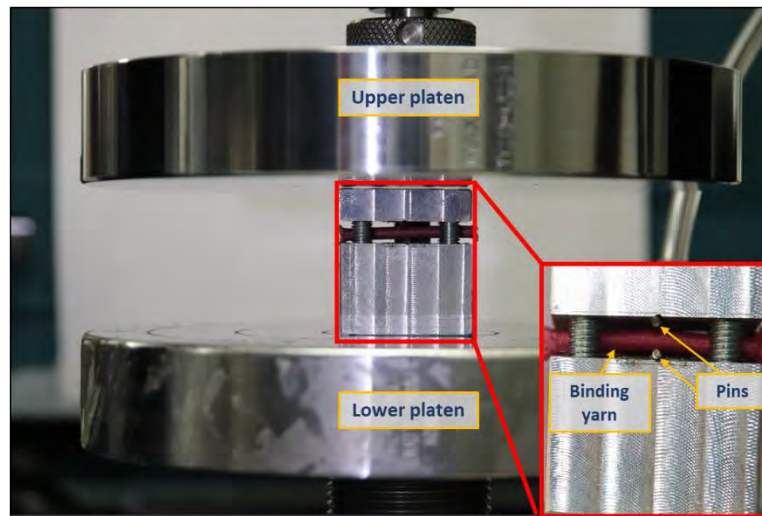


Figure 5.2 Binding yarn compression test assembly.

5.2.3 Geometric model

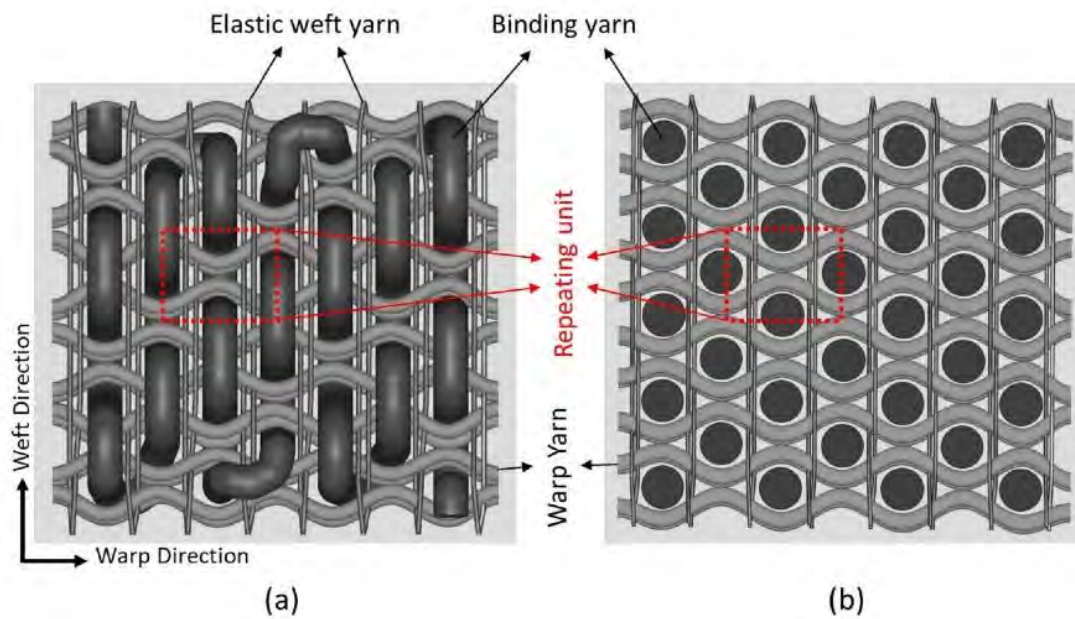


Figure 5.3 Schematic diagram of 3-D auxetic woven structure: (a) Top view, (b) Top cross-sectional view.

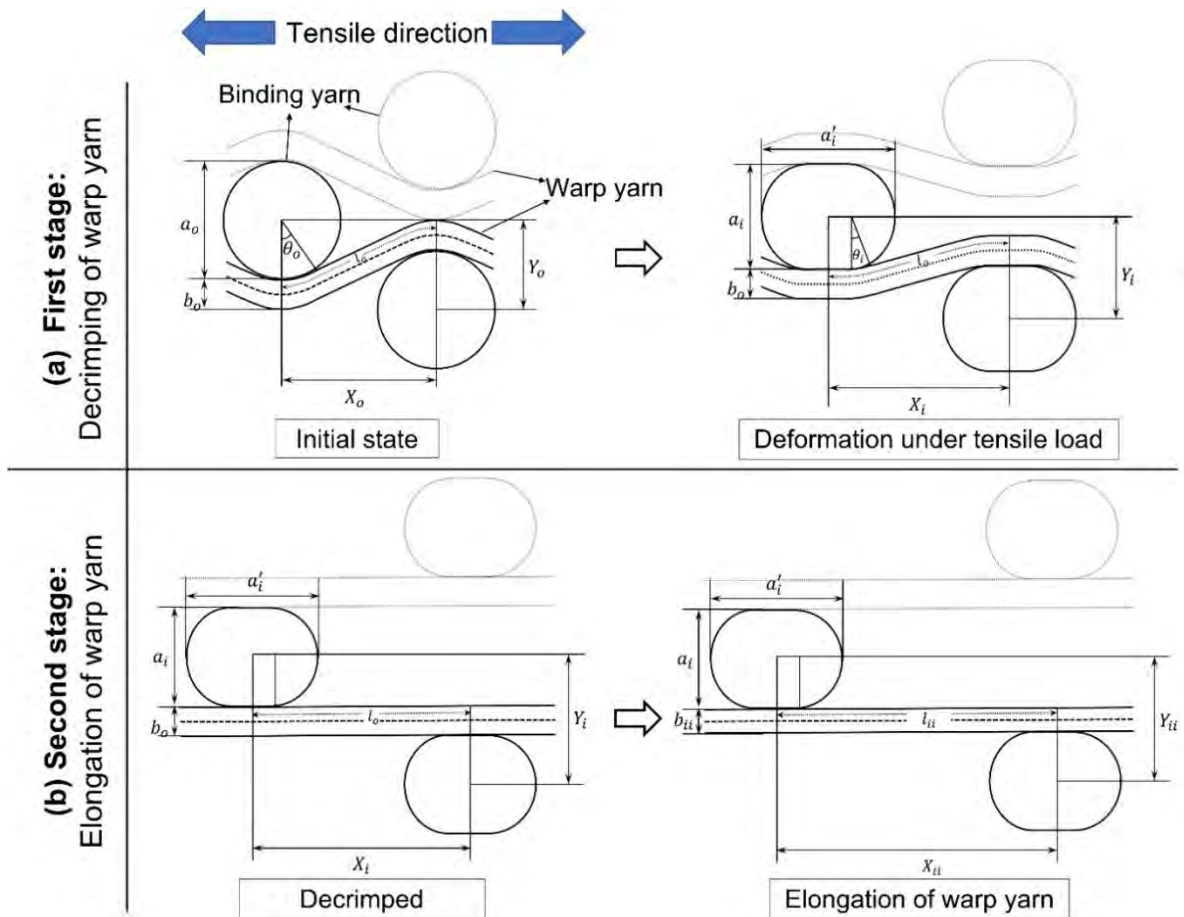


Figure 5.4 Geometrical model of 3-D auxetic structure: (a) decrimping of warp yarns under tensile deformation, (b) elongation of warp yarns under tensile deformation.

The parametric terms used in this geometrical analysis are given below:

a_o – initial diameter of binding yarn

b_o – diameter of warp yarn at the initial state and during the first stage of deformation

b_{ii} – diameter of warp yarn during the second stage of deformation

l_o – length of warp yarn between the centers of the two binding yarns at the initial state and during the first stage of deformation

l_{ii} – length of warp yarn between the centers of the two binding yarns during the second stage of deformation

θ_o – initial inclination angle of warp yarn

θ_i – inclination angle of warp yarn at a deform state

D_o – sum of the radii of binding yarn and warp yarn at the initial state

D_i – sum of the radii of binding yarn and warp yarn during the first stage of deformation

D_{ii} – sum of the radii of binding yarn and warp yarn during the second stage of deformation

a_i – height of binding yarn after compression

a'_i – width of binding yarn after compression

To propose a geometric model for the prediction of NPR of the 3-D auxetic woven structure, the below assumptions can be made on the basis of the deformation behavior of the 3-D auxetic woven fabric during the tensile deformation:

1. Figure 5.3 illustrates a unit cell geometry of the 3-D auxetic woven structure shown in Figure 5.4. It is assumed that the unit cell the whole structure and all the repeating unit cells are equal in size at pre-deform state and elongate symmetrically upon tensile extension.
2. The inclusion of an elastic weft yarn has been omitted from the geometric model since the warp and binding yarn analysis is enough to predict the auxetic behavior. Instead, its effect on the binding yarn, i.e., compression caused to the binding yarn by elastic weft yarn, has been included.

3. Initially, the binding yarn is circular in diameter and changes to a race-track shape due to the compression caused by the warp yarns and elastic weft yarns. However, the cross-sectional area is assumed to be constant all the time.
4. At the initial state, the warp yarns are laterally crimped by the binding yarns. It is assumed that at their contact point, the warp yarn is circular, while the non-contact part is straight and tangent to the circular part.
5. No slippage is considered at the contact points of binding and warp yarns during the deformation.
6. Under tensile deformation, the structure deforms in two stages: first, the decrimping stage (Figure 5.4(a)), and second, the elongation stage (Figure 5.4(b)) of warp yarn. Additionally, it is assumed that the cross-section of binding yarn only changes at the first stage of deformation, and the diameter of warp yarn remains unchanged. However, during the second stage, the diameter of the warp yarn changes due to elongation.
 - i. First stage: In this stage of deformation, the warp yarns gradually decrimped at a constant rate in response to the tensile strain. Here, the length and diameter of the warp yarn remain unchanged, as shown in Figure 5.4 (a). Based on the above assumptions, the geometrical model of the first stage can be re-illustrated in detail, as shown in Figure 5.5.

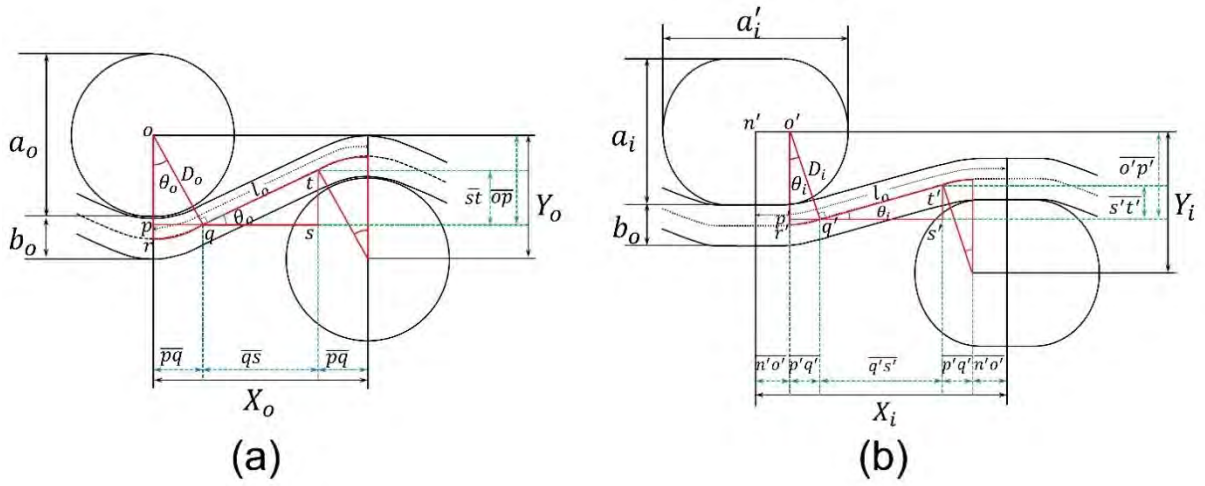


Figure 5.5 First stage of deformation of a unit-cell: (a) initial state, (b) deformed state.

From Figure 5.5, the initial distance (X_o) between the centers of two binding yarns is given by:

$$X_o = 2\overline{pq} + \overline{qs} \quad (5.1)$$

The length of \overline{pq} and \overline{qs} , in terms of yarn's parameters can be calculated by solving right-angle triangles Δopq and Δqst , respectively

$$\overline{pq} = D_o \sin \theta_o \quad (5.2)$$

$$\overline{qs} = \overline{qt} \cos \theta_o \quad (5.3)$$

Whereas:

$$\overline{qt} = l_o - 2\widehat{qr} \quad (5.4)$$

$$\widehat{qr} = D_o \theta_o \quad (5.5)$$

By solving Equation (5.3-5.5), we get

$$\overline{qs} = (l_o - 2D_o \theta_o) \cos \theta_o \quad (5.6)$$

Substituting Equations (5.2) and (5.6) into Equation (5.1) gives the following relation

$$X_o = 2D_o \sin \theta_o + (l_o - 2D_o \theta_o) \cos \theta_o \quad (5.7)$$

Likewise, the initial height (Y_o) between the centers of two binding yarns is given as

$$Y_o = 2\overline{op} - \overline{st} \quad (5.8)$$

By solving Δopq and Δqst , the following relation can be made for \overline{op} and \overline{st}

$$\overline{op} = D_o \cos \theta_o \quad (5.9)$$

$$\overline{st} = \overline{qt} \sin \theta_o \quad (5.10)$$

Substituting Equations (5.4) and (5.5) into Equation (5.10) gives the following Equation

$$\overline{st} = (l_o - 2D_o \theta_o) \sin \theta_o \quad (5.11)$$

Substituting Equations (5.9) and (5.11) into Equation (5.8) gives the following relation

$$Y_o = 2D_o \cos \theta_o - (l_o - 2D_o \theta_o) \sin \theta_o \quad (5.12)$$

This relation can be used for calculating the initial height (Y_o) using the inclination angle (θ_o), however, Y_o can also be calculated simply by using the following relation.

$$Y_o = \frac{a_o}{2} + b_o \quad (5.13)$$

Similarly, the distance between the centers of the two binding yarns at a deformed state (X_i), is given below.

$$X_i = 2\overline{p'q'} + \overline{q's'} + 2\overline{n'o'} \quad (5.14)$$

Whereas:

$$\overline{n'o'} = (a'_i - a_i)/2 \quad (5.15)$$

By solving the right triangles $\Delta o'p'q'$ and $\Delta q's't'$, the lengths $\overline{p'q'}$ and $\overline{q's'}$ can be expressed in Equations (5.16) and (5.17), respectively.

$$\overline{p'q'} = D_i \sin \theta_i \quad (5.16)$$

$$\overline{q's'} = [l_o - 2D_i\theta_i - (a'_i - a_i)] \cos \theta_i \quad (5.17)$$

Substituting Equations (5.15-5.17) into Equation (5.14) gives the following relation

$$X_i = 2D_i \sin \theta_i + [l_o - 2D_i\theta_i - (a'_i - a_i)] \cos \theta_i + (a'_i - a_i) \quad (5.18)$$

The height, Y_i , between the coarse binding yarns can be expressed mathematically as,

$$Y_i = 2\overline{\sigma'p'} - \overline{s't'} \quad (5.19)$$

From $\Delta o'p'q'$ and $\Delta q's't'$, the $\overline{\sigma'p'}$ and $\overline{s't'}$ can be expressed in the following Equations

$$\overline{\sigma'p'} = D_i \cos \theta_i \quad (5.20)$$

$$\overline{s't'} = (l_o - 2D_i\theta_i - (a'_i - a_i)) \sin \theta_i \quad (5.21)$$

Substituting Equations (5.20) and (5.21) into Equation (5.19) gives the following relation

$$Y_i = 2D_i \cos \theta_i - [l_o - 2D_i\theta_i - (a'_i - a_i)] \sin \theta_i \quad (5.22)$$

As both the lateral and longitudinal strains at initial and deform states are known, the Poisson's ratio (ν_i) for the first stage of deformation can be calculated. By putting Equations (5.7), (5.12), (5.18), and (5.22) in Equation (3.2), we get the following relation

$$\nu_{xy}^{(i)} = \frac{[2D_i \cos \theta_i - [l_o - 2D_i\theta_i - a'_i + a_i] \sin \theta_i - 2D_o \cos \theta_o + (l_o - 2D_o\theta_o) \sin \theta_o] \times [2D_o \sin \theta_o + (l_o - 2D_o\theta_o) \cos \theta_o]}{[2D_i \sin \theta_i + [l_o - 2D_i\theta_i - a'_i + a_i] \cos \theta_i + a'_i - a_i - 2D_o \sin \theta_o - (l_o - 2D_o\theta_o) \cos \theta_o] \times [2D_o \cos \theta_o - (l_o - 2D_o\theta_o) \sin \theta_o]} \quad (5.23)$$

- ii. Second stage: As the warp yarn is fully decrimped in the first stage, it will now elongate due to the effective tensile deformation. In addition, the diameter of warp yarn will also decrease due to axial deformation, as shown in Figure 5.6.

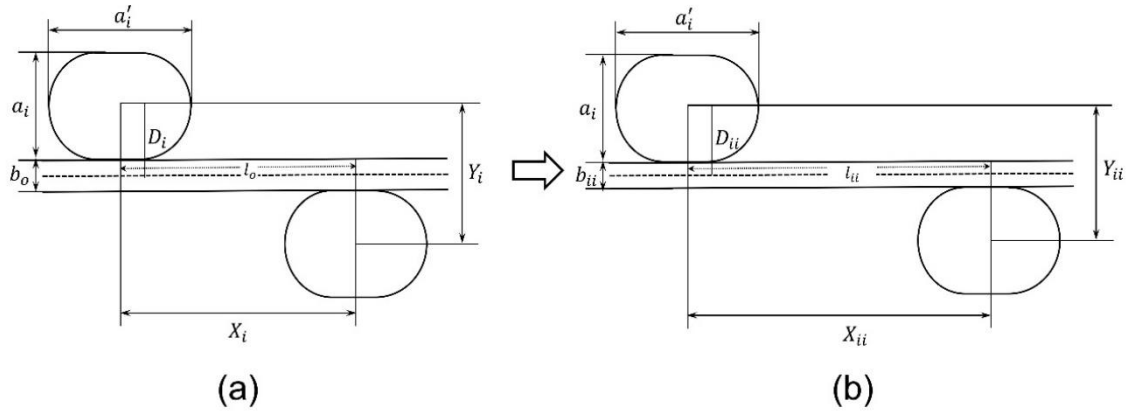


Figure 5.6 Second stage of deformation of a unit-cell: (a) decrimped, (b) elongation of warp yarn

It is important to consider that the height and width of the race-track-shaped binding yarns will remain unchanged. However, based on assumption 6, during the second stage of deformation, the length and diameter of the warp yarn will undergo changes. As a result, the sum of the radii of the warp yarn and binding yarn is denoted as D_i , will be changed to D_{ii} , as expressed in Equation (5.24). Similarly, the length of the warp yarn, initially l_o , will be modified to l_{ii} , as indicated in Equation (5.25).

$$D_{ii} = \frac{a_i}{2} + \frac{b_{ii}}{2} \quad (5.24)$$

$$l_{ii} = l_o + \Delta l \quad (5.25)$$

Where Δl is the change in the length of warp yarn, it can be calculated from the magnitude of tensile extension.

As the warp yarns are decrimped and straight, the inclination angle (θ_i) become "0". By putting $\theta_i = 0$ in Equations (5.18) and (5.22), we get the following relations, respectively

$$X_{ii} = l_{ii} \quad (5.26)$$

$$Y_{ii} = 2D_{ii} \quad (5.27)$$

As the lateral and longitudinal strains at the second stage of deformation are known, the Poisson's ratio ν_{ii} for the second stage of deformation can be calculated by putting Equations (5.7), (5.12), (5.26), and (5.27) in Equation (3.2).

$$\nu_{xy}^{(ii)} = -\frac{[2D_{ii} - 2D_o \cos \theta_o + (l_o - 2D_o \theta_o) \sin \theta_o] \times [2D_o \sin \theta_o + (l_o - 2D_o \theta_o) \cos \theta_o]}{[l_{ii} - 2D_o \sin \theta_o - (l_o - 2D_o \theta_o) \cos \theta_o] \times [2D_o \cos \theta_o - (l_o - 2D_o \theta_o) \sin \theta_o]} \quad (5.28)$$

5.2.4 Experimental observations of geometric parameters and model validation

5.2.4.1 Determining the Poisson's ratio during the first stage of deformation

To validate the geometric model, it is essential to ensure that the calculated tensile strain and Poisson's ratio results are based on the same geometric parameters as those of the developed 3-D woven fabric sample. Determining all the parameters at the initial state is relatively straightforward. For instance, the radii of the coarse binding yarn ($\frac{a_o}{2}$) and warp yarn ($\frac{b_o}{2}$) can be obtained from Table 5.1. The initial distance (X_o) between two coarse binding yarns can be calculated by dividing the total length of a sample by the total repeats of the coarse binding yarn. The initial height (Y_o) can be determined using Equation (5.13). With these parameters known, the initial inclination angle (θ_o) and length (l_o) of the warp yarn can be calculated using Equation (5.7) and Equation (5.12), respectively.

On the other hand, calculating the compression effect of the binding yarn in a deformed state is more complex. According to assumption (3), the cross-section of the binding yarn changes to a race-track shape due to the compression of the warp yarns caused by the restoring force of the elastic weft yarns. Therefore, it is necessary to first calculate the magnitude of the restoring force of elastic yarn. Due to lateral expansion of the structure during tensile deformation, the force applied by the elastic weft yarn increases. Hence, calculating the lateral expansion of the structure can provide information on the force by the elastic yarns. To do so, the lateral expansion of the structure can be calculated without assuming compression of the coarse

binding yarn. Equations (5.7), (5.12), (5.18), and (5.22) can be used for this purpose, supposing $a'_i = a_i = a_o$. Once the lateral expansion of the structure is calculated, the amount of force applied by the elastic weft yarn can be calculated from the force-strain curve of the elastic weft yarn, as illustrated in Figure 5.7. Finally, the compression induced in the binding yarn at a given force can be determined from the force-compressive extension curve of the coarse binding yarn, as shown in Figure 5.8.

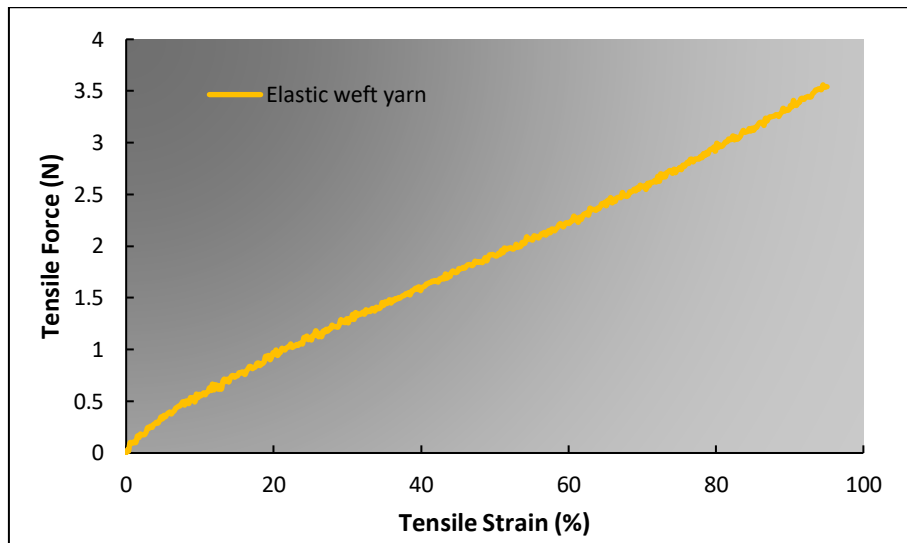


Figure 5.7 Tensile force-strain curve of elastic weft yarn.

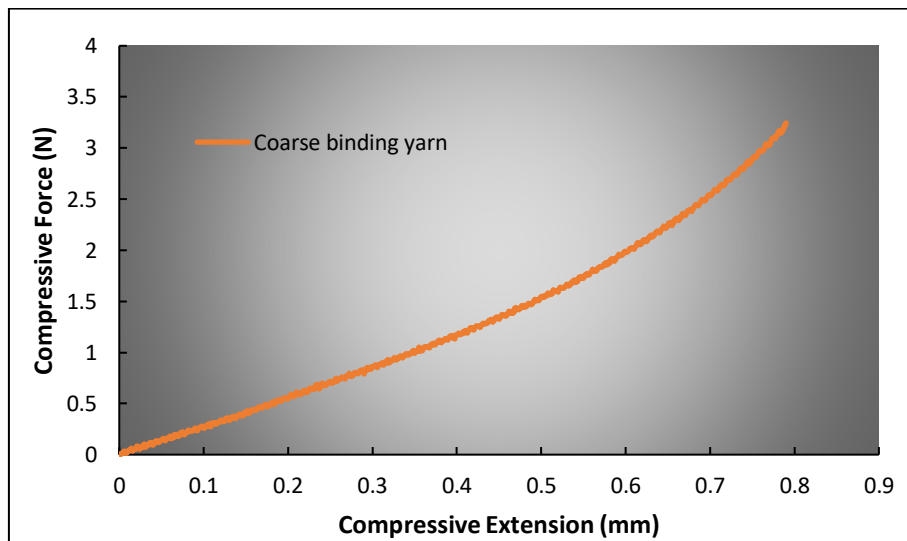


Figure 5.8 Compressive force-extension curve of coarse binding yarn.

After the compression to the binding yarn at the deform state is calculated, the unknown parameters such as the final height (a_i) and width (a'_i) of the compressed race-track-shaped binding yarn can be determined based on assumption 3. With these known values, the inclination angle (θ_i) can be calculated at a specific tensile deformation (X_i) using Equation (5.18). Since all the variables are now calculated, the Poisson's ratio (ν_i) during the first stage of deformation can be determined using Equation (5.23). The calculated values of Poisson's ratio for the first stage of deformation can be found in Table 5.2.

5.2.4.2 Determining the Poisson's ratio during the second stage of deformation

The inclination angle (θ_i) reaches 0 when the tensile strain reaches 8.07%, indicating that the warp yarn becomes fully straight. At this point, the second stage of deformation starts. This specific point is referred to as the "critical strain," and the corresponding Poisson's ratio is known as the "critical Poisson's ratio." After reaching the critical strain, the warp yarns elongate at the same rate as the tensile strain, which is a known parameter. However, it is necessary to calculate the decrease in the diameter of the warp yarn (b_{ii}) at a particular tensile strain. To achieve this, a customized tensile test was conducted on the warp yarn, where the cross-head of the universal testing machine was paused after every 1% strain for 10 seconds to measure the diameter of the warp yarn using a thickness gauge. The variation trend of the warp yarn's diameter (b_{ii}) with respect to the tensile strain (ε) is illustrated in Figure 5.9. It can be observed that the change in b_{ii} follows a polynomial trend. Therefore, based on a second-degree polynomial trend, the following assumption can be established

$$b_{ii} = m_1 \varepsilon_i^2 + m_2 \varepsilon_i + m_3 \quad (5.29)$$

Where ε_i is the tensile strain and m_1 , m_2 , and m_3 are the constants that can be determined from the experimental results of the warp yarn. Substituting Equation (5.29) in Equation (5.24) gives the following relation

$$D_{ii} = \frac{a_i}{2} + \frac{m_1 \varepsilon^2 + m_2 \varepsilon + m_3}{2} \quad (5.30)$$

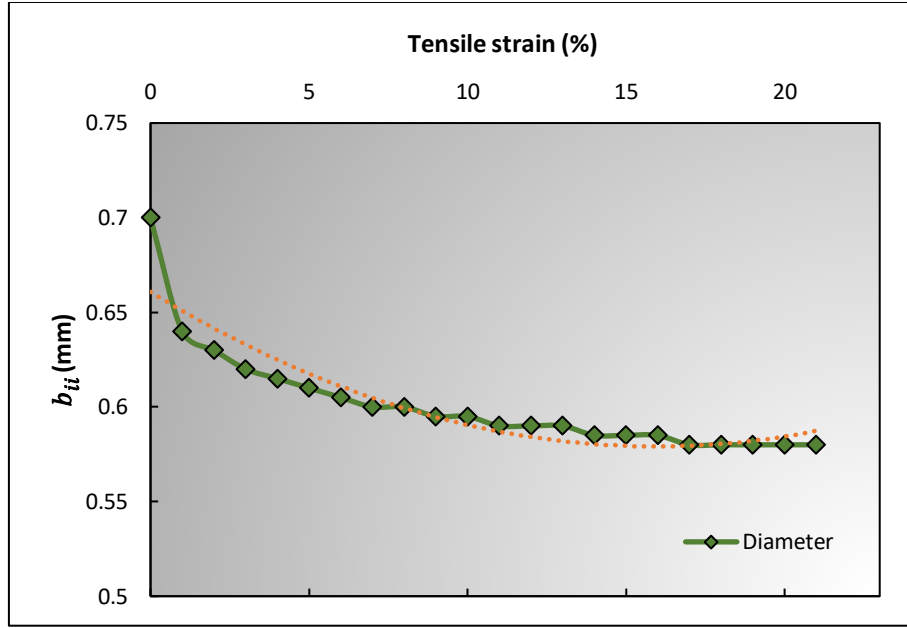


Figure 5.9 Trend of the diameter of warp yarn against the tensile strain.

Based on Equation (5.30), the parameter a_i is known, while the remaining three constants are determined experimentally from the relationship between the diameter of the warp yarn and the tensile strain. These constants are calculated as follows: $m_1 = 0.003$, $m_2 = -0.0102$, and $m_3 = 0.6608$.

Once the sum of the radii of the binding yarn and warp yarn (D_{ii}) is known at a particular tensile extension (X_{ii}), the Poisson's ratio for the second stage of deformation can be calculated using Equation (5.28). The yarn's parameters, the structural variables of the geometric model, and the calculated Poisson's ratios are presented in Table 5.2.

It is important to note that if the tensile strain is lower than the critical tensile strain, the Poisson's ratio $\nu_{xy}^{(i)}$ (calculated using Equation (5.23)) will be used. However, if the tensile strain

exceeds the critical value, the Poisson's ratio $\nu_{xy}^{(ii)}$ (calculated using Equation (5.28)) will be used.

Table 5.2 Structural parameters and the calculated Poisson's ratio results of 3-D auxetic woven fabric.

State	Tensile strain (%)	a_o or a_i (mm)	b_o or b_{ii} (mm)	D_o or D_i or D_{ii} (mm)	X_o or X_i or X_{ii} (mm)	Y_o or Y (mm)	θ_o or θ_i (rad)	l_o or l_{ii} (mm)	PR	
Initial state	0	2.28	0.70	1.490	3.000	1.840	0.460	3.242	0	
Under tensile deformation	First stage	1	2.19	0.70	1.447	3.030	1.845	0.436	3.242	-0.29
		2	2.12	0.70	1.410	3.060	1.862	0.408	3.242	-0.61
		3	2.05	0.70	1.377	3.090	1.890	0.376	3.242	-0.90
		4	2.00	0.70	1.351	3.120	1.933	0.337	3.242	-1.26
		5	1.93	0.70	1.316	3.150	1.974	0.295	3.242	-1.46
		6	1.87	0.70	1.286	3.180	2.037	0.243	3.242	-1.79
		7	1.78	0.70	1.245	3.210	2.108	0.177	3.242	-2.08
		8	1.62	0.70	1.158	3.240	2.226	0.047	3.242	-2.61
	8.07	1.62	0.70	1.113	3.242	2.226	0	3.242	-2.59	
	Second stage	9	1.62	0.62	1.110	3.270	2.221	0	3.27	-2.33
		10	1.62	0.61	1.108	3.300	2.216	0	3.3	-2.07
11		1.62	0.60	1.105	3.330	2.211	0	3.33	-1.86	
And so on										

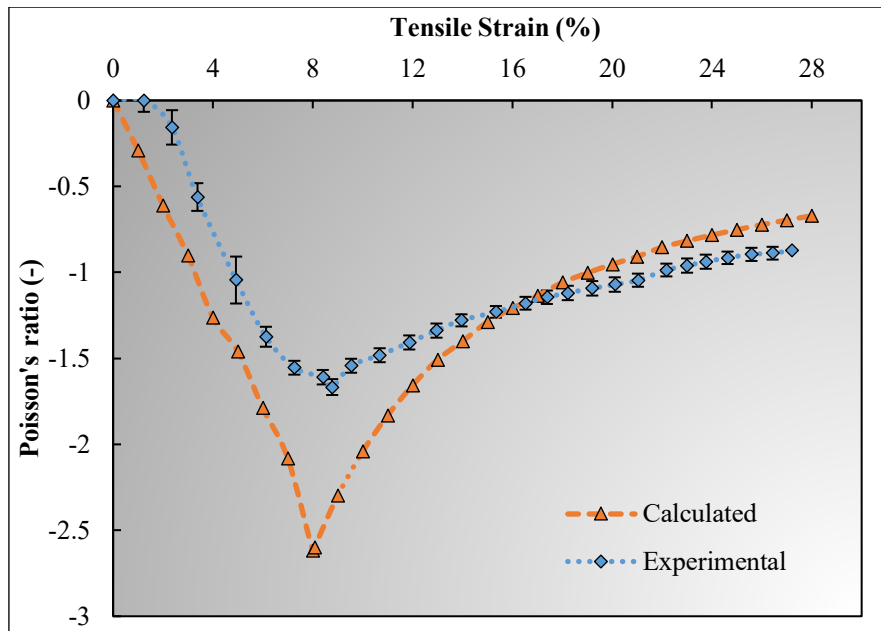


Figure 5.10 Comparison of calculated and experimental results of Poisson's ratio against the tensile strain.

Figure 5.10 illustrates Poisson's ratio curves plotted against the tensile strain for the developed 3-D auxetic woven fabric, along with the corresponding calculated results obtained from the geometric model. It can be observed that both the experimental and calculated Poisson's ratios exhibit a similar trend. This agreement between the calculated and experimental data confirms the reliability of the geometric model. Initially, the Poisson's ratio decreases and reaches a minimum at a tensile strain of 8.07%. This behavior can be attributed to the lateral crimp of the warp yarn, which plays a significant role in the fabric's auxetic response under tensile extension. As the tensile deformation progresses, the warp yarn starts to decrimp, leading to a decrease in the Poisson's ratio. This decrimping effect continues until the warp yarn becomes fully straight, which occurs at the 8.07% tensile strain. After reaching this critical point, there is no further decrimping of the warp yarn, indicating that there will be no additional lateral extension with continued tensile extension. However, the diameter of the warp yarns decreases

due to longitudinal extension. Consequently, the Poisson's ratio increases beyond the 8.07% tensile strain as a result of these changes in the warp yarn's geometry.

5.2.5 Prediction of auxetic behavior

5.2.5.1 Effect of binding yarn compression

In a previous study¹¹³, it was claimed that the binding yarn undergoes compression during tensile extension. The experimental evaluation of the fabric structure confirmed the occurrence of compression, attributed to the elastic yarn's restorative force. However, the extent to which the compression of the binding yarn affects the auxetic behavior remained unanswered. By contrast, the geometrical model can assess the impact of binding yarn compression on the auxetic behavior of the 3-D woven fabric. Figure 5.11 shows the Poisson's ratio versus tensile strain curves. The two curves, labeled with compression (W-C) and without compression (W/O-C), are calculated using the geometrical model while keeping all parameters constant except for the effect of binding yarn compression. In the case of W/O-C, it is assumed that the diameter of the binding yarn (a_o) remains unchanged during tensile strain. On the other hand, for W-C, the diameter of the binding yarn decreases as the structure elongates both longitudinally and laterally. It is important to note that the compression experienced by the binding yarn is determined experimentally, as explained in Section 3.1. From Figure 5.11, it can be observed that the auxetic behavior of W-C is 54% lower than that of W/O-C. This indicates that the compressive stiffness of the binding yarn is crucial and should be actively considered during the development of the 3-D auxetic woven fabric.

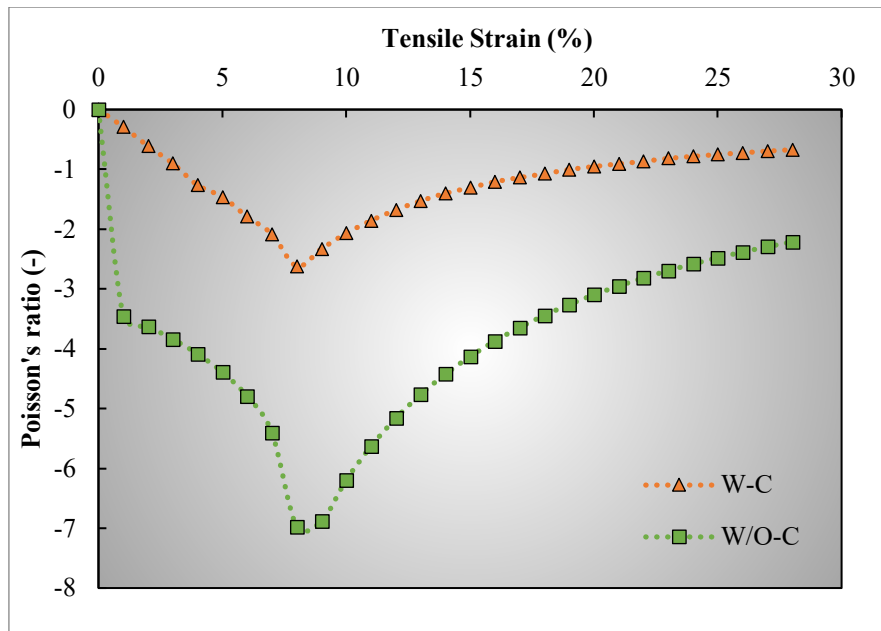


Figure 5.11 Effect of binding yarn's compression on auxetic behavior of 3-D woven structure.

5.2.5.2 Effect of binding yarn diameter

Initially⁵⁷, it was known that the diameter of both the warp and binding yarns has a significant impact on the NPR of 3-D auxetic structures. This finding was further reinforced by an experimental study¹¹³. While the effect of yarn diameter on auxetic behavior has been recognized since then, a scientific explanation for the observed differences has been lacking. In order to provide a solid reason, the Poisson's ratio of the 3-D woven structure was calculated using a geometric model. In this study, three different diameters of binding yarns, specifically 1.9 mm, 2.28 mm, and 2.75 mm, were utilized while keeping other parameters constant. The Poisson's ratio-tensile strain curves of the 3-D woven fabrics associated with these different binding yarn diameters are presented in Figure 5.12.

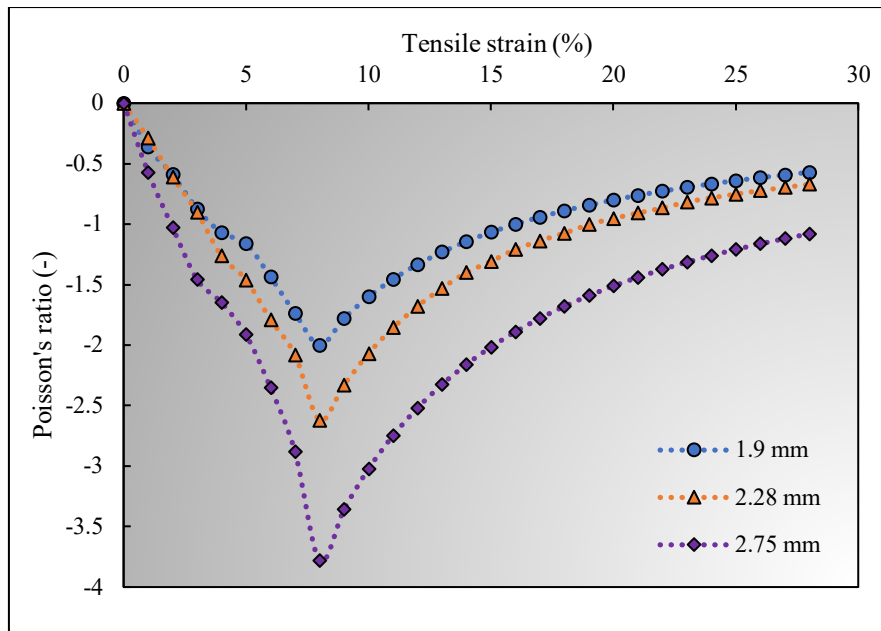


Figure 5.12 Effect of binding yarn diameter on auxetic behavior of 3-D woven structure.

It can be found that the auxetic effect increases by increasing the diameter of the binding yarn, which validates the literature. To establish a solid explanation for this observation, we further analyze the numerical values generated by the geometric model. Upon analysis, it is concluded that the initial percentage of lateral crimp in the warp yarn decreases as the diameter of the binding yarn increases. The crimp percentage can be calculated using Equation (5.31). Specifically, for binding yarn diameters of 1.9 mm, 2.28 mm, and 2.75 mm, the corresponding crimp percentages are 8.086, 8.011, and 7.949, respectively. A lesser degree of lateral crimp in the warp yarn implies that the lateral expansion of the auxetic structure will be initiated at a lower longitudinal strain, and the structure will reach its maximum lateral deformation at a lower strain. Considering that the longitudinal strain is inversely proportional to the NPR (as per Equation (3.2)), it follows that a structure with reduced lateral crimp exhibits a higher degree of auxetic behavior, while a higher degree of lateral crimp leads to a lower auxetic response.

$$Crimp \% = \frac{l_o - X_o}{X_o} \times 100 \quad (5.31)$$

5.2.5.3 Effect of binding yarn spacing

In a similar manner to the effects of binding yarn compression and binding yarn diameter, the spacing between the two binding yarns plays a significant role in evaluating the auxetic behavior of the 3-D auxetic woven structure. To assess this influence, a similar methodological approach was adopted, wherein all other parameters were held constant while the initial distance between the two binding yarns (X_o), referred to as binding yarn spacing, was varied across three measurements. Three specific values were selected for X_o : 2.8 mm, 3 mm, and 3.2 mm. Subsequently, Poisson's ratio values were calculated using the developed geometric model, as shown in Figure 5.13.

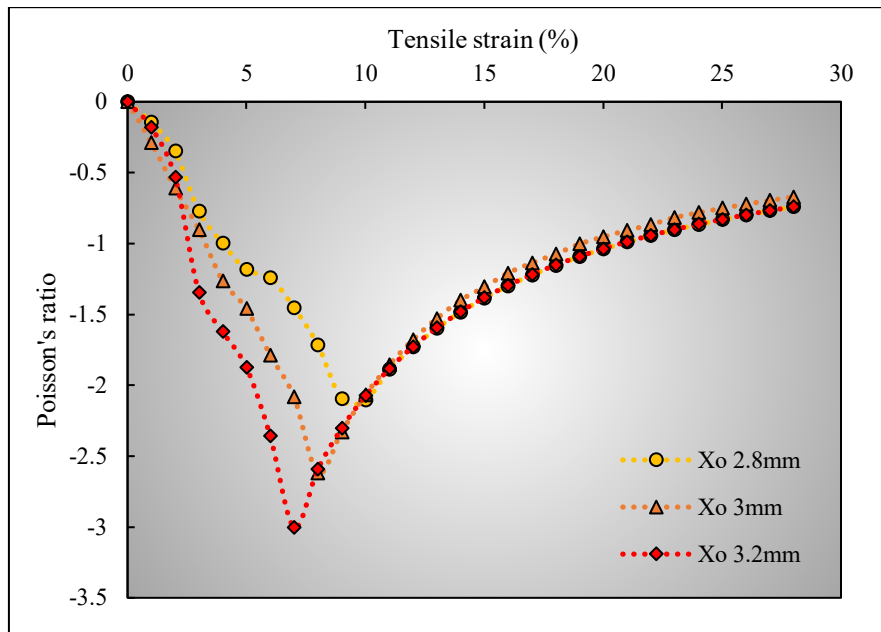


Figure 5.13 Effect of binding yarn spacing on auxetic behavior of 3-D woven structure.

The relationship between binding yarn spacing (X_o) and the NPR effect can be explained. It is observed that the NPR increases with an increase in the yarn spacing, and conversely, decreases when the spacing is reduced. Upon evaluating the measured values for each parameter, we also

discovered that binding yarn spacing has an impact on the lateral crimp of the warp yarn. A higher yarn spacing leads to a reduction in the crimp of the warp yarn, resulting in a more obvious NPR effect at a lower longitudinal strain. The calculated lateral crimp values for X_o of 2.8 mm, 3 mm, and 3.2 mm are 9.74 mm, 8.01 mm, and 6.97 mm, respectively.

5.3 Conclusions

In this chapter, the 3-D woven structure that produces an auxetic effect on the bases of a special geometry resembling a re-entrant hexagon is put forward for geometrical analysis. A meso-level geometrical model is proposed based on the arrangement of yarns in the structure, aiming to establish a relationship between Poisson's ratio and tensile strain through semi-empirical equations. During the practical deformation of the structure, it is observed that the auxetic behavior is primarily generated by the structure's geometry. However, it is also recognized that factors other than geometry can influence auxetic behavior. One such factor is the behavior of the binding yarn, which undergoes compression during tensile deformation, affecting the Poisson's ratio. Therefore, in addition to geometrical parameters, the model also considers the compression behavior of the binding yarn. The Poisson's ratio results obtained from the geometrical model are compared with experimental results, which demonstrates a good agreement. Following validation, the model was used to calculate and discuss critical geometrical parameters that affect the auxetic behavior of the structure. As the developed geometrical model is based on the meso-level (yarn-level) analysis of the structure, therefore, it is useful to predict the auxetic behavior with given yarn parameters. Additionally, it can help to find specific reasons for the NPR effect related to a particular parameter.

The geometrical analysis suggests that the compression that occurs in binding yarns during the lateral expansion significantly affects the NPR of the structure. Therefore, the compressive stiffness of binding yarn should be considered carefully. The diameter of the binding yarn and

the spacing between the two binding yarns inversely affect the lateral crimp percentage of the warp yarn. While the lateral crimp of warp yarn has a strong relationship with the NPR of the structure e.g., the NPR increases if the crimp is less and vice versa.

In the next chapter, the structure will be modeled and simulated using the finite element method. The simulated results obtained from the finite element model will be compared and validated against experimental results. Following verification, the model will be employed to identify the reasons behind the auxetic behavior of the 3-D structure at different longitudinal strains, as well as the behavior of the warp and binding yarns. Furthermore, the model will be utilized to assess the effect of yarn properties on the auxetic behavior of the 3-D structure.

CHAPTER 6 FINITE ELEMENT SIMULATION OF THREE-DIMENSIONAL AUXETIC WOVEN FABRICS

6.1 Introduction

In the previous chapters, the design, development, and analysis of three-dimensional (3-D) auxetic woven fabrics were conducted to explore their negative Poisson's ratio (NPR) effect. However, due to practical constraints in terms of time and resources, it was not feasible to experimentally study all the parameters that influence the designed structure. To overcome this limitation, a geometrical model of the 3-D auxetic woven structure was proposed, which utilized geometrical parameters such as yarn diameters and distances between yarns to predict the auxetic behavior. However, this geometrical model cannot consider material properties, limiting its usefulness in guiding the design of 3-D auxetic woven structures. In addition, the geometric model of the structure is based on a very small unit cell (1/4 of the repeating unit of structure), which may not represent the actual behavior of the structure.

In this chapter, numerical modeling of the 3-D auxetic woven structure will be presented. The finite element (FE) method will be employed to simulate the auxetic structure by incorporating both the geometrical information and material properties of the yarns. Once a good agreement is achieved between simulated and experimental results, the structure will be further studied by varying the properties of the binding yarn. It is anticipated that the FE analysis will offer new insights and stimulate discussions regarding the auxetic behavior of the 3-D woven structure. By utilizing the FE method, the numerical modeling approach enhances the understanding of the auxetic behavior of the 3-D auxetic woven structure. This modeling technique allows for the consideration of both geometrical parameters and material properties, providing a more

comprehensive analysis of the structure's behavior. The insights gained from the FE analysis can contribute to optimizing the design of 3-D auxetic woven structures and exploring their potential applications in various fields.

6.2 Simulation of three-dimensional auxetic woven structure

6.2.1 Background of three-dimensional auxetic woven structure

A conventional 3-D multi-layer orthogonal through-the-thickness structure was modified to visualize auxetic property. Typically, this type of structure consists of three yarn systems: warp, weft, and binding yarns in X-, Y-, and Z-directions respectively, as shown in Figure 6.1 (a). The warp and weft yarns are straight, while the binding yarn is woven through the thickness of the structure in an orthogonal manner along the warp direction. To convert this structure into an auxetic one, the three-yarn system was arranged in a special configuration with the desired diameters and properties of yarns. In this study, a relatively thicker binding yarn was used by replacing the warp direction and 1/1 plain weave with the weft direction and 2/2 twill weave, respectively, as shown in Figure 6.1 (b). This arrangement creates alternating space throughout the structure. In a subsequent modification stage, the weft yarn was replaced by a fine elastic yarn, as shown in Figure 6.1 (c), causing the structure to shrink and fill the spaces by crimping the warp yarns around the orthogonal binding yarn in the lateral direction, as shown in Figure 6.1 (d). With this modified arrangement, the 3-D woven structure becomes auxetic, expanding in the lateral direction when a tensile deformation is applied in the warp direction. Therefore, the structure will switch from position “d” to position “c” under tensile deformation and from position "c" to position "d" under a relaxed state.

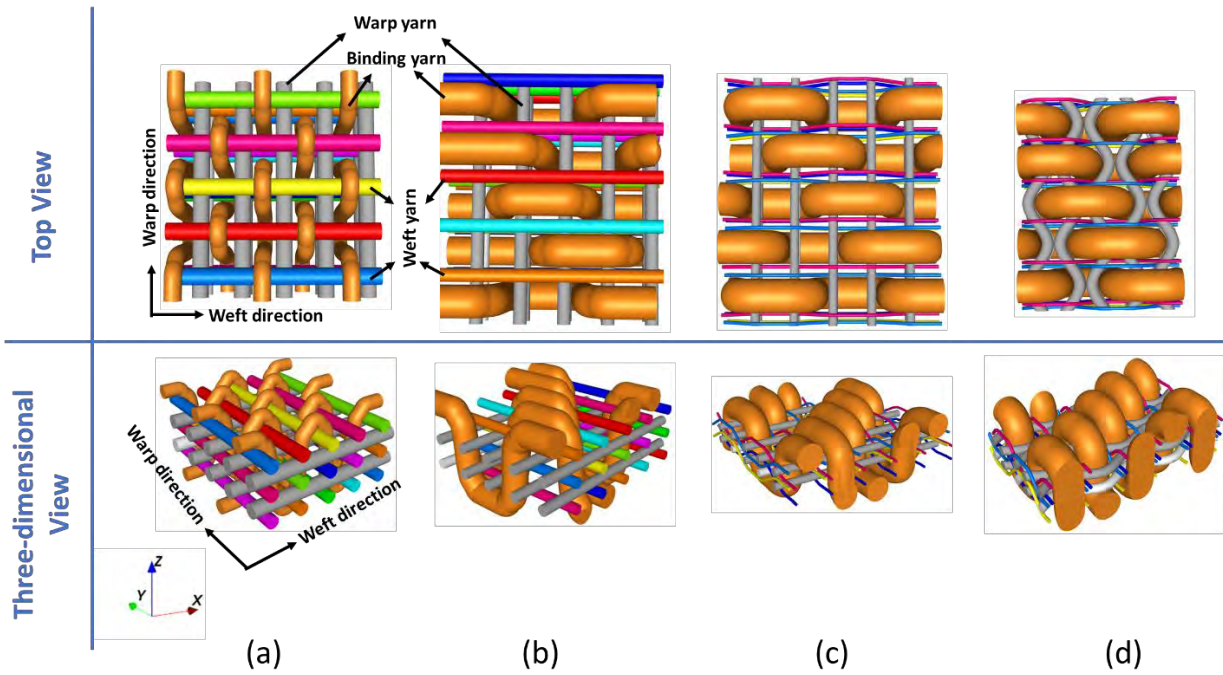


Figure 6.1 Schematic illustration of (a) conventional three-dimensional orthogonal through-the-thickness structure, (b) modification of binding yarn, (c) modification of weft yarn, and (d) modified three-dimensional auxetic structure.

It is important to note that during the fabrication process, the elastic weft yarns were inserted in stretched form, as shown in “stage c” of Figure 6.1. It was intended to make the elastic yarn work as a restoring spring that can shrink the fabric structure when cutting off the weaving machine, as illustrated in “stage d” Figure 6.1. At this stage, the 3-D woven structure is referred to as an “initial state” or “relaxed state” because no external force or deformation is acting on it. Although the 3-D auxetic woven structure is in a relaxed state, the elastic weft yarns are still in stretched form as they did not fully return to their initial length due to close ends (fabric selvage). Therefore, at the initial state, the elastic weft yarns are under a pre-stretched state.

6.2.2 Numerical modeling

Modeling the textile structure at the mesoscale (yarn level) is considered as a challenging task due to architectural complexity, material anisotropy, and meshing challenges. Before

establishing the FE model, the following assumptions are made based on the findings of the experimental analysis conducted on the textile structure:

1. In the FE model, the initial state will be referred to as the post-developed state of the fabric structure under no external force. While the deform state is referred to as the fabric structure under tensile deformation.
2. At the initial state, the two adjacent warp yarns within the same layer are in contact with each other.
3. The warp yarns are in contact with the binding yarns and weft elastic yarns.
4. At the initial state, the elastic weft yarn is under a pre-stretch of 14.8 %, while warp and binding yarns are under zero extension or compression.
5. During the tensile extension, the deformation is applied to one end of the structure in the warp direction, while the other end will remain fixed.
6. The ends of the structure in the weft direction (along the width) should act as fabric selvage (i.e., fixed ends of weft yarns).

These assumptions are expected to enhance the accuracy of the FE modeling and ensure that the simulated results obtained will closely align with the experimental findings.

6.2.2.1 Establishing a model of the fabric structure

The process used to develop the model for the 3-D auxetic textile structure is explained in detail, ensuring the reproducibility of the model. To reduce processing time, a relatively small yet adequately representative geometric area was chosen for the FE model. This area consists of 4 by 4 geometric unit cells in both the warp and weft directions, representing a single repeat of the weave pattern, specifically a 2/2 twill weave as shown in Figure 6.2 (a). The geometric

arrangement of yarns forming a 3-D textile assembly was initially generated using an open-source TexGen software¹¹⁴, and the resulting geometry was extracted as a STEP file extension for further processing. The STEP file was then imported into commercially available Abaqus software for simulation as shown in Figure 6.2 (b). The geometric parameters of the fabric model such as the diameter of yarns, the distance between yarns, etc. are illustrated in Figure 6.2 (b), while their respective values are provided in Table 6.1.

Table 6.1 Geometric parameters of fabric structure for FE model

Description	Symbol	Value
Diameter of binding yarn	D_b	2.28 mm
Diameter of warp yarn	D_p	0.7 mm
Diameter of weft yarn	D_f	0.25 mm
Distance between the axial lines of two consecutive binding yarns	A_o	3 mm
Distance between the surfaces of two consecutive elastic yarns or elastic yarn and binding yarn	B_o	0.073 mm
Distance between the axial lines of the warp yarns of top and bottom layers	T_o	0.95 mm
Length of the representative model structure	L_o	12 mm
Width of the representative model structure	W_o	7.36 mm

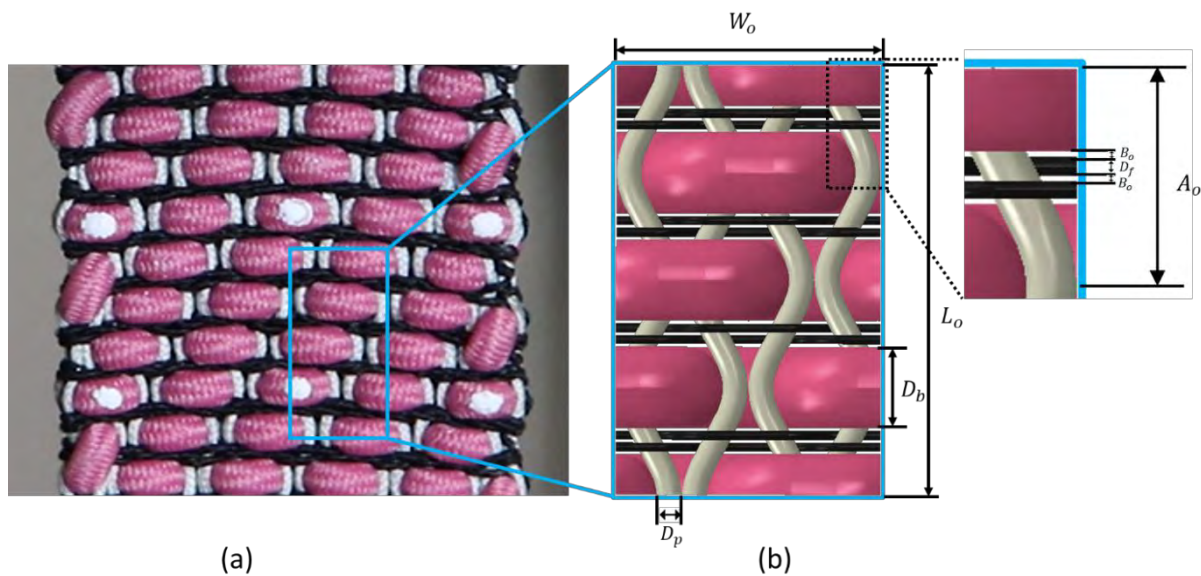


Figure 6.2 Establishment of fabric structure model for finite element analysis; (a) real fabric structure, (b) modeled fabric structure.

6.2.2.2 Determining material properties for the model

The material composition and properties of the three yarn systems forming the textile assembly are provided in Table 6.2. In the FE model, the warp yarn was defined as an isotropic elastic material, considering its braided structure, in which component yarns are oriented in various directions to form a quasi-isotropic structure. The elastic modulus of warp yarn was calculated from region A (elastic deformation) of the stress-strain curve, as illustrated in Figure 6.3. Due to its braided structure, the individual filaments of yarn adjust to the applied tensile force, resulting in an initial low modulus at a negligibly small strain of 0.11 %. As the filaments align, the yarn starts to resist the deformation, leading to an increase in modulus as highlighted in yellow (region A). This modulus of the warp yarn represents the elastic modulus, therefore, it is considered for the FE model. Subsequently, the yarn enters the plastic deformation stage at 2.34 % tensile strain, highlighted in green (region B). Hence, region A was defined with isotropic property by inputting the axial modulus and Poisson's ratio, while region B, which

reflects the plastic deformation of the warp yarn, was defined with plastic property by inputting the plastic engineering stress-strain data points of the curve. In contrast to the warp yarn, the binding yarn was defined with transversely isotropic material property due to the presence of polyurethane (PU) in its core, which imparts transverse isotropy to its nature. In addition, the radial modulus of binding yarn is crucial in the structure as the yarn undergoes compressive loads during deformation. A discrete local orientation of the binding yarn was defined to specify its axial modulus (E_x) and radial modulus (E_y). It is important to note that the E_x was calculated from the tensile stress-strain data within the elastic limit, while the E_y was obtained from a compression test performed on the binding yarn. The elastic weft yarn demonstrates substantially significant deformation of over 400% strain, and it was defined with the hyperelastic property. The deformation of the elastic weft yarn remained within an elastic limit during the tensile process of the 3-D woven fabric. Hence, assigning the hyperelastic property to elastic weft yarn is appropriate for the FE model. To assign the property of the weft yarn, the uni-axial test data (nominal stress-strain) was initially inputted into the hyperelastic mechanical property. Subsequently, the material was evaluated to calculate the strain energy potential constants based on Equation 6.1 (incompressible materials) of the Ogden model of elasticity ¹¹⁵. The calculated value of strain-energy potential constants, Mu (μ) and Alpha (α), are provided in Table 6.3. Furthermore, based on the nominal stress-strain data of weft yarn, the strain-energy potential constants remained stable with the Ogden model of order 2.

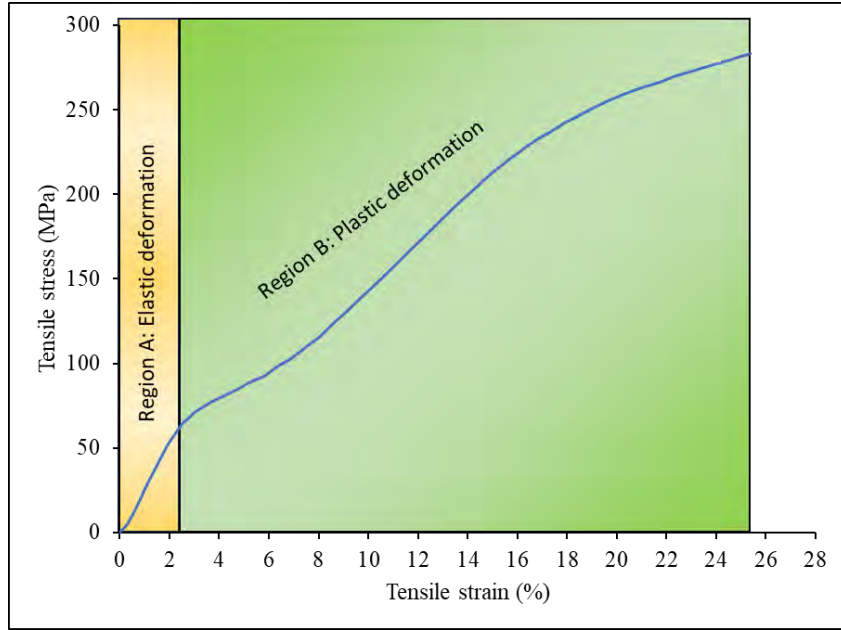


Figure 6.3 Tensile stress-strain curve of warp yarn.

Table 6.2 Material properties of warp yarn and binding yarn.

Yarn type	Material and structure	Young's modulus (MPa)		Poisson's ratio (-)
		Axial (E_x)	Radial (E_y)	
Warp yarn	Polyester-based braided	1645.8	1645.8	0.35
Binding yarn	Polyester-wrapped PU-based braided	39.7	9.9	0.35

$$W = \sum_{i=1}^N \frac{\mu_i}{\alpha_i} (\lambda_1^{-\alpha_i} + \lambda_2^{-\alpha_i} + \lambda_3^{-\alpha_i} - 3) + W_{volume} \quad (6.1)$$

Where N is an order of the model that ranges from 1 to 3, μ_i and α_i are material constants, λ_1 , λ_2 and λ_3 are variables of principal stretches in the three directions of strain, W_{volume} indicates volume change of the material that can be eliminated in case of incompressible materials.

Table 6.3 Material law parameters for elastic weft yarn.

Order	Mu (μ)	Alpha (α)
1	2.555e-10	5.981
2	0.561	-3.401

6.2.2.3 *Setting up the testing environment and executing the model*

The three yarn components that make up the assembly were relatively straightforward for the FE model. However, the pre-stretch condition of elastic weft yarn (according to assumption 4) complicates the model. Specifically, the elastic weft yarns are under 14.8% strain at the initial state. To accurately carry this argument, a two-step simulation method using a dynamic explicit solver was chosen. More specifically, the pre-stretch condition of elastic weft yarn is achieved in the first step (step-1) of analysis by applying a displacement of 1.09mm (equivalent to 14.8% strain) to the ends of the elastic weft yarns in positive and negative y-directions, as shown in Figure 6.4 (a). In addition, other yarns were temporarily fixed during this step to prevent unintended displacements. In step-2, a tensile deformation of 4.2mm (equivalent to 35% tensile strain) was applied to one end of the model in the positive x-direction, while the other end remained fixed, as shown in Figure 6.4 (b). Moreover, the end columns of the binding yarns were fixed in the z-direction to prevent undesired rotation.

The interaction among yarns in the textile assembly is both crucial and challenging. To address this, a general contact was established for step-1 with a global property of frictionless behavior to smoothly attain the pre-stretch condition of elastic weft yarn. However, the general contact was modified for step-2 by enabling a penalty friction formulation of 0.4¹¹⁶ for the binding and elastic weft yarns with the warp yarns. Additionally, to satisfy assumption 6, a rough interaction

was defined between the ends of the elastic weft yarns and the warp yarns, effectively acting as fabric selvage, with specific conditions of no slip and no separation after contact.

For meshing, the element size was determined based on the yarn diameter. For example, elastic weft yarn was seeded with an element size of 0.17mm, the warp yarn with 0.2mm, and the binding yarn with 0.25mm. Due to non-linearity in the yarn's initial geometry, a tetrahedral element shape with linear element type (C3D4) was assigned to warp and binding yarns, while a hybrid element type (C3D4H) was chosen for the weft yarn. The selection of the hybrid element for the weft yarn was based on the strain energy potential constants, as weft yarn material was considered incompressible by the model, which can only be used with hybrid elements.

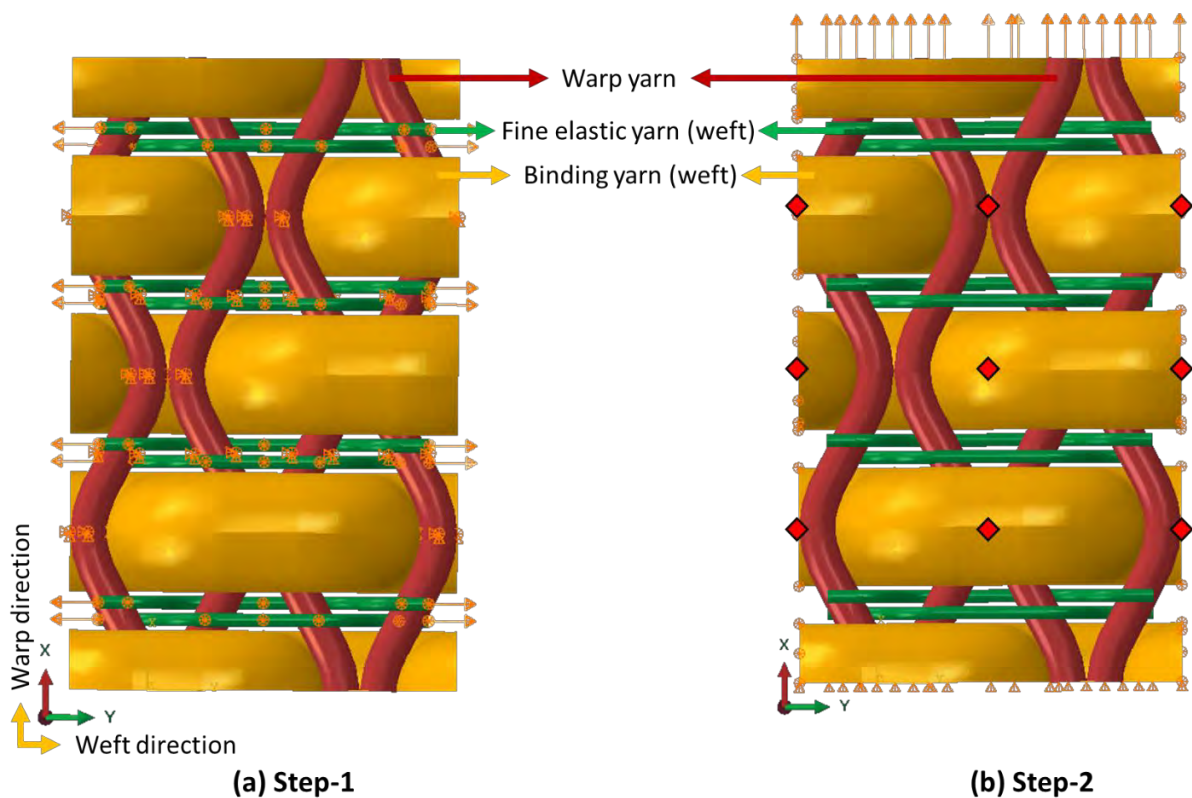


Figure 6.4 Boundary conditions of finite element model at (a) step-1, and (b) step-2.

To calculate the FE simulated Poisson's ratio (PR) of the 3-D auxetic structure, sets of two nodes from a specific region (as specified in Figure 6.4 (b) by red dots) were selected, from the length (x-), and the width (y-) directions. The data point at each deformation state was then extracted. The distance between the two points in the x-direction can be used to calculate longitudinal deformation, while the distance in the y-direction can be used to calculate transverse deformation. Once the two deformations are known, the PR of the structure can be calculated using Equation (6.2).

$$\nu_{xy} = -\frac{\varepsilon_y}{\varepsilon_x} = -\frac{(y-y_0)/y_0}{(x-x_0)/x_0} \quad (6.2)$$

Where ε_x is longitudinal strain and ε_y is transverse strain; y_0 and x_0 are the initial width and length; y and x are width and length under deformation respectively.

6.2.3 Simulation results

6.2.3.1 Model validation

To verify the FE model, the simulated PR and tensile stress of the 3-D auxetic structure are compared with those of real fabric calculated experimentally in our previous study¹¹³, as shown in Figure 6.5 (a) and (b), respectively. From Figure 6.5 (a), it can be seen that both simulated and experimental PR of the 3-D textile structure exhibited a decrease at the initial tensile strain, reaching to the lowest PR values of -1.66 and -1.61 at tensile strains of 7.77% and 7.26%, respectively. After reaching the minimum PR, both curves began to increase again, though at a slower pace. Since the simulated PR followed the same trend as the experimental PR, it can be concluded that the simulated and experimental results of the 3-D auxetic structure are in good agreement. However, it should be noted that the PR at the initial tensile strain is lower for the FE model compared to the experimental PR. This difference can be attributed to the ideal arrangement of the warp yarns in the FE model. Another reason for the difference is the

non-linear tensile modulus of the warp yarn, specifically, the modulus at initial stain from 0% to 0.9% is 10.1 MPa, followed by an increase in modulus to 27.18 MPa during tensile strain of 0.9% to 3%. The modulus 27.18 MPa is the elastic modulus of the yarn while the initial lower modulus of 10.1 MPa is caused by the alignment of filaments to the tensile force. However, the modulus of 27.18 MPa is considered in the FE model, resulting in the initial difference in PR.

From Figure 6.5 (b), it can be found that although there is some difference in the simulated and experimental tensile stress-strain, still they are in good agreement. The difference could be due to the slippage phenomenon occurring in experimental testing, while no condition of slippage is assumed in FE analysis. Based on the tensile stress-strain and Poisson's ratio-tensile strain results, the model is considered validated, and it can be used to predict and analyze the auxetic behavior of the 3-D auxetic woven structure.

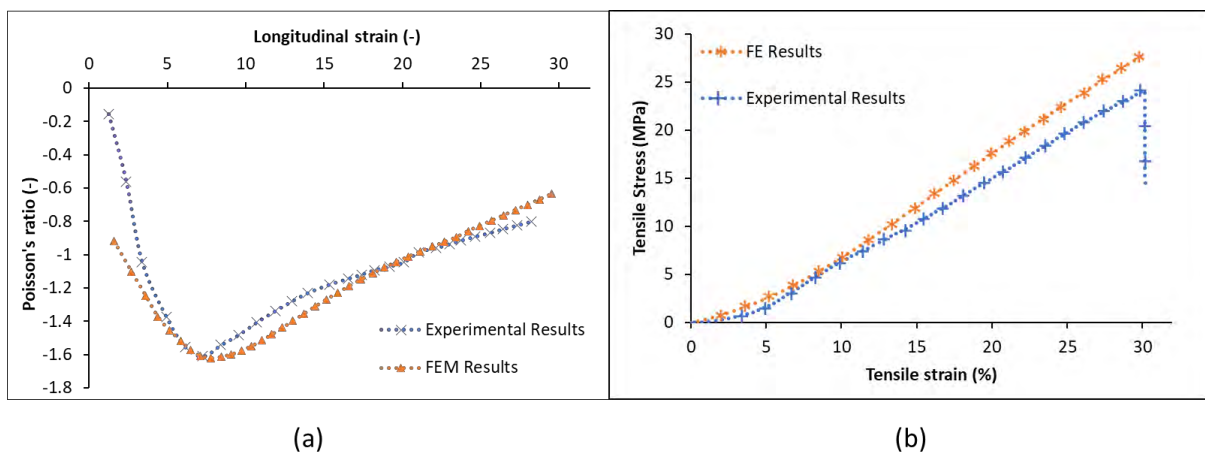


Figure 6.5 Comparison of experimental and simulated results: (a) Poisson's ratio-tensile strain, (b) tensile stress-tensile strain.

6.2.3.2 *Deformation of structure and stress distribution analysis*

In the geometry, the initial length of the elastic weft yarns was intentionally kept smaller than the total width of the model to attain the pre-stretching condition as explained before. Consequently, the weft yarns were subjected to an initial condition of 14.8% tensile strain in step-1, as shown in Figure 6.6 (a-b). Once the initial strain conditions of the elastic weft yarns were met in step-1, the structure was subjected to an axial tensile extension in the warp (x-) direction. In step-2, at zero strain, the warp yarns were perfectly crimped by the elastic yarns in the 3-D structure, as shown in Figure 6.6 (b). However, when a tensile displacement is applied, the warp yarns start to straighten in response to the applied force. This causes the binding yarns to be pushed laterally by warp yarns, resulting from the unique alternating arrangement of these two types of yarn. This causes a lateral expansion of the whole structure, as shown in Figure 6.6 (c-h), and leads to negative PR.

Due to the application of a 14.8% initial strain to the elastic weft yarns, they exhibit comparatively higher stresses than the warp yarns at the initial strains in step-2. However, at higher longitudinal strain, as shown in Figure 6.6 (h), the stresses in the warp yarns become dominant over those in the elastic weft yarns. Since the displacement in step-2 was applied to the warp yarns, they play a central role in bearing the applied tensile load and exhibit a higher stress contribution. The binding yarns experience compression forces due to the pushing force exerted by the warp yarns, which contributes to the lateral expansion of the structure. Therefore, compressive stresses are generated in the binding yarns, as shown in Figure 6.7.

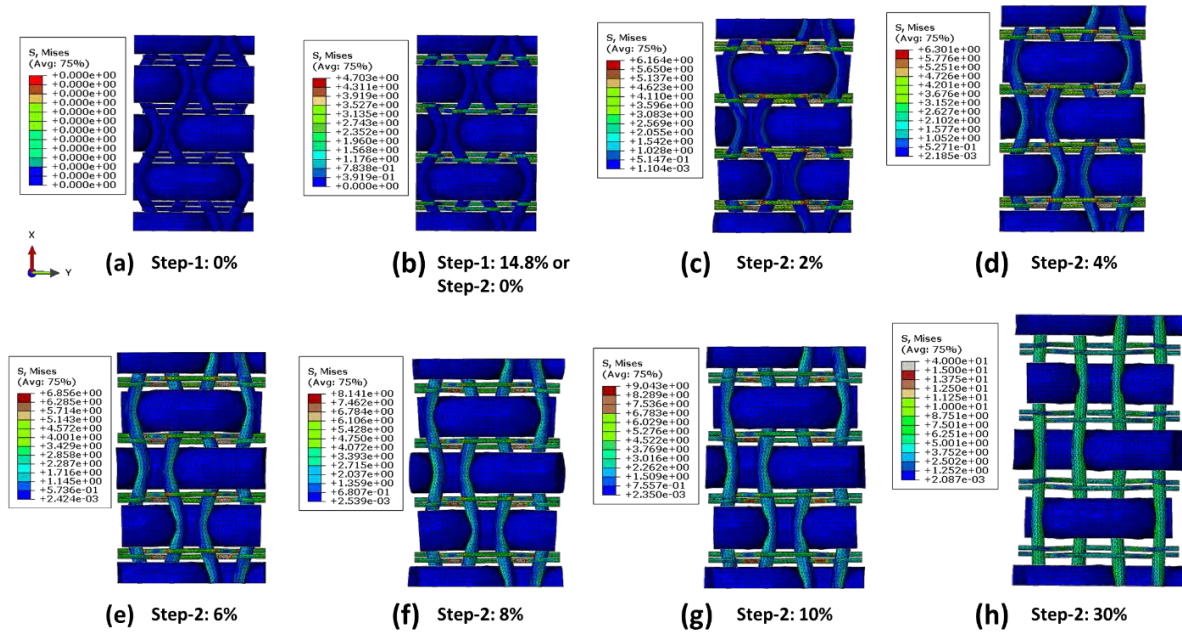


Figure 6.6 Deformation and Mises distribution of 3-D structure at different tensile strains in step-1 (elastic weft yarn extension) and step-2 (warp yarn extension).

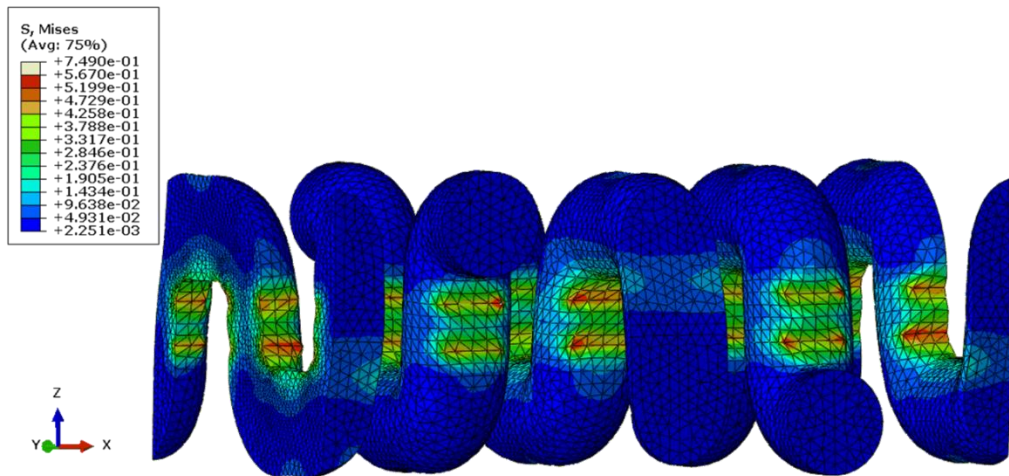


Figure 6.7 Mises stress distribution in binding yarns at a deform state.

6.2.3.3 Insights into the deformation behavior of the 3-D auxetic structure

In the experimental study, the results were discussed based on overall physical assessments of the 3-D auxetic structure under tensile deformation²³. Based on those assessments, a geometrical model was developed to predict the auxetic behavior of the structure²⁴. However,

it is evident that general physical assessments cannot provide detailed information about the behavior of the individual yarns during structural deformation. Due to this limitation, the PR results obtained from the geometrical model²⁴ did not fit with the experimental results, as shown in Figure 6.8. Nonetheless, the FE model is based on the true material properties used in the experiment study along with a significantly higher geometrical unit representing the whole 3-D auxetic structure. Therefore, the FE model provides a more accurate and justifiable calculation of the PR.

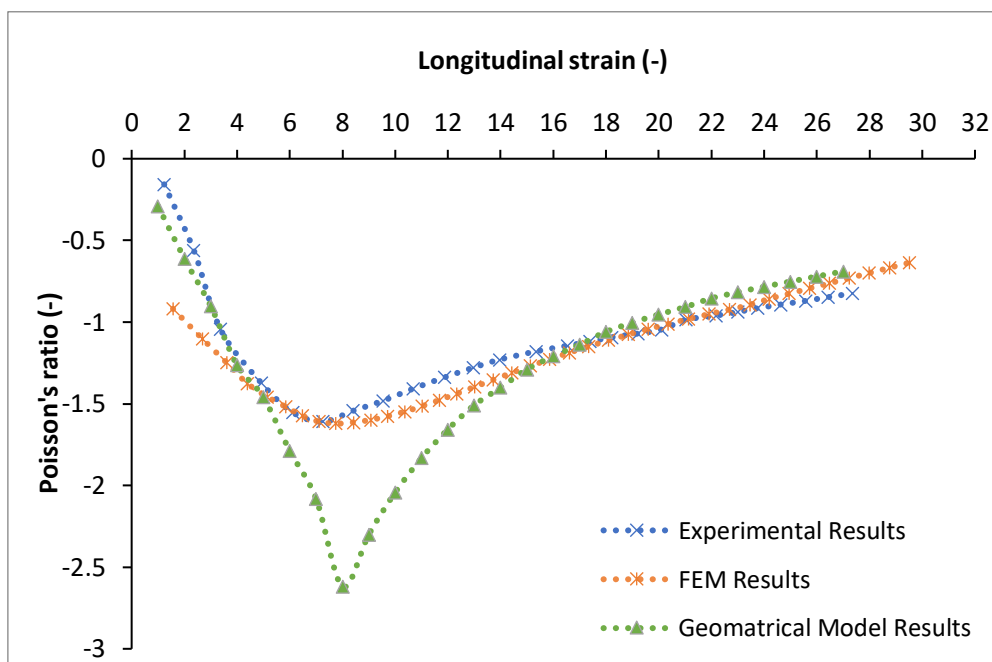


Figure 6.8 Comparison of FE simulated and geometrically calculated PR with experimental PR of the 3-D auxetic woven structure.

During the experimental and geometrical studies of the 3-D auxetic structure, it was previously believed that the compression experienced by the binding yarns during deformation was solely caused by the restoring force of elastic weft yarns. Although the analysis was true, however, it was only one of the two factors causing the compression of the binding yarn. The FE model revealed an additional factor that contributes to the compression of the binding yarn, which is

the uniaxial stretching of pairs of neighboring warp yarns that attempt to come closer to each other during the decrimping process. To comprehend this phenomenon, the graphical representation of the structure was modified to display a top cross-sectional view with the elastic weft yarns omitted, as shown in Figure 6.9 (a). If the binding yarns are assumed absent from the geometry, as shown in Figure 6.9 (b), the pair of neighboring warp yarns (referred to as pair-1 and pair-2) would certainly move closer to each other under the defined boundary conditions, as represented partially transparent in Figure 6.9 (b). However, due to the presence of binding yarns in the actual scenario, the warp yarns experience a lateral displacement in the y-direction, as shown in Figure 6.9 (c). As a result, the tendency of the warp yarns to approach each other generates an additional compressive force on the binding yarns, which acts as a second factor that influences the negative PR of the structure.

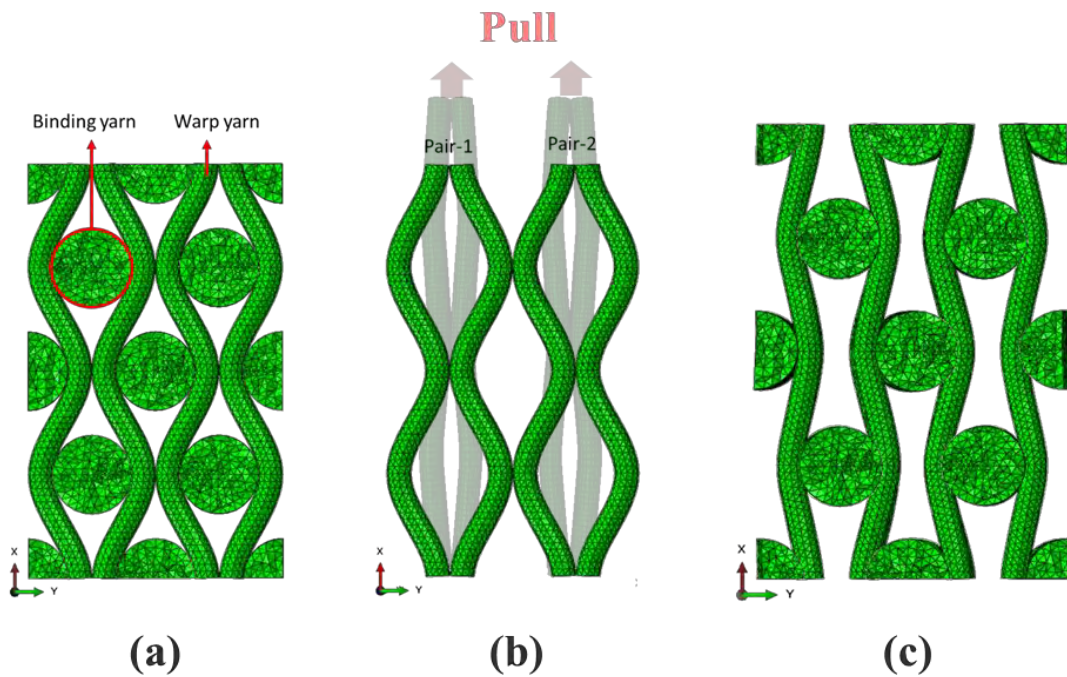


Figure 6.9 Illustration of the top cross-sectional of 3-D auxetic structure: (a) top cross-section of warp and binding yarns at initial state, (b) only warp yarns at initials and deform state (shown as partially transparent), and (c) warp and binding yarns under 10 % tensile strain.

6.2.3.4 Prediction of auxetic behavior with FE model

In science, FE analysis holds significant importance in predicting the properties and behavior of material, product, or structure under specific conditions. Hence, the FE model developed in this study can be utilized to assess the auxetic behavior of the 3-D auxetic woven fabric, considering different geometrical parameters and material properties. However, the previously developed geometrical model²⁴ of the 3-D auxetic structure was primarily employed to predict and analyze its auxetic behavior based on various geometrical parameters, such as warp or binding yarn diameters. Therefore, the developed FE model will only be used to predict the auxetic behavior by changing the material properties. Although the geometrical model successfully predicted the PR with different geometrical parameters, it has limitations in predicting the auxetic behavior with varying material properties. Thus, the FE model is employed to predict the PR of the 3-D auxetic structure by modifying the most important factor i.e., the stiffness of binding yarn.

During the development of the 3-D auxetic woven fabric on the weaving machine, it was observed that the bending stiffness, also known as axial stiffness, of the binding yarn played a critical role in both the weaving process and the auxetic behavior of the structure. However, there was no available physical tool to assess and quantify the effect of the bending stiffness of the binding yarn on the auxetic behavior of the 3-D fabric. In addition, as explained in the previous section, the binding yarn undergoes a compression process during tensile deformation, which also affects the PR of the 3-D auxetic structure. Therefore, it can be concluded that both the axial and radial stiffnesses, which are correlated with the bending and compression of binding yarn, respectively, play a significant role in the auxetic behavior of the 3-D auxetic fabric structure. To investigate these two factors, the model was modified solely for binding yarn. The binding yarn was assigned different moduli for axial (E_x) and radial (E_y)

directions of the binding yarn. The values of E_x and E_y provided in Table 4 represents the moduli used in this study to obtain conclusive results explaining the effect of binding yarn moduli on the auxetic behavior of the 3-D woven structure. The 3-D auxetic structure exhibited intriguing outcomes when the given values of E_x and E_y for the binding yarn were employed to predict the auxetic behavior.

Table 6.4 Axial and radial moduli of binding yarn.

Factor	Level						
Axial modulus, E_x (MPa)	40	40	40	40	50	60	70
Radial modulus, E_y (MPa)	10	20	30	40	10	10	10

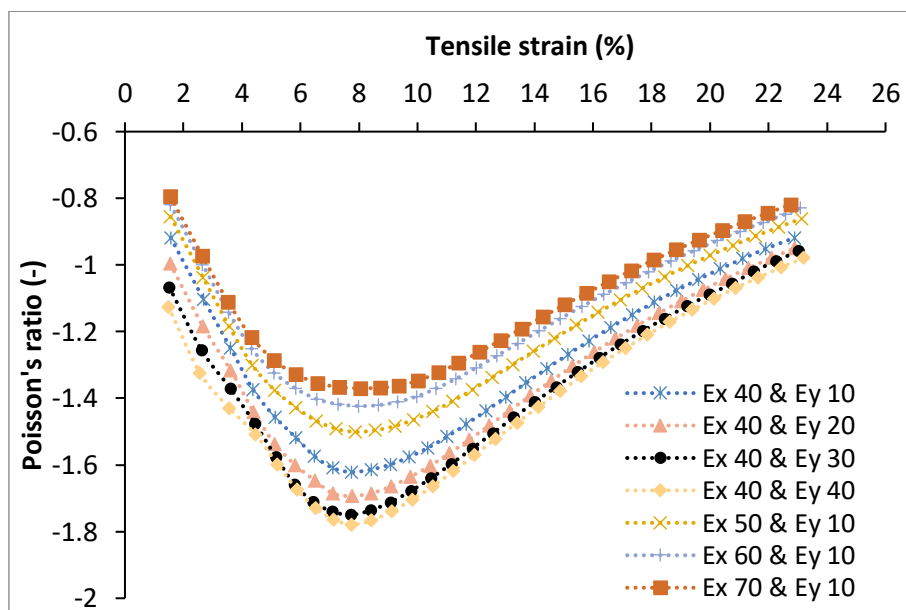


Figure 6.10 PR results of three-dimensional auxetic structure with different axial and radial moduli of binding yarn.

Figure 6.10 provides clear information about the relationship between the axial and radial moduli of binding yarn and NPR of the 3-D auxetic structure. The auxetic behavior of the 3-D structure increases when the radial modulus of binding yarn is increased while keeping the axial modulus constant. In contrast, the auxetic behavior decreases when the axial modulus of binding yarn is increased with a fixed radial modulus.

In the first scenario, increasing the radial modulus makes the binding yarn stiffer in the thickness direction. As a result, it becomes more difficult for the warp yarn to compress the binding yarn under tensile deformation. This reduced compression of the binding yarn leads to a higher NPR of the 3-D auxetic structure. This claim is supported by Figure 6.11, which illustrates the compressive strain of the binding yarn against the tensile strain of the 3-D auxetic structure. It can be observed that the compressive strain decreases as the radial modulus increases. A lower compressive strain indicates a lesser decrease in the diameter of the binding yarn. Additionally, the compressive strain remains the same for samples with similar out-of-plane modulus, regardless of the change in axial modulus.

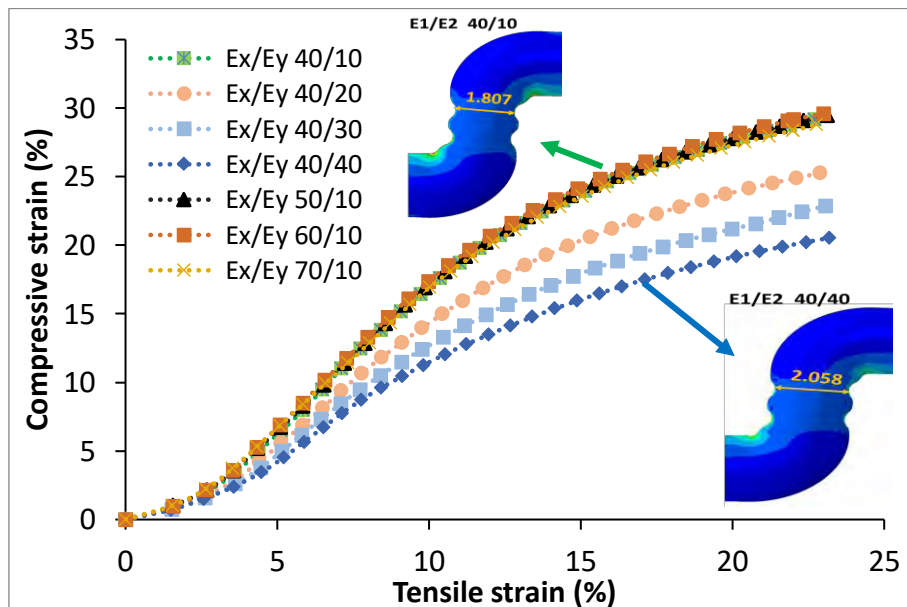


Figure 6.11 Compressive strain of binding yarn against the tensile strain of the 3-D auxetic structure.

In the second scenario, a higher axial modulus indicates a higher bending stiffness of the binding yarn. This higher bending stiffness causes two problems for the 3-D structure: the first problem is related to the practical weaving process of the 3-D woven structure, where a binding yarn is more difficult to bend when it alternately changes its movement direction from the top face to the bottom face and from the bottom face to the top face of the structure. The second problem is relevant to the stress concentration as shown in Figure 6.12 (a-b) where significantly higher stresses are developed in binding yarn with a higher axial modulus compared to the one with a lower axial modulus. From the aforementioned scenarios, it could be concluded that better auxetic behavior can be achieved by using a binding yarn that possesses the unique property of being easy to bend but difficult to compress.

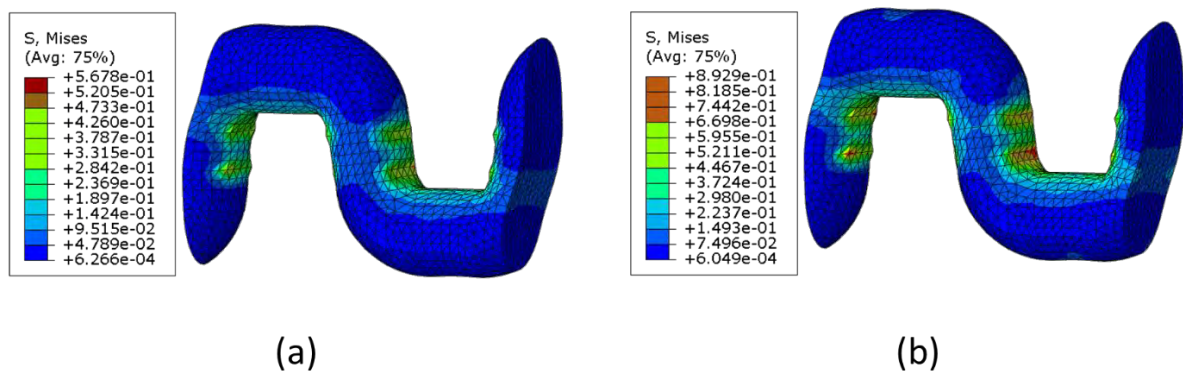


Figure 6.12 Mises stress distribution in binding yarn, (a) E_x/E_y 40/10 and (b) E_x/E_y 70/10.

6.3 Conclusions

This research has successfully demonstrated the potential of finite element (FE) analysis in providing detailed insights into the auxetic behavior of 3-D woven structures at the yarn level, which was previously a challenging task. The study has established a reliable 3-D FE model

that simulates the behavior of the structure effectively, bridging the gap left by experimental and geometrical studies. The main findings from the study are stated below:

1. The FE model provides a significant advantage over the previously developed geometrical model in predicting the Poisson's ratio of the 3-D auxetic structure considering the material's property as well as a comparatively bigger unit cell. Thereby more accurate results are achieved through the developed FE model.
2. The FE analysis highlighted the critical role of the uniaxial stretching of neighboring warp yarns that causes compression of the binding yarn during the decrimping process.
3. Based on the findings from the FE analysis, an important question regarding the disparity between the experimental PR and the geometrically calculated PR of the 3-D auxetic structures has been addressed. Specifically, it has been determined that the compression of binding yarns during the lateral expansion of the structure is not solely caused by the elastic weft yarns, but the warp yarns themselves also contribute to this compression.
4. The analysis also revealed the significant impact of the axial and radial moduli of the binding yarn on Poisson's ratio of the 3-D woven structure. The results show that a better auxetic effect can be achieved by using binding yarn with a lower axial modulus (easy to bend) and higher radial modulus (difficult to compress).

CHAPTER 7 CONCLUSIONS AND SUGGESTIONS FOR FUTURE RESEARCH

7.1 Conclusions

This thesis focuses on the study of three-dimensional (3-D) woven fabrics with an in-plane negative Poisson's ratio (NPR) effect. The research methodology can be explained in five steps:

- 1) Designing a novel 3-D woven structure with in-plane auxetic behavior by modifying a conventional 3-D multi-layer through-the-thickness structure.
- 2) Converting the designed 3-D auxetic structure into woven fabrics through the fabric manufacturing process.
- 3) Testing the developed fabric samples to analyze their auxetic behavior.
- 4) Developing a geometrical model of the unique arrangement of yarns that causes the auxetic behavior.
- 5) Conducting finite element simulations of the 3-D auxetic woven fabrics.

The main findings of each objective of the study are summarized below.

7.1.1 Design concept and development

This study explores the possibility of developing a novel 3-D woven structure with in-plane auxetic behavior. To achieve this objective, the existing conventional 3-D woven structures were closely examined for potential modifications. Among these structures, a multi-layer through-the-thickness structure was ultimately chosen due to the orthogonal positioning of warp, weft, and binding yarns in the x, y, and z directions, respectively, which provides flexibility for modification. The structure underwent three significant changes to the yarn system in order to achieve the auxetic effect. The in-plane auxetic behavior was achieved by

introducing an unconventional lateral crimp to the warp yarns, resulting in a unique geometric configuration resembling a re-entrant hexagon. As the structure was stretched longitudinally (warp direction), the lateral crimp in the warp yarns started to straighten, pushing the binding yarn in the lateral direction. Consequently, the structure expanded laterally when subjected to longitudinal deformation, thus exhibiting in-plane auxetic behavior. An intriguing aspect of the newly designed structure is that it does not require special production methods or machinery. Conventional elastic and non-elastic yarns, along with a commonly available (semi-automatic) weaving machine, were used to develop the 3-D auxetic woven samples.

7.1.2 Auxetic behavior and factors affecting Poisson's ratio

The results of Poisson's ratio analysis demonstrate a significant in-plane auxetic behavior in the 3-D woven fabrics. These fabrics exhibit a sudden increase in auxetic behavior at the initial stage of tensile strain. This immediate auxetic response is attributed to the lateral crimp in the warp yarn, which begins to straighten during the initial tensile strain, causing the fabric to expand laterally. The fabrics reach their maximum auxetic effect of -1.6 Poisson's ratio at a tensile strain of 8%. At this point, the warp yarns are fully straightened under the tensile load. After reaching 8% tensile strain, the auxetic effect gradually decreases, albeit at a slower pace. This decrease occurs because the longitudinal strain is still active, but there is no additional lateral crimp in the warp yarns to further expand the fabric.

Given the complex design of the structure, several factors influence its auxetic behavior. Therefore, the fabrics were developed with different parameters to analyze their effects on auxetic behavior. The selected parameters for analysis include the diameter of the binding yarn, the repeat size of the elastic yarn, the bending stiffness of the binding yarn, and the stretch percentage of the elastic weft yarn. The results indicate that a larger diameter of the binding yarn can cause weaving issues, resulting in an improper formation of the auxetic structure. On

the other hand, a finer binding yarn only induces minimal lateral crimp in the warp yarns, resulting in a weaker auxetic effect. Additionally, the use of elastic weft yarn contributes to the stability of the fabric structure by keeping it in a relaxed state. However, the magnitude of the restoring force (RF) generated by the elastic weft yarns should be controlled. Insufficient RF can lead to inadequate shrinkage of the structure, while excessive RF can compress the binding yarn and restrict the lateral expansion of the structure. Furthermore, the bending stiffness of the binding yarn also affects the auxetic properties. For instance, a lower bending stiffness of the binding yarn can produce a higher auxetic effect. Therefore, it is important to select a suitable binding yarn with easy bending properties.

7.1.3 Geometrical analysis

The auxetic behavior of the 3-D woven fabrics primarily arises from the arrangement of the three-yarn system within the structure. To better understand this behavior, a geometrical model of the 3-D auxetic structure was developed at the meso-level, focusing on yarn parameters. Semi-empirical equations were derived to establish a relationship between tensile strain and the Poisson's ratio of the structure. To enhance the robustness of the geometrical analysis, the model incorporated individual yarn behavior observed during experimental tests of the 3-D auxetic woven fabrics. Notably, the model took into account the compression of the binding yarn, which was observed during the fabric deformation process. The model was then utilized to calculate the Poisson's ratio of the structure at various tensile strains, and the calculated results were validated by comparing them with experimental data from the 3-D auxetic woven structure. The trend variation of the calculated Poisson's ratio demonstrated a better agreement with the experimental results. However, it should be noted that the Poisson's ratio at the negative peak in the calculated results was slightly higher than the experimental values. This discrepancy can be attributed to the model's limitation, as it solely considered geometric

parameters and did not incorporate material properties. Despite this minor limitation, the model proved to be a valuable tool for predicting the auxetic behavior of the structure by manipulating its geometrical parameters. Consequently, the structure was thoroughly examined by investigating different geometrical factors related to the yarns and the overall structure that influence its Poisson's ratio behavior. The proposed geometrical model provided essential insights into the fundamental geometric analysis of the structure, offering valuable information for further exploration.

7.1.4 Finite element analysis

To overcome the limitations of the previous geometrical model, a finite element (FE) model was developed to simulate the in-plane Poisson's ratio behavior of the 3-D auxetic woven fabrics. The FE model provided a more accurate representation by incorporating the material properties of each element within the structure. A precise geometry of the structure was created using TexGen software and imported into Abaqus CAE for simulation. The FE model underwent a tensile test, and the in-plane Poisson's ratio was simulated and compared with experimental results. The simulated outcomes demonstrated a strong agreement with the experimental data. This FE model offers a significant advantage over the previous geometrical model as it considers the material properties, leading to more accurate predictions of Poisson's ratio for the 3-D auxetic structure. The developed FE model was utilized to analyze and elucidate the auxetic behavior of the structure at the yarn level, which was previously challenging. For instance, the FE analysis highlighted the crucial role of uniaxial stretching of neighboring warp yarns, which results in compression of the binding yarn during the decrimping process. It was observed that this compression by the warp yarns only occurs in alternate binding yarns, and its effect is not substantial enough to significantly reduce the overall lateral expansion of the 3-D structure. Furthermore, the analysis revealed the significant

impact of the in-plane and out-of-plane moduli of the binding yarn on Poisson's ratio of the 3-D woven structure. The results indicated that a better auxetic effect can be achieved by utilizing a binding yarn with a lower in-plane modulus (easy to bend) and a higher out-of-plane modulus (difficult to compress). These findings provide valuable insights for optimizing the auxetic behavior of the 3-D woven structure.

7.2 Contributions

The development of 3-D woven fabrics with in-plane NPR effect represents a significant advancement in this research. Unlike the previously available 2-D auxetic woven fabrics, which exhibit low in-plane auxetic effects and poor mechanical performance, the novel 3-D auxetic woven fabrics introduced in this study offer improved properties. These fabrics have the potential to address high-performance applications that were previously unattainable with non-auxetic 3-D structures or low mechanical 2-D auxetic structures. To understand the auxetic behavior of the 3-D woven fabrics, experimental studies were conducted, investigating various structural parameters and material properties. However, textile fabrics possess numerous parameters that can affect different properties, and in the case of 3-D textiles, the number of parameters increases further. Conducting experiments to study each parameter individually would be impractical, requiring significant time and resources. Therefore, to overcome these challenges, this research extended its scope to include geometric and numerical modeling of the 3-D auxetic woven fabrics. This modeling approach enables the design of 3-D structures with desired performance characteristics before actual production. The combination of experimental studies and geometric/numerical modeling provided valuable insights into the auxetic behavior of 3-D woven fabrics. These models serve as a foundation of knowledge for future research and can be instrumental in designing textile fabrics for specific applications. By considering the effects of various parameters, researchers and fabric designers can optimize

the performance of 3-D fabrics for specific requirements, thereby expanding their potential applications.

7.3 Limitations

Although in this research the novel auxetic fabrics were designed, fabricated, and modeled successfully, still the study has some limitations due to limited time and resources, which are mentioned below:

1. This study is limited to the use of a conventional semi-automatic weaving machine for sample production, therefore, only coarser yarns are used. In addition, the 3-D auxetic fabrics are developed with narrow width and tested in one direction only.
2. No special binding yarn was developed to improve the auxetic behavior of the 3-D woven fabrics. For example, a binding yarn can be designed with lower in-plane modulus, and higher out-of-plane modulus, which has the ability of easy to bend but difficult to compress.
3. The geometrical model of the structure only predicts and explains the auxetic behavior based on the geometrical parameters of the structure and the material properties cannot be included in it.
4. In the finite element model, more material information can be provided to get more accurate results. For example, the warp yarn can be defined with transverse isotropic properties.
5. The 3-D woven fabrics were studied for their auxetic property to understand the deformation mechanism, while other performance properties were not evaluated.

7.4 Suggestions for future research

This research brings several outcomes for the new 3-D auxetic woven fabrics, however, many improvements can be made in the future to increase the scope of the auxetic fabrics. Some suggestions for future research are as follows:

1. Improvements can be made to the 3-D auxetic woven fabrics if a three-dimensional (3-D) weaving machine is used to produce the designed fabrics more efficiently.
2. The current study uses certain warp and elastic weft yarn diameters, and only the diameter of coarse binding yarn was changed. So, 3-D auxetic woven fabric can be developed and checked with finer yarns.
3. Further experiments can be conducted to study the effect of the number of layers on the mechanical performance, structural stability, and deformation behavior of the 3-D auxetic fabrics.
4. Using 3-D weaving machine, the binding yarn can be used in the warp direction and the corresponding deformation behavior can be assessed.
5. The fabrics can be studied with other performance properties for targeted applications such as composite reinforcements, auxetic sensors, safety belts, etc.

REFERENCES

1. Liu Y, Hu H. A review on auxetic structures and polymeric materials. *Sci Res Essays* 2010; 5: 1052–1063.
2. Nguyễn H, Figueiro R, Ferreira F, et al. Auxetic materials and structures for potential defense applications: An overview and recent developments. *Text Res J* 2023; 93: 5268–5306.
3. Ntintakis I, Stavroulakis GE, Karathanasopoulos S. Auxetics, Theory and Textile Applications. In: *Proceedings of the Joint International Conference: 10th Textile Conference and 4th Conference on Engineering and Entrepreneurship*, pp. 509–517.
4. Liu Y, Zhao C, Xu C, et al. Auxetic meta-materials and their engineering applications: a review. *Eng Res Express* 2023; 5: 042003.
5. Parisi M, Allen T, Colonna M, et al. Indentation and impact response of conventional, auxetic, and shear thickening gel infused auxetic closed cell foam. *Smart Mater Struct* 2023; 32: 074004.
6. Duncan O, Alderson A, Allen T. Fabrication, characterization and analytical modeling of gradient auxetic closed cell foams. *Smart Mater Struct* 2021; 30: 035014.
7. Alderson K., Evans K. The fabrication of microporous polyethylene having a negative Poisson's ratio. *Polymer (Guildf)* 1992; 33: 4435–4438.
8. Caddock BD, Evans KE. Microporous materials with negative Poisson's ratios. I. Microstructure and mechanical properties. *J Phys D Appl Phys* 1989; 22: 1877–1882.
9. Zahra T. Behaviour of 3D printed re-entrant chiral auxetic (RCA) geometries under in-plane and out-of-plane loadings. *Smart Mater Struct* 2021; 30: 115011.

10. Etemadi E, Zamani AMM, Scarpa F, et al. Modified re-entrant auxetic metamaterials with energy absorption enhancement. *Mater Today Commun* 2024; 38: 108079.
11. Etemadi E, Gholikord M, Zeeshan M, et al. Improved mechanical characteristics of new auxetic structures based on stretch-dominated-mechanism deformation under compressive and tensile loadings. *Thin-Walled Struct* 2023; 184: 110491.
12. Mizzi L, Salvati E, Spaggiari A, et al. Highly stretchable two-dimensional auxetic metamaterial sheets fabricated via direct-laser cutting. *Int J Mech Sci* 2020; 167: 105242.
13. Gonçalves C, Magalhães R, Rana S, et al. Novel high performance auxetic fibrous structures for composite reinforcement. *IOP Conf Ser Mater Sci Eng* 2018; 406: 012046.
14. Ren X, Das R, Tran P, et al. Auxetic metamaterials and structures: a review. *Smart Mater Struct* 2018; 27: 023001.
15. Mizzi L, Salvati E, Spaggiari A, et al. 2D auxetic metamaterials with tuneable micro-/nanoscale apertures. *Appl Mater Today* 2020; 20: 100780.
16. Ravirala N, Alderson KL, Davies PJ, et al. Negative Poisson's Ratio Polyester Fibers. *Text Res J* 2006; 76: 540–546.
17. Alderson KL, Alderson A, Smart G, et al. Auxetic polypropylene fibres: Part 1 - Manufacture and characterisation. *Plast Rubber Compos* 2002; 31: 344–349.
18. Miller W, Hook PB, Smith CW, et al. The manufacture and characterisation of a novel, low modulus, negative Poisson's ratio composite. *Compos Sci Technol* 2009; 69: 651–655.
19. Sloan MR, Wright JR, Evans KE. The helical auxetic yarn – A novel structure for

- composites and textiles; geometry, manufacture and mechanical properties. *Mech Mater* 2011; 43: 476–486.
20. Gao Y, Chen X, Studd R. Experimental and numerical study of helical auxetic yarns. *Text Res J* 2021; 91: 1290–1301.
 21. Ali M, Zeeshan M, Qadir MB, et al. Development and Comfort Characterization of 2D Woven Auxetic Fabric for Wearable and Medical Textile Applications. *J Cloth Text* 2018; 36: 199–214.
 22. Ali M, Zeeshan M, Qadir MB, et al. Development and mechanical characterization of weave design based 2D woven auxetic fabrics for protective textiles. *Fibers Polym* 2018; 19: 2431–2438.
 23. Chen Y, Zulifqar A, Hu H. Auxeticity from the Folded Geometry: A Numerical Study. *Phys status solidi* 2020; 257: 1900361.
 24. Kamrul H, Dong W, Zulifqar A, et al. Deformation behavior of auxetic woven fabric made of foldable geometry in different tensile directions. *Text Res J* 2021; 91: 87–99.
 25. Kamrul H, Zulifqar A, Hu H. Deformation behavior of auxetic woven fabric based on re-entrant hexagonal geometry in different tensile directions. *Text Res J* 2020; 90: 410–421.
 26. Cao H, Zulifqar A, Hua T, et al. Bi-stretch auxetic woven fabrics based on foldable geometry. *Text Res J* 2019; 89: 2694–2712.
 27. Zulifqar A, Hu H. Geometrical analysis of bi-stretch auxetic woven fabric based on re-entrant hexagonal geometry. *Text Res J* 2019; 89: 4476–4490.
 28. Zulifqar A, Hua T, Hu H. Single- and Double-Layered Bistretch Auxetic Woven Fabrics

- Made of Nonauxetic Yarns Based on Foldable Geometries. *Phys Status Solidi Basic Res* 2020; 257: 1–13.
29. Zeeshan M, Ali M, Riaz R, et al. Optimizing the Auxetic Geometry Parameters in Few Yarns Based Auxetic Woven Fabrics for Enhanced Mechanical Properties Using Grey Relational Analysis. *J Nat Fibers* 2022; 19: 4594–4605.
 30. Zulifqar A, Hua T, Hu H. Development of uni-stretch woven fabrics with zero and negative Poisson's ratio. *Text Res J* 2018; 88: 2076–2092.
 31. Ge Z, Hu H. A theoretical analysis of deformation behavior of an innovative 3D auxetic textile structure. *J Text Inst* 2015; 106: 101–109.
 32. Ge Z, Hu H, Liu Y. A finite element analysis of a 3D auxetic textile structure for composite reinforcement. *Smart Mater Struct* 2013; 22: 084005.
 33. Ahmed HI, Umair M, Nawab Y, et al. Development of 3D auxetic structures using para-aramid and ultra-high molecular weight polyethylene yarns. *J Text Inst* 2021; 112: 1417–1427.
 34. Ma P, Chang Y, Jiang G. Design and fabrication of auxetic warp-knitted structures with a rotational hexagonal loop. *Text Res J* 2016; 86: 2151–2157.
 35. Shuaiquan Z, Yuping C, Yadie Y, et al. Auxetic behavior of warp knitted fabric under repeating tension. *Text Res J* 2021; 91: 1732–1741.
 36. Yuping C, Liu Y, Shuaiquan Z, et al. Design and manufacture of three-dimensional auxetic warp-knitted spacer fabrics based on re-entrant and rotating geometries. *Text Res J*. Epub ahead of print 2021. DOI: 10.1177/00405175211037204.
 37. Wang Z, Hu H. 3D auxetic warp-knitted spacer fabrics. *Phys status solidi* 2014; 251:

- 281–288.
38. Zhao S, Chen Y, Chang Y, et al. Finite Element Modeling of Auxetic Warp-Knitted Fabric Made of Re-entrant Geometry. *Phys status solidi* 2021; 258: 2100107.
 39. Zhao S, Hu H, Kamrul H, et al. Development of auxetic warp knitted fabrics based on reentrant geometry. *Text Res J* 2020; 90: 344–356.
 40. Yuping C, Liu Y, Shuaiquan Z, et al. Design and manufacture of three-dimensional auxetic warp-knitted spacer fabrics based on re-entrant and rotating geometries. *Text Res J* 2022; 92: 467–478.
 41. Glazzard M, Breedon P. Weft-knitted auxetic textile design. *Phys status solidi* 2014; 251: 267–272.
 42. Hong Hu, Zhengyue Wang, Su Liu. Development of auxetic fabrics using flat knitting technology. *Text Res J* 2011; 81: 1493–1502.
 43. Boakye A, Chang Y, Rafiu KR, et al. Design and manufacture of knitted tubular fabric with auxetic effect. *J Text Inst* 2018; 109: 596–602.
 44. Verma P, Smith CL, Griffin AC, et al. Wool nonwovens as candidates for commodity auxetic materials. *Eng Res Express* 2020; 2: 045034.
 45. Bhullar SK, Ko J, Cho Y, et al. Fabrication and Characterization of Nonwoven Auxetic Polymer Stent. *Polym Plast Technol Eng* 2015; 54: 1553–1559.
 46. Verma P, Shofner ML, Lin A, et al. Inducing out-of-plane auxetic behavior in needle-punched nonwovens. *Phys status solidi* 2015; 252: 1455–1464.
 47. Khan MI, Akram J, Umair M, et al. Development of composites, reinforced by novel

- 3D woven orthogonal fabrics with enhanced auxeticity. *J Ind Text* 2019; 49: 676–690.
48. Xu W, Sun Y, Lin H, et al. Preparation of soft composite reinforced with auxetic warp-knitted spacer fabric for stab resistance. *Text Res J* 2020; 90: 323–332.
49. Steffens F, Oliveira FR, Figueiro R. Energy absorption from composite reinforced with high performance auxetic textile structure. *J Compos Mater* 2021; 55: 1003–1013.
50. Zhou L, Jiang L, Hu H. Auxetic composites made of 3D textile structure and polyurethane foam. *Phys status solidi* 2016; 253: 1331–1341.
51. Miller W, Ren Z, Smith CW, et al. A negative Poisson's ratio carbon fibre composite using a negative Poisson's ratio yarn reinforcement. *Compos Sci Technol* 2012; 72: 761–766.
52. Wang Z, Zulifqar A, Hu H. Auxetic composites in aerospace engineering. In: Rana S, Figueiro R (eds) *Advanced Composite Materials for Aerospace Engineering*. Cambridge: Woodhead Publishing, pp. 213–240.
53. Bhattacharya S, Zhang GH, Ghita O, et al. The variation in Poisson's ratio caused by interactions between core and wrap in helical composite auxetic yarns. *Compos Sci Technol* 2014; 102: 87–93.
54. Wright JR, Burns MK, James E, et al. On the design and characterisation of low-stiffness auxetic yarns and fabrics. *Text Res J* 2012; 82: 645–654.
55. Ng W, Hu H. Woven Fabrics Made of Auxetic Plied Yarns. *Polymers (Basel)* 2018; 10: 226.
56. Zulifqar A, Hu H. Development of Bi-Stretch Auxetic Woven Fabrics Based on Re-Entrant Hexagonal Geometry. *Phys Status Solidi Basic Res* 2019; 256: 1–8.

57. Ge Z, Hu H. Innovative three-dimensional fabric structure with negative Poisson's ratio for composite reinforcement. *Text Res J* 2013; 83: 543–550.
58. Liaqat M, Samad HA, Hamdani STA, et al. The development of novel auxetic woven structure for impact applications. *J Text Inst* 2016; 108: 1264–1270.
59. Hu H, Zhang M, Liu Y. Applications of auxetic textiles. In: Hu H, Zhang M, Liu Y (eds) *Auxetic Textiles*. Cambridge: Woodhead Publishing, 2019, pp. 337–350.
60. Voigt W. *Lehrbuch der Kristallphysik* (Leipzig: B G Teubner). 1928; 741.
61. Gibson LJ, Ashby MF, Schajer GS, et al. The mechanics of two-dimensional cellular materials. *Proc R Soc London A Math Phys Sci* 1982; A 382: 25–42.
62. Lakes R. Foam Structures with a Negative Poisson's Ratio. *Science (80-)* 1987; 235: 1038–1040.
63. Ge Z, Hu H, Liu S. A novel plied yarn structure with negative Poisson's ratio. *J Text Inst* 2016; 107: 578–588.
64. Verma P, Wagner KB, Griffin AC, et al. Reversibility of Out-of-Plane Auxetic Response in Needle-Punched Nonwovens. *Phys status solidi*; 259. Epub ahead of print 17 December 2022. DOI: 10.1002/pssb.202200387.
65. Ullah T, Ahmad S, Nawab Y. Development of helical auxetic yarn with negative Poisson's ratio by combinations of different materials and wrapping angle. *J Ind Text* 2020; 152808372094111.
66. Shah AA, Shahid M, Hardy JG, et al. Effects of Braid Angle and Material Modulus on the Negative Poisson's Ratio of Braided Auxetic Yarns. *Crystals* 2022; 12: 781.

67. Cuthbert TJ, Hannigan BC, Roberjot P, et al. HACS: Helical Auxetic Yarn Capacitive Strain Sensors with Sensitivity Beyond the Theoretical Limit. *Adv Mater*; 35. Epub ahead of print 6 March 2023. DOI: 10.1002/adma.202209321.
68. Liu S, Gao Y, Chen X, et al. A Theoretical Study on the Effect of Structural Parameter on Tensile Properties of Helical Auxetic Yarns. *Fibers Polym* 2019; 20: 1742–1748.
69. Liu S, Du Z, Liu G, et al. Study on the tensile behavior of helical auxetic yarns by modeling and mechanical analysis. *J Text Inst* 2021; 112: 1531–1537.
70. Razbin M, Jamshidi Avanaki M, Jeddi AAA, et al. A systematic study on the predictability of different methods to predict the maximum Poisson's ratio of helical auxetic yarn. *J Text Inst* 2022; 113: 90–100.
71. Starbuck M, Anand SC, Ravirala N, et al. *FABRICS HAVING KNIT STRUCTURES EXHIBITING AUXETIC PROPERTIES AND GARMENTS FORMED THEREBY*. US 2008/0011021 A1, 2008.
72. Ugbolue SC, Kim YK, Warner SB, et al. *AUXETIC FABRICSTRUCTURES AND RELATED FABRICATION METHODS*. US 8772187 B2, 2014.
73. Attard D, Grima JN. Auxetic behaviour from rotating rhombi. *Phys status solidi* 2008; 245: 2395–2404.
74. Attard D, Manicaro E, Grima JN. On rotating rigid parallelograms and their potential for exhibiting auxetic behaviour. *Phys status solidi* 2009; 246: 2033–2044.
75. Grima JN, Evans KE. Auxetic behavior from rotating triangles. *J Mater Sci* 2006; 41: 3193–3196.
76. N. Grima J, Gatt R, Alderson A, et al. On the Auxetic Properties of `Rotating

- Rectangles' with Different Connectivity. *J Phys Soc Japan* 2005; 74: 2866–2867.
77. Yuping C, Liu Y, Hong H. Deformation behavior of auxetic laminated fabrics with rotating square geometry. *Text Res J* 2022; 92: 4652–4665.
 78. Luan K, Newman Z, West A, et al. Efficient Poisson's Ratio Evaluation of Weft-Knitted Auxetic Metamaterials. *Textiles* 2023; 3: 275–286.
 79. Khalid R, Jamshaid H, Mishra R, et al. Performance analysis of socks produced by auxetic yarns for protective applications. *J Ind Text* 2022; 51: 6838S-6863S.
 80. Sun Y, Xu W, Wei W, et al. Stab-resistance of auxetic weft-knitted fabric with Kevlar fibers at quasi-static loading. *J Ind Text* 2021; 50: 1384–1396.
 81. Chang Y, Liu Y, Hu H. A finite element analysis of auxetic composite fabric with rotating square structure. *J Ind Text* 2023; 53: 152808372311731.
 82. Verma P, Shofner ML, Griffin AC. Deconstructing the auxetic behavior of paper. *Phys status solidi* 2014; 251: 289–296.
 83. Yanping Liu, Hong Hu, Lam JKC, et al. Negative Poisson's Ratio Weft-knitted Fabrics. *Text Res J* 2010; 80: 856–863.
 84. Wang Z, Hu H. 3D auxetic warp-knitted spacer fabrics. *Phys status solidi* 2014; 251: 281–288.
 85. Zhou L, Zeng J, Jiang L, et al. Low-velocity impact properties of 3D auxetic textile composite. *J Mater Sci* 2018; 53: 3899–3914.
 86. Alderson KL, Simkins VR, Coenen VL, et al. How to make auxetic fibre reinforced composites. *Phys status solidi* 2005; 242: 509–518.

87. Carneiro VH, Meireles J, Puga H. Auxetic materials — A review. *Mater Sci* 2013; 31: 561–571.
88. Alderson KL, Coenen VL. The low velocity impact response of auxetic carbon fibre laminates. *Phys status solidi* 2008; 245: 489–496.
89. Herakovich CT. Composite Laminates with Negative Through-the-Thickness Poisson's Ratios. *J Compos Mater* 1984; 18: 447–455.
90. Miller W, Hook PB, Smith CW, et al. The manufacture and characterisation of a novel , low modulus , negative Poisson ' s ratio composite. *Compos Sci Technol* 2009; 69: 651–655.
91. Boakye A, Raji RK, Ma P, et al. Compressive Property of an Auxetic-Knitted Composite Tube Under Quasi-Static Loading. *Autex Res J* 2020; 20: 101–109.
92. Poźniak AA, Wojciechowski KW, Grima JN, et al. Planar auxeticity from elliptic inclusions. *Compos Part B Eng* 2016; 94: 379–388.
93. Zhang M, Ho MMP, Hu H. Low velocity impact performance of <sc>3D</sc> auxetic composites embedded with re-entrant triangle inclusions. *Polym Compos* 2023; 44: 5070–5086.
94. Zhang M, Hu H, Kamrul H, et al. Three-dimensional composites with nearly isotropic negative Poisson's ratio by random inclusions: Experiments and finite element simulation. *Compos Sci Technol* 2022; 218: 109195.
95. Jiang L, Gu B, Hu H. Auxetic composite made with multilayer orthogonal structural reinforcement. *Compos Struct* 2016; 135: 23–29.
96. Xu W, Ma P, Wu L, et al. Low-velocity impact properties of composite reinforced by

- auxetic warp-knitted spacer fabric. *J Sandw Struct Mater* 2021; 23: 1972–1986.
97. Li T, Liu F, Wang L. Enhancing indentation and impact resistance in auxetic composite materials. *Compos Part B Eng* 2020; 198: 108229.
 98. Wang Z, Hu H. Auxetic materials and their potential applications in textiles. *Text Res J* 2014; 84: 1600–1611.
 99. Ma P, Chang Y, Boakye A, et al. Review on the knitted structures with auxetic effect. *J Text Inst* 2017; 108: 947–961.
 100. Hu H, Zulifqar A. Auxetic Textile Materials - A review. *J Text Eng Fash Technol*; 1. Epub ahead of print 2016. DOI: 10.15406/jteft.2016.01.00002.
 101. Evans KE, Alderson A. Auxetic Materials: Functional Materials and Structures from Lateral Thinking! *Adv Mater* 2000; 12: 617–628.
 102. Alderson A, Alderson K. Expanding materials and applications: exploiting auxetic textiles. *Tech Text Int* 2005; 777: 29–34.
 103. Critchley R, Corni I, Wharton JA, et al. A review of the manufacture, mechanical properties and potential applications of auxetic foams. *Phys status solidi* 2013; 250: 1963–1982.
 104. Khokar N. 3D-Weaving: Theory and Practice. *J Text Inst* 2001; 92: 193–207.
 105. Chen X, Potiyaraj P. CAD/CAM of Orthogonal and Angle-Interlock Woven Structures for Industrial Applications. *Text Res J* 1999; 69: 648–655.
 106. Khokar N. 3D Fabric-forming Processes: Distinguishing Between 2D-weaving, 3D-weaving and an Unspecified Non-interlacing Process. *J Text Inst* 1996; 87: 97–106.

107. Umair M, Hamdani STA, Asghar MA, et al. Study of influence of interlocking patterns on the mechanical performance of 3D multilayer woven composites. *J Reinf Plast Compos* 2018; 37: 429–440.
108. Msalilwa LR, Kyosev Y, Rawal A, et al. Investigation of the Bending Rigidity of Double Braided Ropes. In: Yordan Kyosev (ed) *Recent Developments in Braiding and Narrow Weaving*. Cham: Springer International Publishing, pp. 47–57.
109. Phoenix SL. Mechanical Response of a Tubular Braided Cable with an Elastic Core. *Text Res J* 1978; 48: 81–91.
110. Gokarneshan N. Double Cloths. In: Gokarneshan N (ed) *FABRIC STRUCTURE AND DESIGN*. New Delhi: New age international publishers, 2004, pp. 100–115.
111. Bilisik K, Karaduman NS, Bilisik NE, et al. Three-dimensional fully interlaced woven preforms for composites. *Text Res J* 2013; 83: 2060–2084.
112. Yüksekaya ME, Howard T, Adanur S. Influence Of The Fabric Properties On Fabric Stiffness For The Industrial Fabrics. *Tekst ve Konfeksiyon* 2008; 4: 263–267.
113. Zeeshan M, Hu H, Zulifqar A. Three-dimensional narrow woven fabric with in-plane auxetic behavior. *Text Res J* 2022; 92: 4695–4708.
114. Brown LP, Long AC. Modeling the geometry of textile reinforcements for composites: TexGen. In: *Composite Reinforcements for Optimum Performance*. Elsevier, pp. 237–265.
115. Ogden RW. Large deformation isotropic elasticity – on the correlation of theory and experiment for incompressible rubberlike solids. *Proc R Soc London A Math Phys Sci* 1972; 326: 565–584.

116. Gao Y, Chen X. Finite element analysis study of parameters influencing the Poisson's ratio of auxetic woven fabrics. *Text Res J*; 0. Epub ahead of print 5 January 2024. DOI: 10.1177/00405175231221598.